Search for the lightest MSSM Higgs boson in cascades of supersymmetric particles in ATLAS

Eirik Gramstad

Department of Physics

University of Oslo

Norway

Thesis submitted in partial fulfillment

of the requirements for the degree of

Master of Science

June 2008

Acknowledgements

I would like to thank my supervisor Prof. Farid Ould-Saada for helping me with my this work. I also would like to thank the rest of the Experimental Particle Physics group at Blindern (EPF) at the Univeristy of Oslo for always gladly answering my questions.

A special thank goes to those who has read through my thesis and given me ideas and suggestions.

A very special thank goes of course also to my girlfriend Marte Skogen Evje for always supporting me.

Introduction

One of the most exciting things happening in particle physics today is the imminent start-up of the Large Hadron Collider (LHC) experiments at the European Organization for Nuclear Research, CERN. Situated on the border between Switzerland and France. The main goal of this experiment is to search for the Higgs boson(s), whose existence(s) is (are) necessary in order for other particles to acquire mass according to the Standard Model (SM). This is the only unconfirmed part of the electroweak sector of the SM. There are also strong reasons to believe that the SM is not the final theory of the fundamental objects and their interactions, and that some new physics beyond the Standard Model will be discovered.

One of the new theories trying to give explanations to the problems within the Standard Model is Supersymmetry (SUSY). SUSY predicts additional particles to the ones already discovered and described by the Standard Model, and if SUSY is the correct description of nature, supersymmetric particles are expected to be discovered at the LHC. This theory in fact also predicts several Higgs bosons, in contrast to the prediction of only one Higgs boson in the Standard Model.

This thesis will try to reveal the possibilities of discovering SUSY and the lightest supersymmetric Higgs boson in the ATLAS experiment at LHC. Since the experiment has not yet started to operate[1] one has to rely on computer-simulated data.

Chapter 2 gives a short introduction to particle physics today and the Standard Model. It also gives an introduction to the Higgs mechanism. In chapter 3 motivations for new physics beyond the Standard Model is presented with the supersymmetric solutions to the problems. The Supersymmetric theory is then described shortly with the emphasize on the Minimal Supersymmetric Standard Model (MSSM). After having presented an alternative to the current SM of particle physics, it is time to mention a tool to test such a supersymmetric theory, and in chapter 4 the ATLAS experiment at the Large Hadron Collider (LHC) is described. The experiment has not yet started to operate. It has been a long

---

[1]planning to start summer 2008

process of construction, development and commissioning of the ATLAS detector. While working on this thesis, I have visited CERN several times and participated in the process of making the detector ready for use. The work I have been involved in is described at the end of chapter 4.

In chapter 5 the production and decay of the lightest supersymmetric Higgs boson in ATLAS is discussed. This study relies on the ability to separate b-jets from other jets, since $h \to b\bar{b}$ will be the dominant decay-mode of Higgs. Therefore a pedagogical introduction to b-tagging in ATLAS, what performance one could expect, and the current results on b-tagging performance from another particle experiment, CDF at TEVATRON, is discussed. At the end of the chapter the various cascade patterns expected in each of the SUSY models is carefully studied. Based on this information, chapter 6 tries to see which set of cuts and strategies should be followed in order to extract a Higgs resonance from the simulated data and how to tackle the SM and SUSY backgrounds. In chapter 7 the results of the study are presented.

Contents

Chapter 1

Theory of particle physics today

The standard model was established after a series of discoveries in 1960s and 1970s. It explains in a consistent way most of the phenomena that are observed experimentally. However there are strong reasons to believe that this is not the final theory of the fundamental objects and their interactions.

1.1 The Standard Model

The Standard Model is formulated as a relativistic quantum field theory, and describes three of the four forces that are seen in nature: the weak and strong nuclear force and the electromagnetic force. The fourth force, gravity, is described by a different theory, the general relativity. With these forces we are able to describe the behaviour of all matter known to us.

In the Standard Model each type of interaction has a characteristic set of force carrier particles, called bosons. In the electromagnetic interaction the photon (γ) is the mediator, for the weak force it is the massive vector bosons $W^{\pm}$ and Z and for the strong force it is eight gluons. All these particles have spin 1.

The electromagnetic force explains interactions between charged particles. It is explained by the Quantum Electrodynamic (QED) theory. All particles that have charge interact through the electromagnetic force. Because the γ is massless, the force range is infinite.

The range of the weak interaction is about 10^{-18} m, approximately 1000 times smaller than the diameter of an atomic nucleus. Beta decay, which changes the number of protons in the nucleus of an atom, is mediated by the weak force's massive vector bosons W^{+} and W^{-}. The electromagnetic force and the weak force are understood to be two aspects of the same force, unified in the electroweak

theory.

The strong force becomes important at distances comparable to the size of a nucleus, $\sim 10^{-15}$ m, and is described by the Quantum ChromoDynamic (QCD) theory. It was believed that this force was a fundamental force acting directly on the protons and neutrons. Today this force is called the nuclear force, while the strong force is the force acting directly on the particles inside the protons and neutrons. All particles that carry color charge interact through the strong force.

The particles that make up matter and are "influenced" by the fundamental forces are leptons and quarks and have $1/2$ in spin. They are called fermions in the Standard Model and are divided into three generations/families, each consisting of two leptons and two quarks, like in (1.1).

$$
1^{st} \text{ generation} \qquad 2^{nd} \text{ generation} \qquad 3^{rd} \text{ generation}
$$

$$
\begin{pmatrix} u \\ d \end{pmatrix}, \begin{pmatrix} \nu_e \\ e^- \end{pmatrix} \qquad \begin{pmatrix} c \\ s \end{pmatrix}, \begin{pmatrix} \nu_\mu \\ \mu^- \end{pmatrix} \qquad \begin{pmatrix} t \\ b \end{pmatrix}, \begin{pmatrix} \nu_\tau \\ \tau^- \end{pmatrix} \qquad (1.1)
$$

Leptons only interact through the electroweak interaction. The two leptons in each of the generations in (1.1) are the charged lepton and its neutrino partner. In the first generation, for instance, we have the electron (e^-) and the electron neutrino (ν_e). The neutrinos are extremely light ($m_\nu = [0.0000022 - 15.5]$ MeV). Originally their masses were believed to be zero. But experimental results revealed that this was not the case. Neutrinos are electrically neutral and do not carry color, so they only interact through the weak interaction.

Each generation of quarks consists of one up-type quark (up (u), charm (c) and top (t)) and one down-type quark (down (d), strange (s), bottom (b)). They carry one of three colors[1] (red, green and blue), and therefore are the only particles in the standard model, apart from the gluon itself, that interact through the strong force. Quarks of the 1st generation are the constituents of protons (u,u,d) and neutrons (u,d,d). Because of a feature of the strong force called confinement we do not see free quarks. They always come in colour-less bound states of baryons (such as the proton an neutron) or mesons. Baryons consist of three quarks (qqq), while mesons are combinations of quark anti-quark pairs.

The 1st generation particles: up, down and the electron, are the particles that make up all known matter. The electron-neutrino is involved in processes where matter is transformed, such as in nuclear β decay and muon decay.

---

[1] these have no relations to visible colors

In addition to the ordinary particles, every particle has an antiparticle with opposite electric charge. For instance, the electron has an antiparticle, the positron (e^+) and the up quark an antiparticle, anti-u ($\bar{u}$). The neutral bosons are their own antiparticles and the antiparticle of the W^- is the W^+, and vice-versa.

1.1.1   Standard Model formalism

As we know from classical mechanics, a Lagrangian, L, is a function that describes the dynamics of a system. Classically we have the

$$L = T(\dot{q}) - U(q) = \frac{1}{2}m\dot{q}^2 - U(q),$$

where T is the kinetic energy and U the potential energy term, while q is the four space-time coordinates. The equation of motions follows from the Euler Lagrange equations

$$\frac{\partial L}{\partial q} - \frac{d}{dt}\left(\frac{\partial L}{\partial \dot{q}}\right) = 0$$
$$\Longrightarrow F = \frac{dU}{dq} = ma,$$

which is the usual Newtons law. In a field theory one defines the Lagrangian density, $\mathscr{L}$, as a function of the fields, $\Phi(x_\alpha)$ and its gradient

$$\mathscr{L} = \mathscr{L}\left(\Phi(x_\alpha), \frac{\partial \Phi(x_\alpha)}{\partial x^\alpha}\right).$$

The integration over the three dimensional space leads to L

$$L = \int \pounds\left(\Phi, \partial_\alpha \Phi\right).$$

The Euler-Lagrange equations become

$$\frac{\partial \pounds}{\partial \Phi} - \partial_\alpha\left[\frac{\partial \pounds}{\partial\left(\partial_\alpha \Phi\right)}\right] = 0$$

and represent the corresponding Dirac equation solutions for the wave function. Observed conservation laws can be obtained by requiring this Lagrangian to be invariant under a set of global gauge transformations.

The Standard Model is based on the group $U(1)_Y \times SU(2)_L \times SU(3)_c$. For instance, the conservation of color charge are related to the gauge symmetry of the $SU(3)_c$ group. The electromagnetic

forces, related to the group $U(1)_Y$, and weak forces, à priori very different, have been unified by Glashow, Salam and Weinberg. One of the most important confirmation of the model, is, without doubt, the 1983 discovery in $p\bar{p}$ annihilations at the CERN $Sp\bar{p}S$ collider of the intermediate bosons $W^\pm$ and Z, propagators of weak interactions, at a mass of ~ 80 and $\sim 90\ GeV$, respectively.

The electromagnetic and weak interactions are unified within the frame of a gauge theory based on the group $U(1)_Y \times SU(2)_L$. The abelian group $U(1)_Y$ and the non-abelian $SU(2)_L$ are related to the hypercharge Y and to the weak isospin T, respectively. Hypercharge is again related to the electric charge Q and the weak charge T_3 (third component of weak isospin T) through:

$$Q = T_3 + \frac{Y}{2}.$$

The existence of transitions of type $\nu_e \to e$ and $\nu_\mu \to \mu$ in weak interactions and the occurrence in weak charged currents of fermions of only negative helicity states suggested the classification of fermion fields in weak isodoublets of negative helicity and in weak isosinglets of positive helicity. Therefore particles with negative helicity, left-handed (L)[2], are grouped in isospin doublets and particles with positive helicity, right-handed (R), in isospin singlets. For the electron and its neutrino, for example, we have

$$\begin{pmatrix} \nu_e \\ e_L^- \end{pmatrix} = \frac{1}{2}(1 - \gamma_5) \begin{pmatrix} \nu_e \\ e^- \end{pmatrix} \ ; \ e_R = \frac{1}{2}(1 + \gamma_5)e^-$$

The neutrino and the left-handed electron have weak charges $T_3 = +1/2$ and $-1/2$, respectively. The right-handed electron has no weak charge, and hence is not sensitive to weak interactions. The fact that the right-handed neutrino does not intervene in the theory means that either it does not exist or it is non-interacting. The three fermions generations of the standard model, known today, are recapitulated in table 1.1. The corresponding properties of the force particles are summarized in table 1.2.

1.2 The Higgs Mechanism

The gluons and the photon are massless, but all the other particles in the Standard Model are proved by experiments to have mass. Since the insertion of a mass term in the Standard Model Lagrangian

---

[2]A left-handed particle refers to a particle where the momentum (p) and the projection of the spin (S) are anti-parallel. For a right-handed fermion, p and S are parallel. Since an anti-fermion is a fermion "going backward in time", a left-handed fermion would be a right-handed anti-fermion.

Helicity	Generation			Q	T_3	Y
	1.	2.	3.			
L	$\begin{pmatrix} \nu_e \\ e^- \end{pmatrix}_L$	$\begin{pmatrix} \nu_\mu \\ \mu^- \end{pmatrix}_L$	$\begin{pmatrix} \nu_\tau \\ \tau^- \end{pmatrix}_L$	0 -1	$\frac{1}{2}$ $-\frac{1}{2}$	-1 -1
	$\begin{pmatrix} u \\ d' \end{pmatrix}_L$	$\begin{pmatrix} c \\ s' \end{pmatrix}_L$	$\begin{pmatrix} t \\ b' \end{pmatrix}_L$	$\frac{2}{3}$ $-\frac{1}{3}$	$\frac{1}{2}$ $-\frac{1}{2}$	$\frac{1}{3}$ $-\frac{1}{3}$
R	e_R	μ_R	τ_R	-1	0	-2
	u_R	c_R	t_R	$\frac{2}{3}$	0	$\frac{4}{3}$
	d_R	s_R	b_R	$-\frac{1}{3}$	0	$-\frac{2}{3}$

Table 1.1: *The three generations of fermions in the standard model. The left handed (L) particles are grouped in isospin doublets and the right handed ones (R) are isosinglets of isospin T. The quantum numbers Q, T_3 and Y are respectively the electric charge, the third component of isospin and the hypercharge.*

Force	particle	strength	mass [GeV]	Q [e]	spin
strong	8 gluons	1	0	0	
electromagnetic	photon (γ)	1/137	0	0	1
weak	$W^\pm, Z$	10^{-14}	80.4, 91.2	$\pm, 0$	

Table 1.2: *Force mediators in the Standard Model. The strength is relative to the strong force.*

will destroy gauge invariance, the Higgs mechanism is introduced. This mechanism gives mass to the fermions and the massive vector bosons without destroying gauge invariance, and rely on the concepts of Spontaneous Symmetry Breaking (SSB) [8]. The Higgs field is introduced and the particles acquire their mass by interacting with this field. The strength of the coupling to this field is related to the mass of the particle. To achieve mass we need the Higgs field to take on a non-zero vacuum expectation value (VEV). The quantization of this field gives rise to a new, not yet discovered, particle; the Higgs particle.

1.2.1   Spontaneous Symmetry Breaking (SSB)

To understand the concept of symmetry breaking we consider a system whose Lagrangian L reflects some kind of symmetry. For instance let L be spherically symmetric, which means that it would be invariant under rotation. If a given energy level of this system is non-degenerate, the corresponding energy eigenstate is unique and invariant under a rotation. On the other hand a given energy level may be degenerate and the energy eigenstate is not unique. I.e. there is no unique way to represent the ground state. If we arbitrarily choose one of these energy states as the ground state of our system, the system no longer shares the symmetries of L. This is known as spontaneous symmetry breaking (SSB).

1.2.2   The Goldstone Model

In field theory the lowest energy state is the vacuum state. If the vacuum state is non-unique, spontaneous symmetry breaking may occur. We therefore need some non-vanishing quantity in the vacuum. To get this we assume a scalar field

$$\phi(x) = \frac{1}{\sqrt{2}} \left[\phi_1(x) + i\phi_2(x) \right] \tag{1.2}$$

which has the following Lagrangian density

$$\mathscr{L} = \left[\partial^\mu \phi^*(x) \right] \left[\partial_\mu \phi(x) \right] - V(\phi(x)), \tag{1.3}$$

with the potential given by

$$V(\phi) = \mu^2 |\phi(x)|^2 + \lambda |\phi(x)|^4, \tag{1.4}$$

where μ^2 and λ are real parameters. We require that the potential is bounded from below (i.e. $\lambda > 0$) and that its minimum is non-unique and non-zero. From (1.4) it is clear that we have to chose $\mu^2 < 0$ to achieve this . The minimum of the potential is then given by

$$\phi(x) = \phi_0 = -\frac{\mu^2}{2\lambda}e^{i\theta} = ve^{i\theta} \tag{1.5}$$

We have now a continuous valley of minima in the $\phi_1 - \phi_2$ plane, which is reflected by the $e^{i\theta}$ factor in (1.5). By choosing $\theta = 0$ (we could of course have chosen whatever we wanted) we have chosen a specific ground state and thereby spontaneously broken the symmetry. By considering deviations from this minima, we choose a new basis for $\phi(x)$

$$\phi(x) = \frac{1}{\sqrt{2}}\left[v + \sigma(x) + i\eta(x)\right], \tag{1.6}$$

where $\sigma(x)$ and $\eta(x)$ are two real fields which measure the deviation from the ground state, v. Using this new basis for $\phi(x)$ in the Lagrangian in (1.3) we obtain two neutral scalar boson fields: $\sigma(x)$ and $\eta(x)$. The $\sigma(x)$ bosons become massive, while $\eta(x)$ remains massless. These massless bosons, known as Goldstone bosons, are not seen in nature. The Goldstone bosons often show up in cases with SSB of a global symmetry, but since they are not seen in nature we need to construct a theory with SSB without obtaining these unphysical states. This is done in the next section.

1.2.3   The Higgs Model

The purpose of the Higgs model is to give mass to the $W^{\pm}$ and Z bosons while keeping the photon massless, since this is what we have measured in experiments.

Since we have a method to get the wanted SSB, the remaining problem is to find a theory without getting the unwanted Goldstone bosons. We start with the same Lagrangian as in (1.3) but we now introduce a free field therm, $A_\mu(x)$, and replace the ordinary derivatives with the covariant derivative D_μ[3]. The Lagrangian density of the Higgs model is then given by

$$\mathscr{L} = [D^\mu\phi(x)]^* [D_\mu\phi(x)] - \mu^2|\phi(x)|^2 + \lambda|\phi(x)|^4 - \frac{1}{4}F_{\mu\nu}(x)F^{\mu\nu}(x), \tag{1.7}$$

where $F_{\mu\nu}$ is defined by

$$F_{\mu\nu} = \partial_\nu A_\mu(x) - \partial_\mu A_\nu(x).$$

---

[3]$D_\mu = \partial_\mu + iqA_\mu$

The potential is the same as in the Goldstone model, thus we get the same continuous valley of minima for $\lambda > 0$ and $\mu^2 < 0$. The free field $A_\mu(x)$ also has to vanish for the vacuum, to preserve Lorentz invariance. We then expand the field like in (1.6), except that we eliminate the $\eta(x)$ field by a $U(1)$ local gauge transformation. The Lagrangian then becomes

$$\mathscr{L}(x) = \frac{1}{2} \left[\partial^\mu \sigma(x) \right] \left[\partial_\mu \sigma(x) \right] - \frac{1}{2} (2\lambda v^2) \sigma^2(x) - \frac{1}{4} F_{\mu\nu}(x) F^{\mu\nu}(x)$$
$$+ \frac{1}{2} (qv)^2 A_\mu(x) A^\nu(x) + \text{i.t.,} \tag{1.8}$$

where i.t. denotes interaction terms of order three and higher. The mass terms are represented by the quadratic terms, and the $\sigma(x)$ field becomes a massive real scalar field with mass $m_\sigma = \sqrt{2\lambda v^2}$. The $A_\mu(x)$ field also becomes massive, with $m_A = |qv|$. The particle associated with the $\sigma(x)$ field is the Higgs boson. Which means that we have reached our goal: By starting with a Lagrangian density for a complex scalar field (in (1.2)) and a massless real vector field (A_μ, with two polarization degrees of freedom, ± 1) we have ended up with a Lagrangian density (1.8) for a real scalar field ($\sigma(x)$) and a massive real vector field. The field A_μ acquired a longitudinal polarization thanks to the "to be Goldstone bosons". Moreover we have not destroyed the gauge invariance of the Lagrangian density.

As already mentioned the $SU(2) \times U(1)$ symmetry in the Standard Model is broken and gives rise to the massive vector bosons. Our example above could easily be used to obtain this by introducing a $SU(2)$ weak isospin doublet with four degrees of freedom.

$$\Phi(x) = \left(\begin{array}{c} \phi_a(x) \\ \phi_b(x) \end{array} \right), \tag{1.9}$$

which couple to the vector fields through the Lagrangian in (1.7). In the SM the upper component ($\phi_a(x)$) is electrically charged while the lower ($\phi_b(x)$) is neutral. Since we want to keep the photon massless we are motivated to choose the charged component to be zero in our vacuum state, while the neutral component has the value v in the vacuum state. This gives

$$\Phi_0(x) = \left(\begin{array}{c} \phi_a^0(x) \\ \phi_b^0(x) \end{array} \right) = \frac{1}{\sqrt{2}} \left(\begin{array}{c} 0 \\ v \end{array} \right)$$

Again we parametrize the field in terms of deviations from the vacuum

$$\Phi_0(x) = \left(\begin{array}{c} \eta_1(x) + i\eta_2(x) \\ v + \sigma(x) + i\eta_3(x) \end{array} \right).$$

The $\eta(x)$ field in the unitary gauge can be eliminated by means of a transformation. The three degrees of freedom which we then loose are absorbed by the three vector bosons $W^{\pm}$ and Z, making them massive. The last degree of freedom goes into the Higgs boson.

So far we have only discussed how the massive vector bosons acquire their mass, but what about the fermions? Once the Higgs field is introduced, it is straight forward to add a new term to the SM Lagrangian which introduces couplings between fermions and the Higgs field, so called Yukawa couplings. The fermions then acquire mass by the interaction with the Higgs field. This way of giving mass to the fermions also preserve gauge invariance of the SM Lagrangian.

Chapter 2

Limitations of the Standard Model and the need of Supersymmetry

The Standard Model has been shown to describe to high accuracy all present results from precision measurements at high and low energies including the tests at the level of quantum corrections [16]. Nevertheless, in spite of its impressive success, the SM is not regarded as a final theory. It is rather considered as an effective theory, which works well up to the weak energy scale. The presence of many unexplained parameters may be regarded as one of the SM's limitations. Another limitation, and probably most indispensable, is that the SM does not accommodate gravity.

During the last 30 years theorists have worked fruitfully on constructing theoretically models which could give explanations to the experimentally determined values of the SM parameters and conform quantum physics with gravity. For an experimental researcher it is important that such new theories also predict departures from the SM. One such implications, which is one of the key subjects of the ATLAS experimental program [5], is the prospect for the supersymmetry (SUSY) to be a true symmetry of nature and, as a consequence, the existence of supersymmetric particles.

2.1   Problem 1: Dark Matter

The cosmological data provide good reasons for the new improved theory of particle physics which would be able to accommodate explanation for some of the experimentally estimated features of the universe. During the last years very precise measurements of the Cosmic Microwave Background

(CMB) radiation[1] from especially WMAP have shown that the visible matter (baryonic matter) is not enough to explain the measured properties of the CMB. To be able to explain this disagreement a presence of a significant amount of non-baryonic matter is required. It is believed that 72% of the remaining density comes from dark energy and 23% from dark matter [9]. Dark matter is in some theories assumed to be a stable massive particle which has almost no interaction with ordinary matter, that is does not carry color or charge (often called WIMP - Weakly Interacting Massive Particle). The Standard Model does not provide any candidate for such a particle, except for the neutrinos, but they are too light and have only a very tiny contribution to the total mass density.

2.1.1 Solution

What we need as a Dark Matter candidate is a weakly interacting massive particle (WIMP). If the lightest supersymmetric particle (LSP) is prohibited to decay into SM particles it will be stable, since the other SUSY particles are not kinematically accessible to it. In the early universe the energy was high enough to create the lightest supersymmetric particles. Eventually the universe got cold and started to expanded very fast so the LSPs stopped being created or annihilated. If a gas of these LSPs still fills the whole space, it could be what accounts for the Dark Matter. The WIMPS are extremely hard to detect, because they hardly interact with ordinary matter, and there are several ongoing experiments trying to detect them. Up to now, without any evidence for their existence.

2.2 Problem 2: Hierarchy problem

In the Standard Model the quantum corrections to the Higgs mass coming from loops containing fermions (figure 2.2 (1)) are quadratically divergent in the cut-off scale, Λ, [12]:

(1)   **(2)**
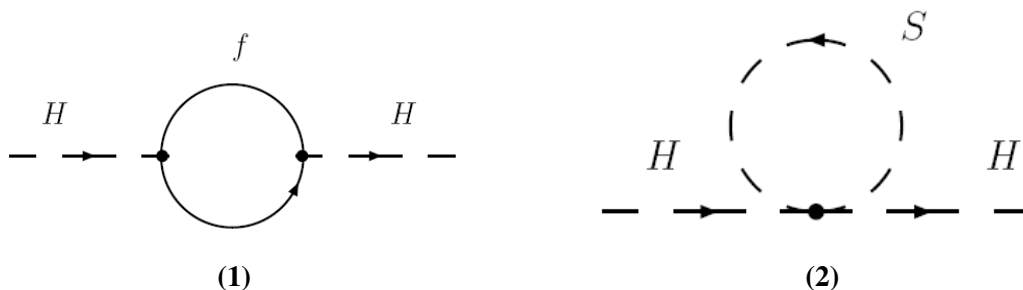
Figure 2.1: *Loop corrections to the Higgs mass from fermion loops (1) and scalar loops (2).*

---

[1]radiation left over from $\sim$ 380.000 years after the Big Bang

$$\Delta m_{H,f}^2 = \frac{\lambda_f^2}{8\pi^2} \left[-\Lambda^2 + 6m_f^2 \ln\left(\frac{\Lambda}{m_f} + \cdots \right) \right], \tag{2.1}$$

where λ_f is the Yukawa coupling strength between fermions and the Higgs boson. The Λ is often chosen to be of the order of the Planck scale ($M_P \approx 10^{19}$GeV). It can be interpreted as the energy scale where the SM is no longer valid and gravity can no longer be neglected. The quadratic divergences destabilize mass, and there is nothing in the SM which could remove them unless there are some delicate cancellations due to the presence of new particles. Therefore one has to assume that there is some fine tuning between the fundamental values and their corrections. However if such new particles exist their masses should be above the electroweak energy scale, but below 1TeV in order to not re-introduce the same divergent corrections.

2.2.1   Solution

The concept of supersymmetry is to relate every Standard Model particle with a super partner whose spin differs by $|\Delta S| = 1/2$. Fermions have scalar super partners while gauge and Higgs bosons have fermionic super partners. For instance, the electron will have a supersymmetric partner with spin 0 (a scalar). This leads, of course, to a doubling of the number of particles, albeit in a very orderly fashion (see the whole list presented in section 2.4). These new scalar particles also couple to the Higgs and thereby contribute to the Higgs mass corrections through loops as in figure 2.2 (2). We do the same as in the Standard Model, and calculate the corrections from these loops. This gives [12]

$$\Delta m_{H,S}^2 = \frac{\lambda_s}{16\pi^2} \left[\Lambda^2 - 2m_s^2 \ln\left(\frac{\Lambda}{m_s} \right) \right]. \tag{2.2}$$

If the relationship between the coupling strength in the loops (1) and (2) in figure 2.2 are $\lambda_f^2 = 2\lambda_s$, which in fact is exactly what supersymmetry predicts, we can combine the two contributions to the corrections of the Higgs mass from (2.1) and (2.2) to get the total correction

$$\Delta m_{H,tot}^2 \simeq \frac{\lambda_f^2}{4\pi^2} \left(m_S^2 - m_f^2 \right) \ln\left(\frac{\Lambda}{m_s} \right).$$

The quadratic divergence cancelled, and we are only left with the logarithmic divergence. This means that the fine tuning problem is solved by introducing a set of new particles which are partners to the SM particles.
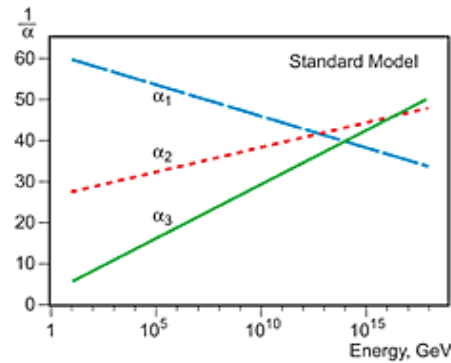
Figure 2.2: *The evolution of the coupling constants according to the SM*

2.3   Problem 3: Unification

The three coupling constants for the three forces in the Standard Model, α_1, α_2 and α_3 are known to very high precision at the weak scale and can be extrapolated to higher energies by using the Renormalization Group Equations (RGE)[2], whose coefficients depend on the nature and number of particles that are contributing to the loop corrections. Figure 2.2 shows the evolution of the inverse of the coupling constants in the Standard Model. As already mentioned the Standard Model has been able to merge electromagnetism and the weak nuclear force into the electroweak theory. This motivates to also be able to unite the electroweak and the strong force at some higher energy scale [10]. This unification of forces is a powerful principle of progress in physics, and the main goal is to construct a theory where all forces could be merged into a *theory of everything*.

If the three forces where the same force in the early universe, one would expect that the evolution of the three force constants would meet at a certain energy level, corresponding to the energy of the early universe. This is almost the case in the Standard Model but not quite, as illustrated in figure 2.2.

2.3.1   Solution

By introducing a new set of heavy supersymmetric particles at a higher energy level (TeV[3] range) the evolution of the coupling constants become altered. At this scale the RGEs have to take into account

---

[2]RGE are a mathematical tool that allows one to investigate the changes of a physical system as one views it at different scales. In particle physics it reflects the scale dependence of the parameters of the theory (e.g the coupling constants, masses,...)[11]

[3]10^3 GeV = 1 TeV
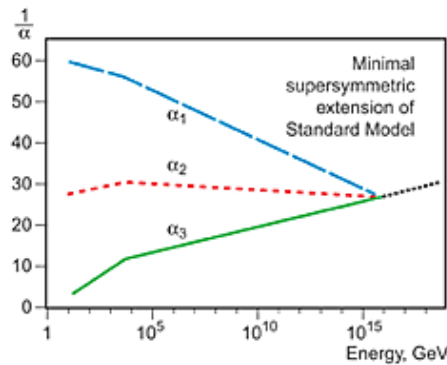
Figure 2.3: *The evolution of the coupling constants with a supersymmetric theory at the TeV scale*

loop contributions from several new particles. Figure 2.3 illustrate how the evolution of the inverse of the coupling constants are affected by the introduction of these new particles. From a certain energy scale (TeV) these new particles contribute to the loop corrections and change the slopes of the three lines so that they meet in a common point. At this point some Grand Unified Theory (GUT) should be valid, and make the three lines continuing as one line.

2.4 Supersymmetry (SUSY)

The last sections illustrate the limitations to the SM which suggest an extension to it. There is a number of theoretical models which could be such an extension [11]. Most of these models suggest supersymmetry (SUSY), that postulates symmetry between fermions and bosons, that is, for every particle there is a super partner whose spin differs by $1/2$. Since the super partners of the SM particles have not yet been observed[4], supersymmetry, if it exist, must be a broken symmetry. This allows the super partners to be much heavier[5], than their SM partner. This is actually what is needed to solve the hierarchy problem mentioned in 2.2. On the other hand the super partners have an upper limit of about 1TeV, to not reintroduce the hierarchy problem.

The structure of the interactions in the supersymmetric models is fully defined by the same gauge invariance and the same coupling constants as in the SM. This puts hard constraints on the super symmetry which should be in accordance with the existent experimental results, like for example the measurements of the anomalous magnetic moment of the muon, rates for the flavor changing neutral

---

[4]as of 1. June 2008

[5]except maybe the super partners of the top quark

current processes (ex. $b \rightarrow s\gamma$) etc. [11]. To further prevent supersymmetry from violating baryon and lepton number conservation, on which there are strong experimental limits, R-parity should be conserved. R-parity is defined as

$$R = (-1)^{3(B-L)+2s},\qquad(2.3)$$

where s is the particle spin, B is the baryon number and L the lepton number[6]. According to (2.3) the Standard Model particles will have R-parity $+1$ while the supersymmetric particles will have R-parity -1. In many of the Supersymmetric models[7] R-parity is conserved. This implies that supersymmetric particles have to be produced in pairs as well as that the Lightest Supersymmetric Particle (LSP) is stable, exactly what is needed for a Dark Matter candidate.

2.4.1   The Minimal Supersymmetric Standard Model (MSSM)

The Minimal Supersymmetric Standard Model (MSSM) is the minimal extension to the Standard Model that realizes supersymmetry. In the MSSM every matter SM particle, is related to a supersymmetric partner, which has exactly the same quantum numbers except that they differ $1/2$ in spin. In the supersymmetry algebra the SM particles and their super partners form super multiplets. A SM fermion with one right- and one left-handed component are accompanied by two scalars, associated to each of the SM components, to form a super multiplet. For example, the up-quark has a supersymmetric spin-0 partner, **s**up[8], the down-quark has a partner called **s**down etc. These supersymmetric partners exist for both the left and the right handed component of the SM fermion. Although they are spin-0 particles, they are usually referred to with the right and left handed notations in the MSSM reflecting the handedness of their fermionic partners. In contrast with the SM the left and right handed super partners are two different particles with different masses, while in the SM the handedness only refers to two components of one particle presentation. In some cases, left- and right-handed **s**fermions mix ($\widetilde{\tau}, \widetilde{t}, \widetilde{b}$, see table 2.1).

The MSSM also requires the existence of at least two Higgs doublets H_d and H_u. Higgs bosons are defined as complex spin-0 fields and also reside in super multiplets with their fermionic super partners called *higgsinos*.

The super partners for the SM gauge bosons are spin-$1/2$ supersymmetric fermions. Unlike the

---

[6](anti)quarks have $B = (-1/3)1/3$ and $L = 0$ while (anti)leptons have $B = 0$ and $L = (-1)1$

[7]in all models studied in this analysis R-parity is conserved

[8]the **s** stands for *scalar*

GROUP	GENERATION		
	1st	2nd	3rd
sleptons	selectron $\widetilde{e}_L,\widetilde{e}_R$	smuon $\widetilde{\mu}_L,\widetilde{\mu}_R$	stau $\widetilde{\tau}_1,\widetilde{\tau}_2$
	sneutrino $\widetilde{\nu}_e$	sneutrino $\widetilde{\nu}_\mu$	sneutrino $\widetilde{\nu}_\tau$
squarks	sup $\widetilde{u}_L,\widetilde{u}_R$	scharm $\widetilde{c}_L, \widetilde{c}_R$	stop $\widetilde{t}_1, \widetilde{t}_2$
	sdown $\widetilde{d}_L, \widetilde{d}_R$	s-strange $\widetilde{s}_L, \widetilde{s}_R$	sbottom $\widetilde{b}_1,\widetilde{b}_2$
Higgs bosons	$h^0,H^0,H^\pm,A^0$		

Table 2.1: *The spin-0 sparticles, scalars, in the MSSM.*

usual SM fermions, the left and right handed components of these supersymmetric fermions have the same gauge transformation properties, which means they have the same properties [12]. The super multiplets which is used to describe the SM vector bosons and their super partners are called gauge or vector super multiplets, and the super partners are called *gauginos*. The $W^\pm$ and B vector bosons, thus, have a super partner called the *Wino* and *Bino*, respectively, while the super partners for the gluons are *gluinos*.

All the new scalar particles in the MSSM are listed in table 2.1. After electroweak symmetry breaking, W^0 and B mix to give Z and γ. The corresponding mixtures of their super partners $\widetilde{W}$ and $\widetilde{B}$ are called *Zino* ($\widetilde{Z}$) and *photino* ($\widetilde{\gamma}$). Moreover the neutral *bosonic* super partners $\widetilde{B}$ and $\widetilde{W}$ mix with the neutral *higgsinos*, $\widetilde{H}_d^0$ and $\widetilde{H}_u^0$ into four mass eigenstates, the *neutralinos* ($\widetilde{\chi}_{1,2,3,4}^0$). Whereas the charged *gauginos* $\widetilde{W}^\pm$ mix with charged *higgsinos* $\widetilde{H}^\pm$ to give two charged mass eigenstates, the *charginos* ($\widetilde{\chi}_{1,2}^\pm$). An overview of these particles are shown in table 2.2

In the MSSM the interactions of supersymmetric particles are obtained from the SM ones by replacing any two lines in a vertex by their super partners. To illustrate the MSSM couplings it is useful to use the convention for the MSSM fields according to which matter super multiplets consist of the fields (ψ,ϕ), where ψ stands for fermion and ϕ stands for the complex scalar. The same goes for the gauge super multiplets which consist of the fields (A, λ) where A being the gauge boson and λ

NAME	Bino	Wino	Higgsino	Wino (ch.)	Higgsino (ch.)
NOTATION	$\widetilde{B}$	$\widetilde{W}^0$	$\widetilde{H}_u^0,\widetilde{H}_d^0$	$\widetilde{W}^{\pm}$	$\widetilde{H}_u^+,\widetilde{H}_u^-$
MIX TO	$\widetilde{\chi}_1^0,\widetilde{\chi}_2^0,\widetilde{\chi}_3^0,\widetilde{\chi}_4^0$			$\widetilde{\chi}_1^{\pm},\widetilde{\chi}_2^{\pm}$	

and those who do not mix:

NAME	Gluino	Gravitino
NOTATION	$\widetilde{g}$	$\widetilde{G}$

Table 2.2: *The spin $1/2$ sparticles, fermions, in the MSSM*

the gaugino. Thus the SM gauge couplings, between a boson and a fermion pair, which can be written as $(A\psi\psi)$, is complemented by the couplings $(A\phi\phi)$ and $(\lambda\phi\psi)$. For example, the gluon-gluon-quark (ggq) coupling will be accompanied with the gluon-**s**quark-**s**quark, glu**ino**-**s**quark-quark couplings with the same coupling constant. The couplings between vector bosons and gauginos are obtained in a similar manner.

The MSSM Higgs sector

In the Standard Model we had one left handed scalar doublet, as in (1.9). This doublet is promoted to a doublet of left-chiral super fields in the MSSM

$$\Phi(x) = \begin{pmatrix} \phi_a(x) \\ \phi_b(x) \end{pmatrix} \rightarrow \hat{H}_u = \begin{pmatrix} \hat{h}_u^+ \\ \hat{h}_u^0 \end{pmatrix}.$$

This doublet carries weak hyper charge $Y = 1$, and can give mass to the up-type fermions. In the Standard Model the right-chiral charge conjugate of the Higgs field Φ^C carries weak hyper charge $Y = -1$ and can give mass to the down type fermions. By definition, a right-chiral super field is not allowed in the Supersymmetric Lagrangian [11]. Therefore one is forced to introduce another left-chiral scalar doublet super field

$$\hat{H}_d = \begin{pmatrix} \hat{h}_d^- \\ \hat{h}_d^0 \end{pmatrix}$$

which carries weak hyper charge $Y = -1$. This doublet can then give mass to the down type fermions. We can set up a potential

$$V_{Higgs} = (|\mu|^2 + m^2_{H_u})(|h^0_u|^2 + |h^+_u|^2) + (|\mu|^2 + m^2_{H_d})(|h^0_d|^2 + |h^-_d|^2)$$

$$+ [B\mu(h^+_u h^+_d - h^0_u h^0_d) + c.c.]$$

$$+ \frac{1}{8}(g^2 + g'^2)(|h^0_u|^2 + |h^+_u|^2 - |h^0_d|^2 - |h^-_d|^2)^2 + \frac{1}{2}g^2|h^+_u h^{0*} + h^0_u h^{-*}_d|^2.$$

Minimizing this potential, exactly as we did in the Standard Model, gives us two conditions necessary for spontaneous breaking of electroweak symmetry

$$B = \frac{\left(m^2_{H_u} + m^2_{H_d} + 2\mu^2\right)\sin 2\beta}{2\mu}$$

$$\mu^2 = \frac{m^2_{H_d} - m^2_{H_u}\tan^2\beta}{(\tan^2\beta - 1)} - \frac{M^2_Z}{2}. \tag{2.4}$$

In-stead of choosing B as a fundamental parameter describing the symmetry breaking we choose $\tan\beta$, which is defined as the ratio of the vacuum expectation values, v_u and v_d, of the up and down-part of the Higgs field respectively.

$$\tan\beta \equiv \frac{v_u}{v_d}. \tag{2.5}$$

The Higgs Bosons

In the Standard Model, with just one complex Higgs doublet, three of the four degrees of freedom (d.o.f.) gave mass to the three vector bosons, the $W^\pm$ and Z. The last d.o.f. gave rise to the Higgs boson. However, since we now have introduced two Higgs doublets, we get eight d.o.f.. Therefore, in addition to give mass to the $W^\pm$ and Z bosons, three neutral spin zero bosons and a pair of charged scalars are created:

$$h^0 \quad \text{lightest Higgs}$$
$$H^0 \quad \text{heavy CP-even Higgs}$$
$$A^0 \quad \text{heavy CP-odd Higgs}$$
$$H^\pm \quad \text{charged Higgs.}$$

The masses of the different Higgs bosons are given by

$$m^2_{H^\pm} = B\mu\left(\cot\beta + \tan\beta\right) + M^2_W$$

$$m^2_{A^0} = B\mu\left(\cot\beta + \tan\beta\right)$$

$$m^2_{h,H} = \frac{1}{2} + \left[\left(m^2_A + M^2_Z\right) \mp \sqrt{\left(m^2_A + m^2_Z\right)^2 - 4m^2_A M^2_Z \cos^2 2\beta}\right].$$

This states that the $H^\pm$ is heavier than the A, and that the lightest Higgs is h. The mass of the h is less than 135 GeV [11]. We see further that once we know the mass of the A and $\tan\beta$ we can calculate all the other parameters in the Higgs sector except for the sign of μ^2. This means that choosing/measuring the value of $\tan\beta$ and m_A, we can obtain the whole Higgs mass spectrum.

2.4.2   mSUGRA

As already mentioned none of the Supersymmetric particles have been detected in any experiment, therefore they need to be heavier than the Standard Model particles. This means that Supersymmetry can not be an exact symmetry which leads us to the concept of soft supersymmetry breaking. This breaking has to be done with care (therefor the term *soft*), to not make the supersymmetric particles too heavy and thereby ruin the cancellation of the corrections to the Higgs mass, section 2.2. One way of describing this breaking are with the mSUGRA model.

In its general form the soft SUSY breaking of the MSSM introduces a large number of free parameters. This could eventually lead to large flavor changing neutral currents or CP violation [12], for which there are strong experimental constraints. To avoid this, a mass universality is assumed in mSUGRA. This means that at the grand unification (GUT) scale there exist one common scalar mass, m_0 and one common gaugino mass, $m_{1/2}$. In addition there is also a common value for the trilinear Higgs-sfermion-sfermion coupling, A_0. Together with the two parameters from the Higgs sector ($\tan\beta$ and μ), this will leave the theory with five free parameters at the GUT scale

$$m_0\,,m_{1/2}\,,A_0\,,\tan\beta\,,sign(\mu), \tag{2.6}$$

where $\tan\beta$ is defined in (2.5) and μ defined in (2.4). Like the coupling constants in the Standard Model, these fundamental parameters evolve with energy through the Renormalization Group Equations (RGE). The m_0 and $m_{1/2}$ parameters split at lower energies, giving rise to all the different fermion sparticle mass-states that we expect at the TeV range. An example, given one set of the fundamental parameters, of the running of the RGE from the GUT scale is showed in figure 2.4. How much the evolution is affected is dependent on the gauge coupling strengths, which give a positive contribution to the mass, and the Yukawa couplings which gives a negative contribution. For instance will the particles having strong interaction and very small Yukawa couplings, i.e. the 1st and 2nd generations squarks, be heavier than for instance the selectron which have only weak interaction, and also negligible Yukawa coupling [11]. The third generations fermions have stronger Yukawa couplings,

Figure 2.4: *The evolution of the M_0, $M_{1/2}$ and the Higgs mass parameters as a function of energy, from [4]*

and will be lighter than the other two generations. We see this in figure 2.4. It is interesting to see that, because of the very large top Yukawa coupling, the up-field of the Higgs doublets are very much altered when we go to lower energies. In fact the H_u component becomes negative. We remember from the Higgs potential in the Standard Model in 1.4 that we just choose the μ to be negative, without any physical justification, to get a degenerate non-zero vacuum expectation value. In the MSSM however we can choose this value to be positive at the GUT scale, and, because of the heavy top-quark, it will be negative just above the weak scale. This explains the whole electroweak symmetry breaking of the Standard Model. At the same time it is important that this does not happen with the other sparticles, because we then would get color- or charge-breaking minima. [11]

After having presented an alternative to the current SM of particle physics, it is time to mention a tool to test such a supersymmetric theory: the ATLAS experiment soon starts to take data at the Large

Hadron Collider (LHC), a collider allowing to break through the TeV scale!

Chapter 3

The ATLAS detector

3.1 The Large Hadron Collider

The Large Hadron Collider (LHC) at CERN is a circular particle accelerator build to collide protons against protons, with a center of mass energy of 14 TeV. The ring is located at the French/Swiss border 100 meters under ground. It has a circumference of nearly 27 km. The current plan is that the experimental activities will start from summer 2008.

To accelerate the protons up to a speed close the speed of light one needs various different accelerators. Therefore there is a complex system of accelerators at CERN (see figure 3.3), containing many smaller sub-accelerators. When the protons are entering the LHC ring, they have already acquired an energy of about 450 GeV from the other accelerators. In the LHC the protons are accelerated to a final energy of 7 TeV. This is achieved using strong electric fields. To keep the protons in a circular orbit superconducting magnets are used, which are cooled down to 1.9 K to provide an eight Tesla magnetic field.

In the LHC the protons are divided into bunches which are compressed as small as possible with use of quadrupole and sextupole magnets. Every proton bunch consists of 10^{11} protons and every beam has 2835 of these bunches. The bunches are separated by 7.5 m (25 ns) and they use approximately 100μs on each lap. To be able to compress these bunches as much as possible is mandatory to acquire high luminosity[1]. The design luminosity of LHC is $10^{34}cm^{-2}s^{-1}$, but it will take some years of running before this is achieved. Until then the LHC will run with a luminosity a factor of ten smaller.

---

[1]Luminosity: the number of particles per cm^2 per second in a beam
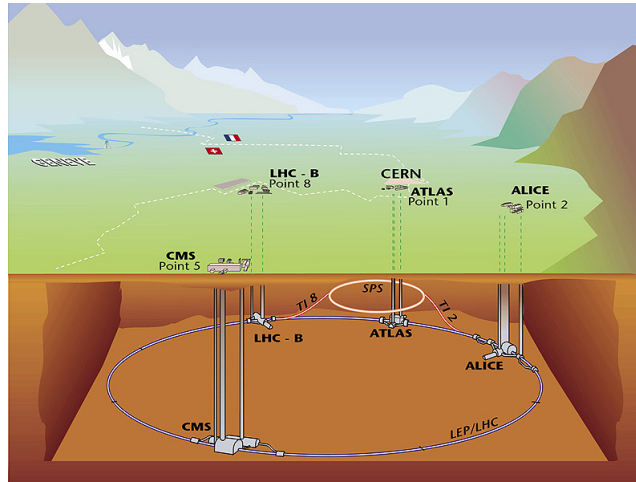
Figure 3.1: *The accelerator system at CERN, together with the location of the main LHC detectors.*

The two proton beams will collide at four different points, where the beam pipes cross. At each of the collision points a complex detector will measure the particles that are produced in every collision. A new collision will take place every 25 ns.

There are in total six detectors placed at the various intersection points; ALICE, LHC-B, TOTEM, CMS, LHC-f and ATLAS. ALICE is a heavy-ion experiment which also would investigate lead-lead collisions to study quark-gluon plasma. LHC-B is specialized in B-physics to shed light on matter-antimatter in the universe. TOTEM will measure total cross section, elastic scattering and diffraction processes and shares interaction point with CMS. The LHC-f (forward) will look at the particles produced in the forward region of the collisions and shares interaction point with ATLAS. CMS and ATLAS are multipurpose detectors and are the most relevant instrument when searching for new physics beyond the Standard Model.

3.1.1   Nomenclature

The coordinate system used in the detector (figure 3.2) is defined such that z axis is in the beam direction, the x axis is transverse to the beam, pointing toward the center of the ring, while the y axis is pointing upward. The azimuthal angle, ϕ, is measured around the beam axis and the polar angle, θ, is the angle with respect to the beam axis. We introduce also a quantity called pseudo rapidity, η,

defined as

$$\eta = -\ln\left[\tan\left(\frac{\theta}{2}\right)\right].$$ (3.1)

This quantity is convenient to use because the particle production in the detector is nearly constant as a function of pseudo rapidity [5]. In fact the pixel elements in the inner detector consist of independent elements with roughly the same area in the (η, ϕ) space. The distance in the (η, ϕ) space is defined as

$$\Delta R = \sqrt{(\Delta\eta)^2 + (\Delta\phi)^2}.$$ (3.2)

To describe a particle trajectory in the detector we use that $\tan\theta = p_T/p_z$ and $\tan\phi = p_y/p_x$, where p_T is the transverse momentum (component of the momenta $\mathbf{p}$ transverse to the z direction) and p_z is the longitudinal component (the component of $\mathbf{p}$ parallel to the z direction). Further p_x and p_y are the components of $\mathbf{p}$ in the x and y direction respectively.

(1) Side view   (2)   Front view   (3) Beamline
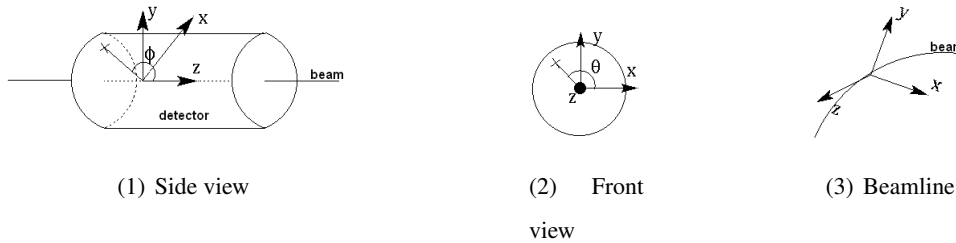
Figure 3.2: *The coordinate system used in the detectors at LHC.*

3.2 The ATLAS detector

ATLAS (figure 3.3) is an abbreviation for A Toroidal LHC ApparatuS and is the largest of the six detectors at the LHC, with its length of 45 m and height of 22 m. It will be used for Standard Model tests, Higgs searches and supersymmetry and other new physics searches. The detector is like an onion with different layers of sub-detectors outside of each other. The three main parts of the detector are The Inner Detector (ID), the Electromagnetic and Hadronic Calorimeters, the Muon Chambers and the Magnet System. These detector parts are again divided into smaller, more specified, sub-detectors. Since the particles produced in the collision will spread in all direction it is important to have a detector which is as closed as possible. Therefore one has, in addition to the central barrel around the collision point, also so called end-caps in the forward and backward directions ($\pm z$-direction), which will measure particles at as high pseudo-rapidity as possible.
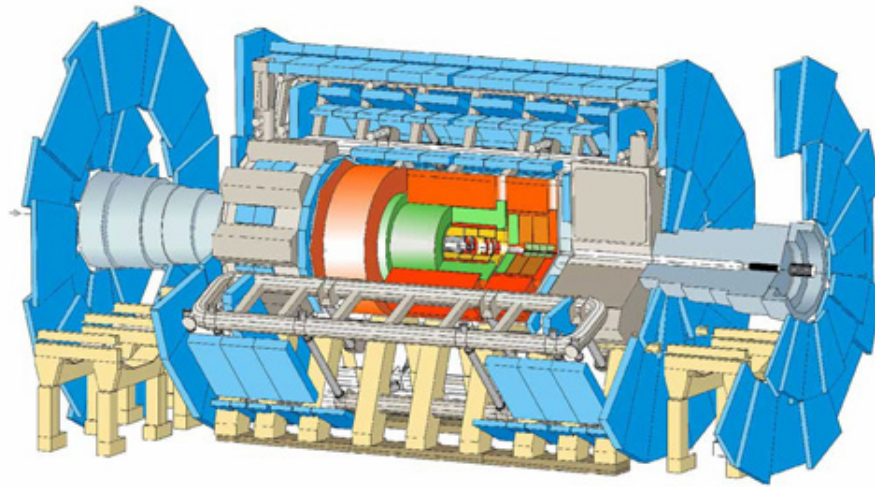
Figure 3.3: *The ATLAS detector*

3.2.1   The Magnet system

The ATLAS detector uses two large magnetic systems to bend charged particles so that the momenta can be measured. The two magnetic systems are:

1. **The inner solenoid**: It produces a homogeneous magnetic field surrounding the Inner detector. Since the field is nearly uniform in both direction and strength the momentum measurements could be done very precisely.

2. **The outer toroidal**: ATLAS has eight very large superconducting magnets in the barrel and two in the end-caps. These are situated outside the calorimeters and provide a magnetic field for the muon system. This magnetic field is not uniform so the momentum measurements are less precise than in the inner detector.

3.2.2   Inner detector

The Inner Detector (ID), sketched in figure 3.4, starts a few centimeters from the beam pipe and extends to a radius of 1.15 m. It is 7 m long and centered at the collision point. The basic functions of the detector are pattern recognition, momentum and vertex measurements and charged particle identification [5]. The vertex measurement is particularly important because good vertex resolution is crucial for identifying b-jets, which are important in B-physics as well as Higgs and Supersymmetry
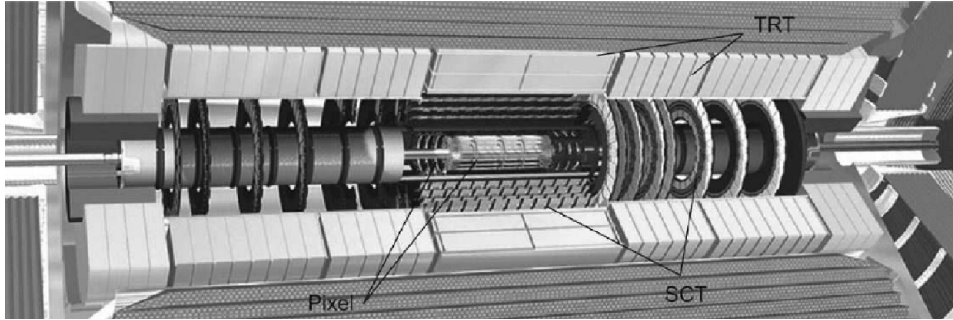
Figure 3.4: The Inner Detector of ATLAS

searches. The momentum measurement in the ID is very precisely with a resolution of $\sigma_{p_T}/p_T = 0.05\% p_T \otimes 1\%$ [1] due to the strong and uniform magnetic field provided by the inner solenoid. The Universities in Bergen and Oslo have been involved in the construction, testing and software developing for one of the ID sub detectors, the Semi Conductor Tracking Detector (SCT). I have also been working with this detector during my stay at CERN, to be summarized in 3.3.3. In addition to the SCT the ID consists of two more sub detectors: the Pixel and Transition Radiation Tracker (TRT).

1. **Pixel** is the inner component of the ID, and contains 1744 modules distributed in the barrel an end-caps. Each module is 2×6 cm and consist of 47.000 pixels each. Each pixel is very small and therefore one can do extremely precise tracking very close to the collision point. The accuracy of the pixels is around $10\mu m$ in $r - \phi$ and $115\mu m$ in z. The innermost pixel layer is called the b-layer, and is located at a radius of 5 cm.

2. **SemiConductor Tracking (SCT)** is the middle component of the inner detector. It has more or less the same concept and function as the Pixel but is made of long, narrow strips and covers a larger area than the Pixel. Because of this large area, SCT is the most critical part of the inner detector when it comes to basic tracking. The SCT is described in more detail in section 3.3.

3. **Transition Radiation Tracker** is the outer detector of the ID. It is a combination of a straw tracker and a transition radiation detector. It contains many very small straws, four millimeters in diameter and 144 cm long. This design makes the resolution worse but that is unavoidable in order to be able to cover a bigger volume and to have a complementary design in comparison with the Pixel and SCT. The detector also consists of materials of very different refractive indices, and uses the phenomena of transition radiation to detect, especially, the lightest charged

particles, i.e electrons.

The tracks reconstructed in the ID are very important for b-tagging. On average a track would consist of three pixel hits, four $3D$ points in the the SCT and about 36 hits in the TRT.

3.2.3 Calorimeters

The Calorimeters are situated outside the solenoidal magnet that surrounds The Inner Detector. Their purpose are to measure the energy from particles when they are absorbed by the material in the detector. The Calorimeters are placed outside the solenoidal magnets. There are two calorimeter systems in ATLAS, an inner electromagnetic calorimeter and an outer hadronic calorimeter. They use the same principle in measuring the energy deposition of a particle going through the high-density materials of the detector. By measuring the shape of the resulting particle shower one can find the initial energy of the particle. The purpose of the two calorimeters are

- **Electromagnetic Calorimeter** absorbs energy from particles that interact electromagnetic (i.e charged particles and photons). It has high precision in both the amount of energy absorbed and the location of the energy deposited. The energy resolution for the electromagnetic calorimeter is $10\%/\sqrt{E} \otimes 0.7\%$ [1].

- **Hadronic Calorimeter** absorbs energy from particles that interact via the strong force (i.e mostly hadrons). This calorimeter is less precise than the electromagnetic with an energy resolution of $50\%/\sqrt{E} \otimes 3\%$ for barrel and end-cap [1].

3.2.4 The Muon Spectrometer

The Muon Spectrometer forms the outer part of ATLAS and is designed to detect charged particles exiting the end-cap and barrel calorimeters and to measure their momentum in the pseudo rapidity range $|\eta| < 2.7$ [1].

The different chambers in the barrel of the muon spectrometer are arranged in three cylindrical shells around the beam axis at radii of approximately 5 m, 7.5 m and 10 m. In the end-cap regions the muons spectrometer form large wheels, perpendicular to the z axis at distances of $|z| \approx 7.4$ m, 10.8 m, 14 m and 21.5 m from the interaction point.

3.3   The Semi Conductor Tracking Detector (SCT)

The SCT consists of one central barrel and two end-caps. The barrel is made up of 2112 modules distributed on four concentric barrels so that four space points per track can be reconstructed. The end-cap sections on each side of the barrel has in total 1976 modules mounted on 18 disks (9 on each side) [7].

The modules are made of single-sided micro-strip detectors glued back-to-back with a displacement of 40 mrad with respect to each other (in some parts of the SCT there are four strip detectors making up one module). This allows two dimensional position information for each hit. The strips in the detectors are $80\mu m$ apart in the barrel and between 55 and $95\mu m$ in the end-cap. This gives a resolution of the position measurement of $16\mu m$ in $R\phi$ and $580\mu m$ in z/R for barrel/end-cap [7]. The whole SCT will cover a range up to $\eta = 2.5$. One end-cap module is shown in figure 3.5 In total the

Figure 3.5: *A SCT end-cap module*

SCT has 63m^2 with silicon micro-strip sensors distributed $40\%/60\%$ among the two end-caps and the central barrel [7]. To operate the SCT modules one needs several power lines. One bias voltage for sensor operation and several low voltages (LV) for readout and conversion from electronic to optical signal. Because of the high radiation damage (due to the position close to the beam pipe) and large heat dissipation the modules need to be cooled down to the operating temperature of -7^oC [7].

3.3.1   SCT Detector Control System (DCS)

To ensure and control that the detector runs under safe conditions a system monitors the detector and its components. The SCT Detector Control System (DCS) will also provide the detector with power and cooling. It should also protect against failure and error conditions. The DCS is divided into two subsystems, the power-supply system (PS) and the environmental monitoring and interlock system.

Power-supply system

The largest subsystem is the power-supply system, and provides all voltages and control signals needed to operate an SCT module. Each module is powered by an independent power-supply. There are both low voltage (LV) and high voltage (HV) supplies. The LV supplies provide all voltages needed by the Detector Module ASIC's (Application Specific Integrated Circuit), the associated opto electronics[2], temperature monitoring, module reset and clock select signals [15]. The HV provides the bias voltage. The LV and HV cards are installed in power-supply (PS) crates, covering 48 modules in one crate. Each crate consists of 12 LV cards, with four channels each and six HV cards with corresponding eight channels each. These crates are served by a common crate controller, crate PS and crate controller software. Figure 3.6 shows a schematic view of a power-supply crate. In addition
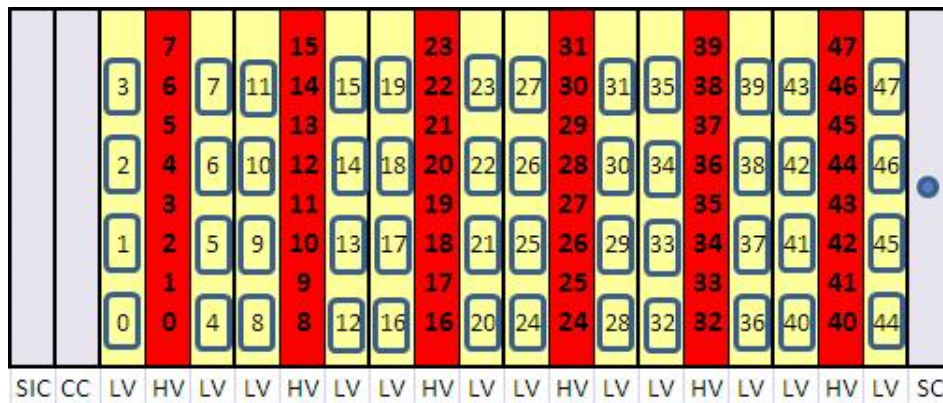
Figure 3.6: *The power-supply crate for the SCT.*

to power, each module is also provided with several other connections in order to be able to read-out signals and to tune and control the power-supply. In total each module has 16 power-supply and corresponding readout values. Figure 3.7 summarize all the readout values and their trip limits.

The environmental DCS and interlock system

The environmental DCS and interlock system consists of four readout quantities:

1. the temperature of the carbon fiber structure of the detector

2. the temperature of the air inside the detector volume

---

[2]electronic devices that interact with light

Param.	Typical	Hard. Trip	Firmware	CC
V_{bias}	150V	500	set value	10 V [1]
V_{cc}	3.5V	10V	-	-
V_{ccPS}	3.6V	10V	-	-
V_{dd}	4.0V	10V	-	-
V_{ddPS}	4.4V	10V	-	-
V_{VCSL}	1.6V - 6.6V	9.6V	-	-
V_{PIN}	5-10V	13 V	-	-
I_{bias}	$0.3\mu A$	5mA	$5\mu A$	$3\mu A$
I_{cc}	900mA	1300mA	-	-
V_{ccRET}	0.08V	10V	-	-
I_{dd}	579mA	1300mA	-	-
V_{ddRET}	0.08V	10V	-	-
I_{VCSL}	4mA	10mA	-	-
I_{PIN}	0.5mA	2.0mA	-	-
$T1_{module}$	$0°C$	$38°C$	$35°C$	$33°C$
$T2_{module}$	$0°C$	$38°C$	$35°C$	$33°C$

Figure 3.7: *The 16 power-supply readout values per module and their trip limits.*

3. the temperature of the cooling pipes and the relative humidity

4. dew point which is calculated from measurements of the temperature inside the detector volume and the humidity.

The purpose of the interlock system is to protect the modules from overheating if the cooling stops. If the interlock is triggered by high temperature on the cooling loop then the associated power-supply channels are switched off in about 1 sec.

3.3.2 Power distributions for the SCT

About 23 kW are needed for the nominal operation of the detector. The design of this system has been challenging since it should satisfy several conflicting requirements. One should minimise material in the detector, the voltage drop and the power dissipation (due to long distances) together with the costs. To satisfy these requirements one need to divide the power path system from the modules to the power supplies into several parts. The first part, from the modules to the patch panel (PPB1 for the barrel and PPF1 for the end-cap), is done by Low Mass Tapes (LMTs). The low mass tapes are made from $25\mu m$ with Kapton and $25\mu m$ of glue substrate with copper conductors covered by another layer of

glue and Kapton. A picture of a rack of low mass tapes is shown in figure 3.8. All lines needed for
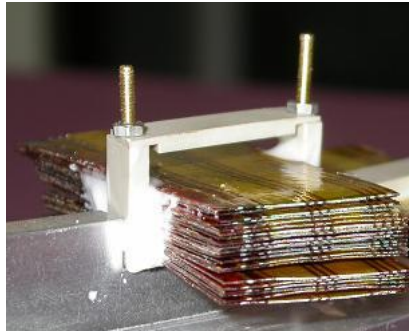
Figure 3.8: *A rack of 24 LMTs.*

the modules in the detector are present on such a tape. The patch panels one (PP1) are situated just outside the detector in the cavern and the length of these cables is therefor between 0.7 m-3 m. In PP1 the LMTs are connected to a new cable which goes to the next patch panel (PP2). This distance is much longer, approx. 9 m, and one need very good conductors to minimize the voltage drop. At PP2 these cables are again connected to a new type of cable going to patch panel three (PP3), a distance of about 20 m. The last part is from PP3 to the power-supply crates, these crates are outside the detector cavern[3].

3.3.3   My Work at CERN

I have been to CERN several times during my master degree, with one longer stay in the summer 2007. During these stays I have contributed to some of the installation and preparation of the SCT detector in ATLAS.

Low Mass Tapes connection and testing

In my stay at CERN during summer 2007 I did some shifts in the ATLAS pit working with the testing of the LMTs and their connection all the way down from the PS crates to the end-cap modules of the SCT detector on side A of ATLAS, since the testing of the barrel was finished already. To be able to do this work I had one weekend where I was taught how to do the testing.

The testing was done at the PS crates in the pit. We used two types of instruments to check the

---

[3]behind the concrete wall

performance of the LMT connections. The Agilent Data Acquisition/Switch measured the resistance between lines, where a high reading indicated an open circuit while a low reading indicated a short. We also used a Keithly Source Meter which measured the High Voltage resistance under forward bias. The testing followed a pattern, stating which HV and LV channels to test on each PS rack. When testing a specific module, a person inside the cryostat[4] of the detector had to connect this module before testing. If anomalies occurred, they where reported to an expert and written down in a logbook. Sometimes when anomalies were discovered an *expert* had to go down the chain from the PS crate and through the three patch panels to find the error. To help with this there is a mapping of every connection between the cables which leads down to the correct module. It is important that this mapping is correct, otherwise connections could be made to the wrong module. Also, when data taking starts, one would rely on the information that a hit comes from a specific module. If the mapping of the connections are wrong this hit can in fact come from a completely different module. Because of this it is extremely important to have this correct, which was also one of the reasons for doing these kind of testing.

Figure 3.9: *Me in front of one of the power-supply racks*
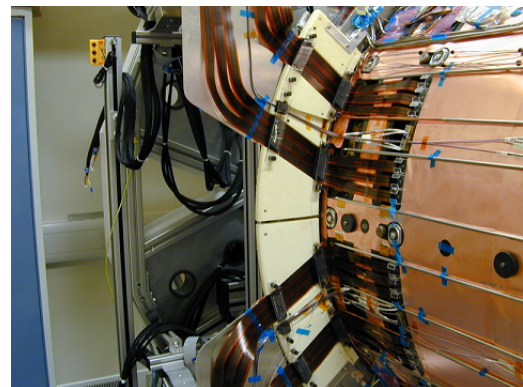
Figure 3.10: *the LMTs are connected to the modules of the SCT detector*

Static web page for SCT DCS

I have also worked within a project related to the SCT detector of ATLAS. My project was to make a static web page for the SCT-DCS. Every day a cron job is run, which connects to the database and collects information about the conditions of the SCT detector. It searches for high temperature spikes and/or high (low) voltage trips. It also checks if there is any danger for condensate in the detector (so

---

[4]inside the ID

called dew point). Previously the cron job only sent a summary by e-mail to people working within

the SCT. Our job has been to make a web page which summaries the result of the cron job. This web

page gives a summary, with different plots of the detector performance and conditions during the day,

as well as plots of the anomalies. One example of this is shown in figure 3.11. (URL to the web page:

`http://egramsta.web.cern.ch/egramsta/DCS_v3/2007-06-11/dailycheck_2007-06-11.html`)

Figure 3.11: *An example of a summary web page and a corresponding plot of the temperature of one of the modules in the SCT.*

Chapter 4

Lightest Supersymmetric Higgs signatures in ATLAS

Since the different mSUGRA scenarios have different properties the cascade pattern leading to a Higgs could look very different from scenario to scenario. However the properties of the lightest supersymmetric Higgs boson, i.e the mass, width and the branching ratios, are almost similar from scenario to scenario. We of course do not know which set of mSUGRA parameters is correct, if anyone. So if the real data from LHC would show some signatures of SUSY only one kind of SUSY will be realized. It is therefor very important to be as unbiased as possible, and find cuts that would reject as few as possible of the mSUGRA scenarios.

In a first step we make use of information from the Monte Carlo production within the different SUSY scenarios. This gives us the possibility to collect the h and Z bosons to see what are their decay products and parents. This is done to get a better understanding of the different cascade patterns in the different models. This information is afterwards used on the real simulated data with detector effects and reconstruction efficiencies to see if it is possible to prove the existence of the SUSY Higgs or an excess of Z bosons from the expected Standard Model.

4.1   SUSY models under study

For studying SUSY events in ATLAS one has defined a set of general points used to describe different scenarios in the mSUGRA parameter space. The points are chosen to lie in regions which allow the
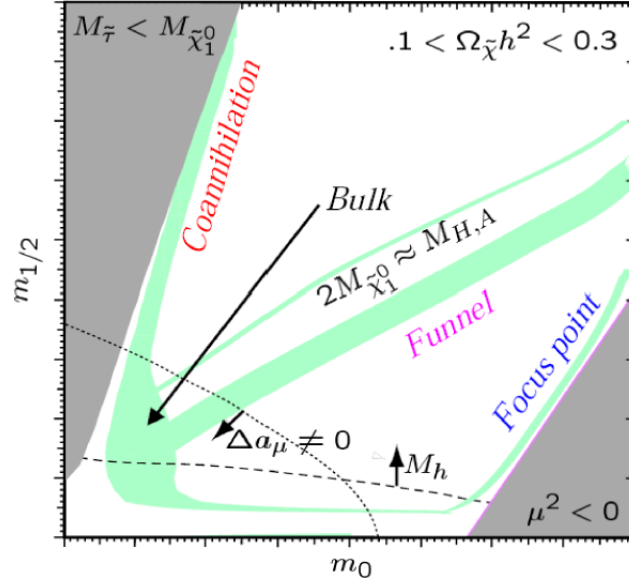
Figure 4.1: *The different mSUGRA regions covered by the ATLAS benchmark points.*

Lightest Supersymmetric Particle (LSP) to roughly fulfill the requirements of a Dark Matter candidate as constrained by the WMAP [9]. These regions are showed in figure 4.1. In addition one has also included one specific point where SUSY Higgs searches are favoured. The name of the different benchmark points comes from the way of describing the relic density of neutralinos.

Point	m_0[GeV]	$m_{1/2}$[GeV]	A_0[GeV]	$\tan\beta$	sign(μ)
Co-annihilation (SU1)	70	350	0	10	+
Focus Point (SU2)	3550	300	0	10	+
Bulk (SU3)	100	300	-300	6	+
Low Mass (SU4)	200	160	-400	10	+
Funnel (SU6)	320	375	0	50	+
Co-annihilation (SU8.1)	210	360	0	40	+
Co-annihilation (SU8.2)	215	360	0	40	+
Co-annihilation (SU8.3)	225	360	0	40	+
Higgs (SU9)	300	425	200	20	+

Table 4.1: *The values of the 5 fundamental mSUGRA parameters for the different ATLAS benchmark points.*

-	All fermions	WW	ZZ
SM Higgs	$\frac{igm_f}{2m_W}$	$igm_W g^{\mu\nu}$	$\frac{igm_Z}{2\cos\theta_W} g^{\mu\nu}$

Table 4.2: *The Standard Model Higgs couplings to fermions and massive gauge bosons*

-	$d\bar{d}$, $s\bar{s}$, $b\bar{s}$, e^+e^-, $\mu^+\mu^-$, $\tau^+\tau^-$	$u\bar{u}$, $c\bar{c}$, $t\bar{t}$	WW, ZZ
h	$-\frac{\sin\alpha}{\cos\beta}$	$\frac{\cos\alpha}{\sin\beta}$	$\sin(\beta-\alpha)$

Table 4.3: *The MSSM correction factors to the Standard Model Higgs couplings listed in table 4.2*

4.2 Higgs Production and Decay

The production cross-sections and decay branching ratios for the lightest MSSM Higgs boson can be calculated, at tree level, from the corresponding SM diagrams by simply multiplying the various amplitudes by the appropriate supersymmetric correction factor. The SM Higgs couplings to fermions and gauge bosons are shown in table 4.2. The corresponding SUSY correction factors, shown in table 4.3 depend on the parameters α[1] and β[2]. This does not yield for processes described by loop-diagrams, since one then has to include contributions from particles which are absent in the Standard Model. Therefore the couplings in table 4.2 and 4.3 are subject to large radiative corrections, especially from loops containing heavy **s**top and **s**bottom quarks. However it is still possible to calculate the expected cross sections, with loop corrections, in the different mSUGRA scenarios as long as the parameters and masses of the sparticles are known.

4.2.1 Production

There are two dominant ways of producing a supersymmetric Higgs bosom in a pp collision at LHC. Either directly through a Standard Model like process, such as gluon-gluon fusion, or through a cascade decay of supersymmetric particles. Given the relatively low mass of h, the first mechanism will be challenging to prepare for due to enormous Standard Model QCD background. However a lot of

---

[1] the mixing angle between the real components in the MSSM Higgs doublet

[2] defined in (2.5)
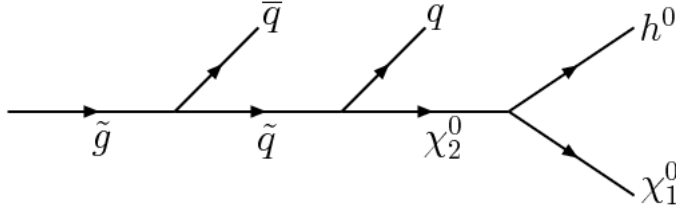
Figure 4.2: A typical cascade of supersymmetric particles producing a Higgs

work is done within this production channel in search for a light SM Higgs boson by using the decay $H \to \gamma\gamma$. In the second case however there are several possibilities of reducing the background, especially by using the missing transverse energy signature. One example of a typical cascade producing a Higgs in the end is shown in figure 4.2. The most promising source of Higgs in such a cascade is usually the final decay of a second lightest neutralino; $\widetilde{\chi}_2^0 \to \widetilde{\chi}_1^0 h$, but the Higgs can also come from decays of the other gauginos, **s**quarks and **s**taus. If the $\widetilde{\chi}_2^0 \to \widetilde{\chi}_1^0 h$ channel is kinematically allowed it will often dominate the $\widetilde{\chi}_2^0 \to \widetilde{\chi}_1^0 Z$ because the two lightest neutralinos are basically gaugino like in mSUGRA models, so that the gaugino-gaugino-Higgs vertex is enhanced with respect to the higgsino-gaugino-gauge one [13]. However, if some of the **s**leptons are light, so that the $\widetilde{\chi}_2^0$ decay into a **s**lepton-lepton pair ($\widetilde{\chi}_2^0 \to \widetilde{l} l$), this will often dominate over $\widetilde{\chi}_2^0 \to \widetilde{\chi}_1^0 h$.

4.2.2 Decay

The decay possibilities for the lightest MSSM Higgs are in general the ones listed in (4.1), but which of them that is kinematically allowed varies from model to model.

$$
\begin{aligned}
h &\to f_i \bar{f}_j, \gamma\gamma \\
h &\to \widetilde{\chi}_i^0 \widetilde{\chi}_{i'}^0, \widetilde{\chi}_j^+ \widetilde{\chi}_{j'}^-, \widetilde{f}\bar{\widetilde{f}}, \\
h &\to AA
\end{aligned}
\tag{4.1}
$$

where f denotes a fermion and A is the heavy CP-odd Higgs. Since $m_h < 135\text{GeV}$, as was discussed in section 2.4.1, in all the SUSY scenarios under study the Higgs boson will not be heavy enough to decay to either W or Z bosons. From the couplings in table 4.2 and 4.3 it is clear that the couplings to the Higgs is proportional to the mass of the particles. The dominant decay for h is therefore into $b\bar{b}$, since it is the heaviest quark kinematically accessible. The exact value on the branching ratio varies from model to model, but it is between 0.7 and 0.85 in all the models studied here. As is clear from 4.1

the Higgs could also decay to a pair of supersymmetric particles. If the decay $h \to \widetilde{\chi}_1^0 \widetilde{\chi}_1^0$ is possible, Higgs would decay invisibly, since $\widetilde{\chi}_1^0$ is the LSP and will leave the detector without detection. In all the models studied here the sparticles are too heavy to be kinematically accessible for the lightest SUSY Higgs to decay into them.

To be able to choose the correct cuts and strategies for discovering the lightest supersymmetric Higgs and reject other SUSY background, it is important to take into account the properties, regarding decay branching ratios and mass hierarchy in each model. Some of the most important properties for the following analysis for each model studied are listed in table 4.4.

sparticle	SU1	SU2	SU3	SU4	SU6	SU8.2	SU9
mass [GeV]							
h^0	115.81	119.01	114.83	113.98	116.85	116.68	114
squarks	$\sim 570 - 830$	$\sim 2100 - 3600$	$\sim 430 - 650$	$\sim 200 - 450$	$\sim 640 - 870$	$\sim 600 - 800$	≈ 900
gluino	**832.33**	856.59	**717.46**	**413.37**	**894.70**	**856.47**	**1000**
$\widetilde{\chi}_1^0$ (LSP)	136.98	103.35	117.91	59.84	149.57	142.48	173
$\widetilde{\chi}_2^0$	263.64	160.37	218.60	113.48	287.97	273.99	325
$A_0{}^3$	512.39	3506.62	511.53	368.18	386.47	428.90	625
decay				**Branching Ratio [%]**			
$\widetilde{\chi}_2^0 \rightarrow \widetilde{\chi}_1^0 h$	4.83	0	0	0	3.60	2.84	86
$\widetilde{\chi}_2^0 \rightarrow \widetilde{\chi}_1^0 Z$	0.73	0	2.56	0	0.83	0.75	12
$h \rightarrow b\bar{b}$	83.04	79.3	83.42	84.69	81.36	81.75	72

Table 4.4: *Some important masses and branching ratios for the ATLAS-benchmark points, the bold face indicate the heaviest particle in the scenario*

---

[3]this is the CP odd Higgs, not the trilinear coefficient

4.3 B-tagging

In this analysis the ability to distinguish b-jets from other types of jets is a crucial point, because we need to separate the two possible b-jet candidates coming from Higgs from all the other abundant jets. B-tagging is one of the main goals of the Inner Detector in ATLAS.

Hadrons containing a b quark have sufficient lifetime ($\sim$ 1.5ps), so that they can travel a short but measurable distance ($\sim$ 4 mm for a 50 GeV particle) in the detector before decaying. This will lead to so called secondary vertices in the detector. The light[4] quark hadrons (i.e u, d, s) lead to jets without secondary vertices. The c-hadrons and τ leptons could also lead to secondary vertices. The ability to distinguish b-jets from the other jet types is crucial, especially in studies of the top quark but also, as we have discussed, in SM and supersymmetric Higgs searches. One therefore needs an inner detector with very good vertexing ability, to be able to separate primary and secondary vertices. Three main ways to tag jets of b quarks are used in ATLAS [1].

1. impact parameter (IP)

2. secondary vertex properties tag

3. soft lepton tag

The most powerful of these methods are 1 and 2, the so called *lifetime tags* [1].

4.3.1 Definitions

There are some general variables that are used by people working with b-tagging to indicate the performance of the various b-tagging algorithms. These are both used at the TEVATRON and LHC.

b-tagging Efficiency

$$\varepsilon_b = \frac{\#\text{of tagged b jets}}{\text{total}\#\text{of b jets}} \qquad (4.2)$$

Rejection of light flavored jets

$$R_l = \frac{\#\text{of all light jets}}{\#\text{of light jets mistagged as b jets}} \qquad (4.3)$$

---

[4]*light* will in the following mean that they have *light* flavor, i.e. they are quarks from one of the two first generations quarks
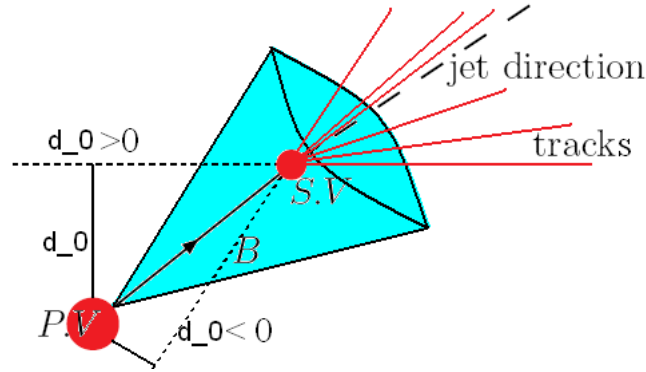
Figure 4.3: *The idea of Impact Parameter. PV = primary vertex, SV = secondary vertex and d_0 is the transverse impact parameter.*

Mistag rate of light flavored jets

$$M = \frac{1}{R_l} \tag{4.4}$$

At TEVATRON the mistag ratio is mostly used when discussing the b-tagging performance. At LHC however, the rejection is mostly used.

4.3.2   Impact parameter (IP)

This method uses the fact that the jets containing a b quark will have tracks which, when extrapolated backward, do not hit the interaction point. This happens because the decay inside the jet did not take place at the interaction point but after the jet had traveled a small distance in the detector. The perpendicular distance between the extrapolated track and the primary vertex (d_0) is the track impact parameter in the transverse plane ($r - \phi$). It is also possible to measure the longitudinal track impact parameter (z_0), which is the z coordinate of the track at the point of closest approach in $r - \phi$. The one mostly used is d_0. A schematic figure of the impact parameter is shown in figure 4.3. The sign of the IP reflects which side of the primary vertex (PV) the track originates from. Per definitions one side of the PV is defined to give positive IP, while the other gives negative IP. For heavy flavored jets the tracks will be displaced in the jet direction, and the IP distribution will therefore have an excess on the positive side (see figure 4.3). The width of the negative IP distribution is mainly due to the detector resolution, beam spot size and multiple scattering. The IP for every reconstructed track in the jet is measured and used to obtain a probability of the jet being a b-jet in the following way:

1. For each track in the jet a significance, S_i, is calculated, where

$$S_i = \frac{\pm d_0}{\sigma(d_0)},$$

(4.5)

where $\sigma(d_0)$ is the uncertainty on the impact parameter, track and beam line position [1]. The division by the uncertainty is done to reduce the badly measured tracks with very high impact parameter.

2. One then calculates the ratio, r_i, between the significance probability distribution functions for b jets and other light jets (l).

$$r_i = \frac{f_b(S_i)}{f_l(S_i)}.$$

3. A weight is then calculated from the sum of the logarithms of r_i

$$W = \sum_i^{\#tracks} \ln r_i.$$

4. The wanted rejection (or mistag rate) of light jets (see eq. (4.3) and (4.4)) and the efficiency for b jets (see eq. (4.2)) are chosen using some specific value for W.

   In all studies the goal is to maximize both the rejection and the efficiency to obtain as good b tagging as possible. The fact that the probability density functions vary from process to process, has to be taken into account when studying different kinds of processes. This will also lead to different cuts in the variable W, to obtain the desired b-tagging efficiency. There are three different kinds of weights used in my analysis

   - **IP1D**: uses only the longitudinal track impact parameters (z_0)

   - **IP2D**: uses only the transverse track impact parameters (d_0)

   - **IP3D**: a combination of the d_0 and z_0, with

$$r_i = \frac{f_b(S_{d_0 i}, S_{z_0 i})}{f_l(S_{d_0 i}, S_{z_0 i})}.$$

An example of the distribution of the transverse IP significance weight (IP2D) is shown in figure 4.4. The light jet curve (solid) has a much shorter tail for high values of W. The b-jet curve (dotted) differs considerably from the distribution for light jets. The tracks that are selected will have different properties. To improve the b-tagging performance one can divide the tracks into different categories
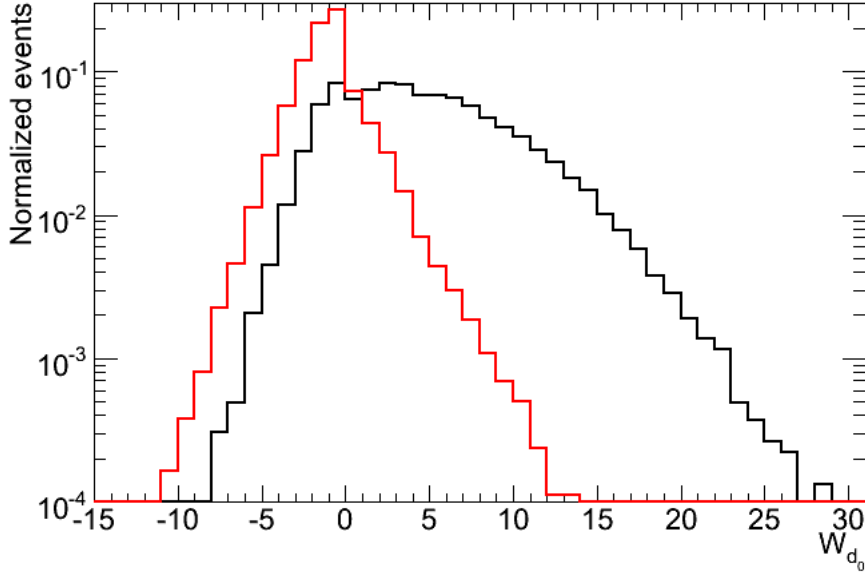
Figure 4.4: *The distribution of the transverse IP significance weight (IP2D) for light jets (light) and b-jets (dark).*

and use specialized probability density functions, f_b^j and f_l^j, for each category j. The weight is then calculated as

$$W = \sum_{j=1}^{N_C} \left(\sum_i^{N_T^j} \ln r_j \right) ,$$

where N_T^j is the number of tracks in each category, N_c the number of categories and r_j is the ratio between the probability density functions for b- and light jets for each category [2].

4.3.3 Secondary vertex properties tag

There are some specific properties that distinguish a primary vertex form a secondary vertex. These different properties can be used in order to distinguish between b-jets and light jets.

- number of 2-track vertices inside the jet (N2T)

- invariant mass of the inclusive secondary vertex (MSVX)

- fraction of total jet energy in the secondary vertex (ESVX = E(charged tracks in vertex)$/E$(charged tracks in jet)

By comparing histograms of these variables with reference histograms one can find a ratio of the probability functions for b jets and light jets

$$r_{SV} = \frac{f_b^{SV}(N2T, MSVX, ESVX)}{f_l^{SV}(N2T, MSVX, ESVX)},$$

where f_b^{SV} and f_l^{SV} are probability functions for b jets and light jets respectively. Again, a weight is calculated from the sum of the logarithm of this ratio. In the analysis two different weights are implemented.

- **SV1**: combine a 1D p.d.f. (probability density function) for *N2T* and a 2D p.d.f. for *MSVX* and *ESVX* to calculate the weight

- **SV2**: same as *SV1*, but the three variables, *N2T*, *MSVX* and *ESVX*, are combined into a 3D p.d.f.

The two lifetime algorithms are based on knowledge of the properties of b and light jets, to get the probability density functions and the typical properties of the secondary vertex. This therefore requires some data for calibration and training before this method of b-tagging can be applied [2]. It is also difficult to extract a pure sample of light jets from the data. Because of this some alternative algorithms are built, which are less powerful, but can be used at the beginning of LHC with less reliance on Monte Carlo [2].

4.3.4   Soft lepton tag

The most powerful way to tag a b-jet is to use the lifetime methods already mentioned, but as a complement to these methods the tagging of soft leptons within a jet could also be used. This method will have very low correlation with the two others and is therefor a very good complementary method [2]. We know that both b and c hadrons could decay semileptonically into an electron or a muon. Since the b quark is heavier than the c quark, the leptons from a b hadron decay will typically have a higher transverse momentum with respect to the jet axis than leptons from a c hadron decay [2].

One or several hits in the muon spectrometer are matched to a track in the inner detector and if this track has a $\Delta R < 0.5$ to a jet, the muon would be assigned as coming from the closest jet. The muon also has to fulfil some requirements on the p_T and d_0 [2].

Nevertheless, due to the relatively low branching ratio for a b to decay to a lepton, this method has its limitation.

The mostly used weight combination, not including the soft lepton tag method, is to combine the *IP3D* with on of the *SV1* or *SV2* taggers into $W = W_{IP3D} + W_{SV1/2}$.

4.3.5   B-tagging in CDF at TEVATRON

Since LHC has not begun to operate it is difficult to say exactly how good b-tagging performance one will achieve, and how long time it will take before we understand the detector well enough to reach the wanted b-tagging performance. It is therefore interesting to look at what is achieved at the TEVATRON experiment since they have been running for a long time already, although at much lower energy than what is expected at the LHC.

There are mainly three different methods of b-tagging used in the CDF and D0 experiments, they are based on the same ideas as the one used in ATLAS, which have been discussed above. Two methods, the *jet probability* and *secondary vertex algorithm*, use the fact that the b-quark travels a small distance before decaying. The third method uses the presence of soft leptons inside a jet, which could come from a semi-leptonic decay of a b-quark, to tag a b-quark.

An efficiency for the secondary vertex algorithm have been calculated. For $350pb^{-1}$ of RUN II data at CDF an efficiency of 0.39 ± 0.01 [14] is measured, integrated over the complete jet E_T range. This efficiency will strongly depend on the E_T and η and one has to consider this efficiency with respect to the process under study. It is interesting to compare the efficiency given by data and by simulations to obtain a scale factor which should be used when working on Monte Carlo data. From this method a scale factor of $0.92 \pm 0.02(\text{stat}) \pm 0.06(\text{syst})$ [14] is achieved. From the second method a scale factor of $0.89 \pm 0.03(\text{stat}) \pm 0.07(\text{syst})$ [14] is measured. Since the scale factor is less than unity the simulations are more optimistic than in the real experiment.

4.3.6   What is expected in ATLAS

The TEVATRON has achieved very good knowledge about the detector and the b-tagging efficiency. This gives optimistic prospects for the CMS and ATLAS detectors at LHC, but there are several things that have to be figured out to get such a high quality b-tagging. First of all it is important to achieve precise alignment of the tracking detectors, since this is crucial for the impact parameter measurements. Also the material, cooling pipes, cables, support structures etc., in the inner part of the detector have significant impact on the tagging rate. It is also very important to use appropriate calibration signals.

From Monte Carlo studies with fully simulated and reconstructed data in ATLAS a b-tagging efficiency of $\sim 60\%$ is achieved with a light jet rejection of more than 100 [1], with the two lifetime methods discussed in the previous sections. The performance is somehow dependent on p_T and $|\eta|$

of the jets. At low p_T the performance is degraded due to the increase of multiple scattering and secondary interactions. At high p_T the fact that more of the B hadrons decay outside the vertexing layer, also decreases the performance [1].

4.4 Cascade patterns

Since the different scenarios will have different cascades leading to Higgs boson production it is interesting to investigate more which kind of signatures are expected in the different signal scenarios. This is done in the following sections. The number of Higgs and Z bosons presented are the total number of Higgs/Z produced in each scenario, regardless of their decay. But as is clear from table 4.4; for h the decay into $b\bar{b}$ is very dominant ($70 - 86\%$). For Z the branching ratio for a decay into $b\bar{b}$ is approximately 15.5% [16]. In the following each of the mSUGRA models are studied more in detail.

4.4.1 Co-annihilation - SU1

The two histograms in figure 4.5 show the mother of the produced Z and h in the $SU1$ mSUGRA point.

| (1) h | (2) Z |
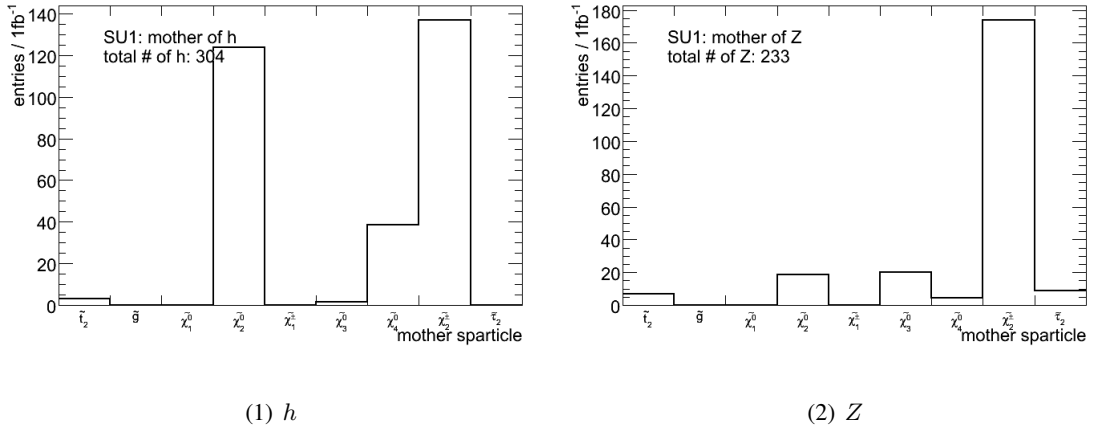
Figure 4.5: *The mother of the produced Z and h bosons in the signal sample $SU1$ for $1 fb^{-1}$.*

We see that the h has mainly two sources, either it comes from a decay of $\widetilde{\chi}_2^0$ or from the heaviest chargino ($\widetilde{\chi}_2^\pm$). A small amount of the Higgses could also originate from the decay of the heaviest neutralino ($\widetilde{\chi}_4^0$). For the Z boson the dominant production is from the decay of $\widetilde{\chi}_2^\pm$. We also see that

there are slightly more Higgs bosons (304) than Z bosons (233) in the sample. The different feynman graphs in figure 4.6 show the most probable decay chains with the production of a Z or a h boson.

(1) BR=0.25(Z)/0.19(h)

(2) BR=0.02(Z)/0.19(h)

(3) BR=0.02(Z)/0.08(h)

(4) BR=0.01(Z)/0.05(h)
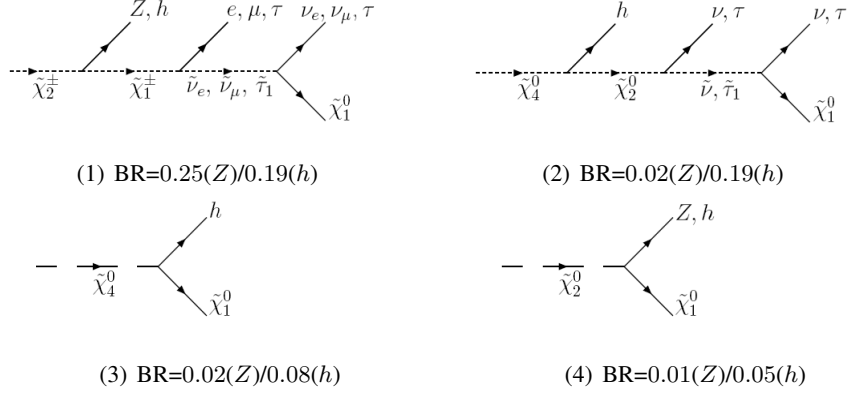
Figure 4.6: *The different diagrams for Z and h production in the signal sample $SU1$. The branching ratio (BR) for the sparticle to decay into h or Z is presented under the graph.*

In both the decay of the $\widetilde{\chi}_2^\pm$ and $\widetilde{\chi}_2^0$ we get a similar cascade pattern. In the case of the $\widetilde{\chi}_2^\pm$ we end up with a lepton and a neutrino, with a branching ratio of 0.75 into the two first generation leptons together with the LSP. In the case where we have $\widetilde{\chi}_2^0$ we get instead two neutrinos, which will contribute to the $\not{E}_T$. For the Z boson the latter decay chain is not probable, and the production will mainly be through the first one. For h however we have also the possibilities of getting shorter chains, without leptons, as in figure 4.6 (3) and (4).

To figure out the most probable cascade of supersymmetric particles that leads to a final state with a h or Z boson we have to look at the initially produced sparticles from the the pp collisions. The histograms in figure 4.7 shows which primary sparticle is most often produced in each leg and the combination of the two sparticles produced per event.
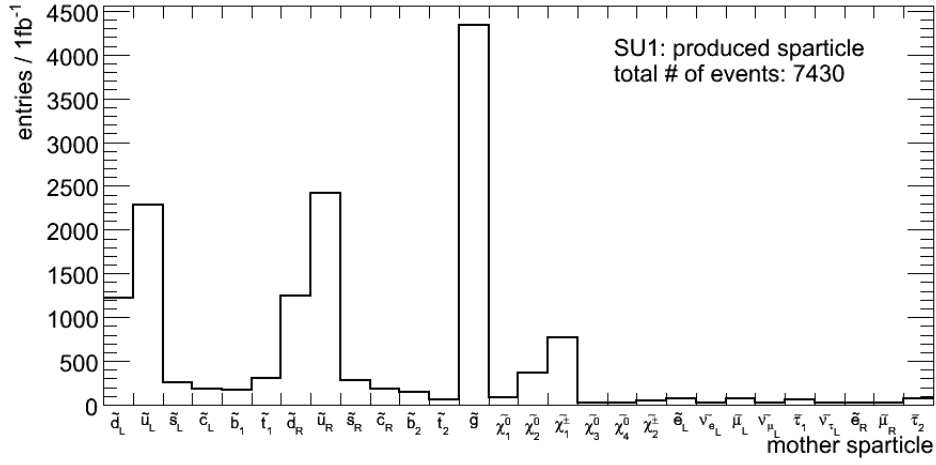
(1) sparticle produced
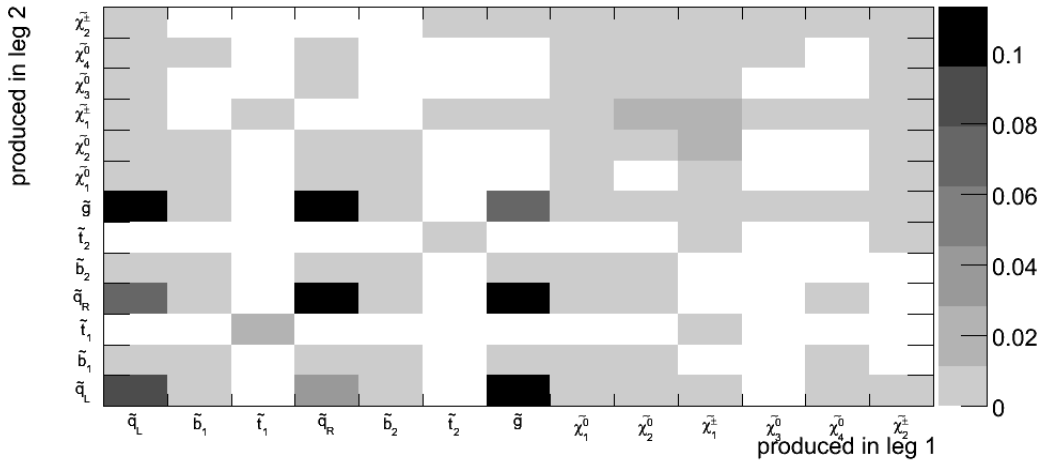
(2) sparticle pair produced

Figure 4.7: *(1): The multiplicity of the initially produced sparticles and (2): the various pairs of produced sparticles from each leg per event.*

The scatter plot in 4.7 (2) shows that the most common pair of produced particles are $\widetilde{g} - \widetilde{q}_L$, where the squark is from one of the first two generations. Also squark-squark and gluino-gluino pairs are produced at relatively high rate.

In the case of direct production of a right/left handed 1st or 2nd generation squark pair, we seldom get production of the heaviest neutralino or chargino. Only in the case of a left handed squark, there is a small branching ratio $(0.01 - 0.05)$ for this. However the decay of a left handed squark into

$\widetilde{\chi}_2^0$ is relatively high (~ 0.3) and this could further lead to the decay in 4.6 (4), although the branching ratio is small (~ 0.05). A right-handed squark will in nearly 100% of the cases go into the LSP and a quark, and is not interesting for this analysis.

To get heavy gaugino production it is crucial to have at least one gluino produced in the pp collisions. The gluino often decays into a 3rd generation squark (BR~ 0.4), which has a decent branching ratio into the $\widetilde{\chi}_4^0(0.01 - 0.2)$ and $\widetilde{\chi}_2^\pm(0.1 - 0.3)$.

The discussion above reveals the most probable decay cascades into a h or Z boson in the $SU1$ mSUGRA point. The feynman graphs for this are shown in figure 4.8.

(1) long cascade, BR=0.43   (2) short cascade, BR=0.31
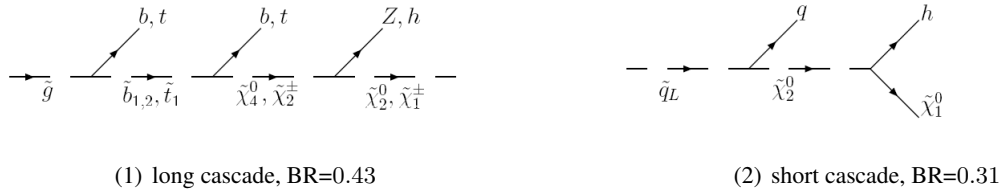
Figure 4.8: *Two of the main cascades of supersymmetric particles that lead to a h production in $SU1$. The branching ratio for the first decay in the chain is presented under the graph (for the q_L the BR is per left-handed squark.*

We define two types of cascades, a short cascade (figure 4.8 (2)) with only one high p_T jet produced, and a long cascade (figure 4.8 (1)) with several high p_T jets and possible leptons or neutrinos. These graphs are then combined with the ones in figure 4.6 to find the typically final states in this scenario. The most probable is the long cascade in figure 4.8 (1), since at least one gluino often is produced initially. This leads to final states with leptons (or neutrinos), LSP and one or two 2nd or 3rd generation high p_t quarks from heavy squark decay. The less probable chain in figure 4.6 (2) will give final states without any additional leptons or neutrinos and with a light flavored jet in stead of the b or t. The scatter plot in figure 4.7 (2) shows that the most common pair of initially particles are gluino and squark, which often will give one short and one long cascade. In case of gluino-gluino production the probability of getting at least one short cascade (not necessarily with Higgs) is also relatively high since the gluino often go to a right-handed squark and $\widetilde{\chi}_2^0$.

It is clear that in $SU1$ the events containing the lightest Higgs typically have one or two high p_T jets, possible leptons and neutrinos and two LSPs.

4.4.2 Focus Point - SU2

The two histograms in figure 4.9 show the mother of the produced Z and h bosons in the $SU2$ mSUGRA point.

(1) h (2) Z
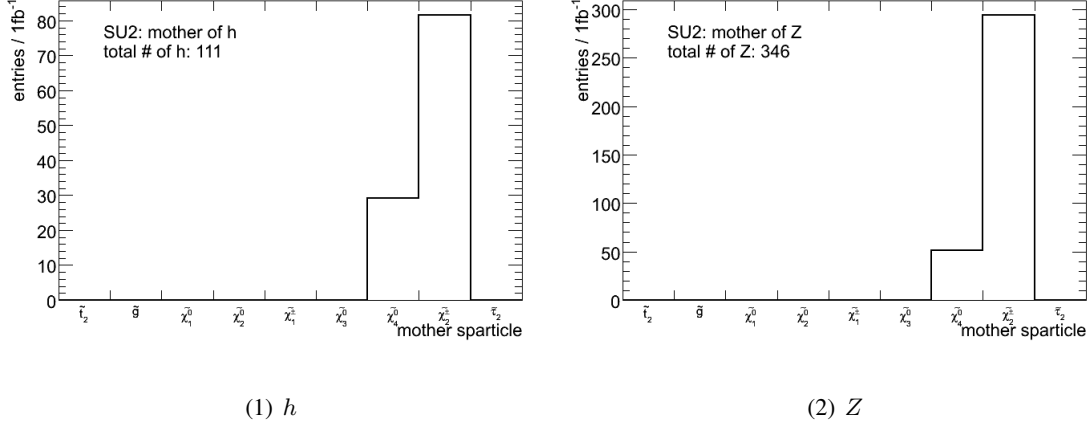
Figure 4.9: *The mother of the produced Z and h bosons in the signal sample $SU2$ for $1fb^{-1}$.*

There are almost three times as many Z bosons (346) as Higgs bosons (111) in the $SU2$ sample. The distributions of the mothers of the two bosons are very similar. Mostly the Z or h comes from the decay of $\widetilde{\chi}_2^{\pm}$ but sometimes the mother could also be the heaviest neutralino, $\widetilde{\chi}_4^0$. The two feynman diagrams in figure 4.10 show the most probable decay patterns.

(1) BR=0.30(Z)/0.08(h)   (2) BR=0.10(Z,into $\widetilde{\chi}_3^0$)/0.06(h,into $\widetilde{\chi}_2^0$)
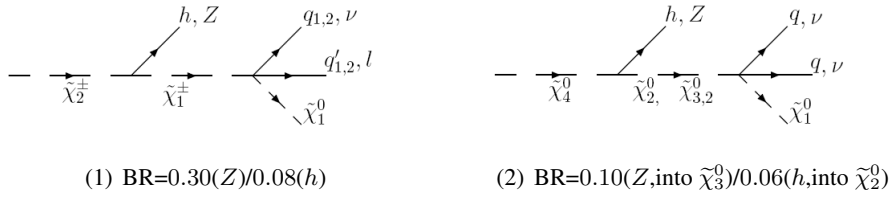
Figure 4.10: *The different diagrams for Z and h production in the signal sample $SU2$. The branching ratio for the decay is shown under the graph. The decay of $\widetilde{\chi}_2^0$ into $\widetilde{\chi}_1^0$ and h or Z has BR=0.01(Z)/0.002(h)*

What is special here is that the neutralinos or charginos decay via a 3-body decay into a neutrino-neutrino/lepton-lepton pair (neutrino-lepton for the chargino) or quark-quark pair. For the chargino the most probable decay is the quark-quark decay (BR=0.67) where the quarks are from the 1st or 2nd generation. Also for the neutralino the quark-quark decay is most probable (BR=0.65), but here we can also have b-quarks. This means that the final states often have several jets.

Figure 4.11 shows the initially produced sparticles in the $SU2$ scenario.
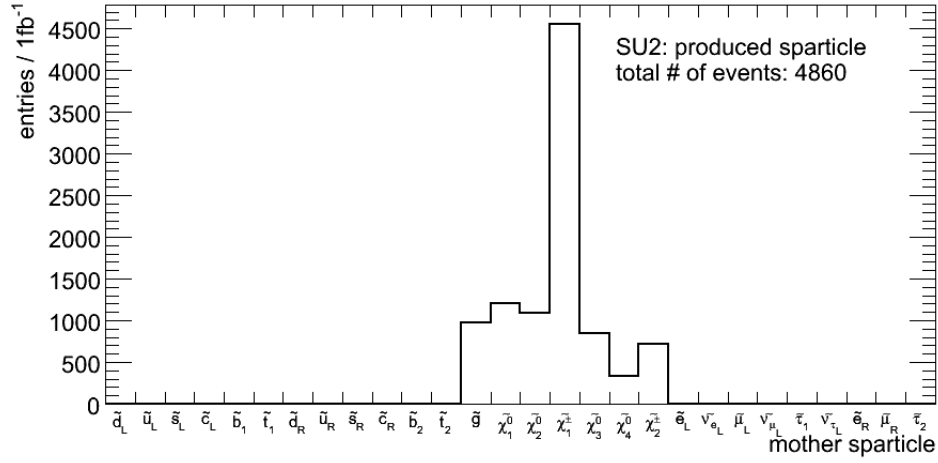
(1) sparticle produced
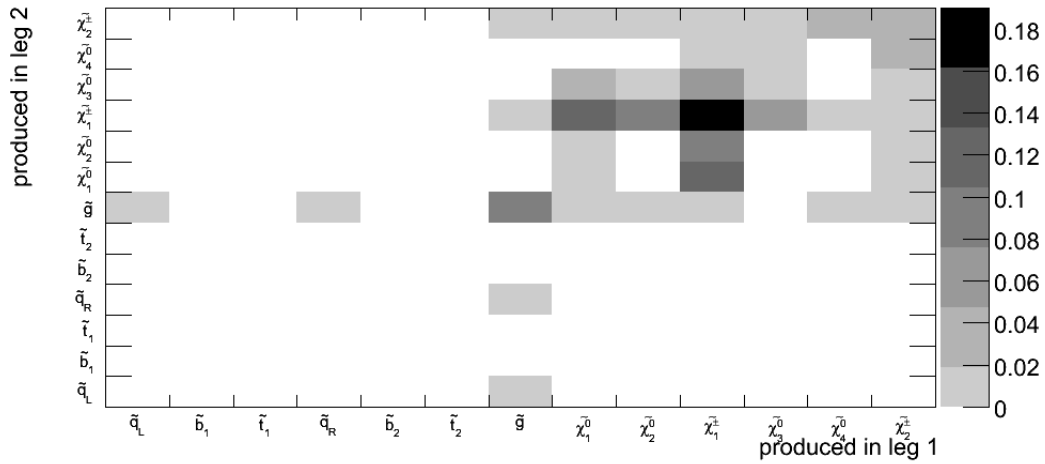
(2) sparticle pair produced

**Figure 4.11:** *(1): The multiplicity of the initially produced sparticles and (2): the various pairs of produced sparticles from each leg per event. Since this scenario has very heavy squarks the production of gauginos dominate, especially $\chi_1^{\pm}$ pair are produced at high rate.*

According to table 4.4, SU2 is a very special sample with extremely heavy squarks (TeV range). This explains the special distribution of the initially produced sparticle compared with the other scenarios. Seldom there are produced squarks or gluinos initially. In-stead gauginos are produce, since they are much lighter. The most dominant produced pair of sparticles is a $\widetilde{\chi}_1^{\pm}$-pair. We already know

that h/Z production is a result of the heaviest chargino, $\widetilde{\chi}_2^\pm$, or neutralino, $\widetilde{\chi}_4^0$, decays. This could happen either through the direct production of $\widetilde{\chi}_4^0$ or $\widetilde{\chi}_2^\pm$ or through an initially produced gluino decaying into a quark-quark pair and the wanted gaugino. These two ways of h/Z production are shown in figure 4.12.

$$q, q \qquad h, Z \qquad\qquad\qquad h, Z$$
$$\widetilde{g} \qquad \widetilde{\chi}_4^0, \widetilde{\chi}_2^\pm \quad \widetilde{\chi}_{1,2,3}^0, \widetilde{\chi}_1^\pm \qquad \widetilde{\chi}_4^0, \widetilde{\chi}_2^\pm \quad \widetilde{\chi}_{1,2,3}^0, \widetilde{\chi}_1^\pm$$
$$q, q'$$

(1) long cascade, $\qquad\qquad$ (2) short cascade,

BR=$0.27(\widetilde{\chi}_2^\pm)$/$0.09(\widetilde{\chi}_4^0)$ $\qquad\qquad$ $BR_{\widetilde{\chi}_4^0}$=$0.11(Z)$/$0.06(h)$,

$\qquad\qquad\qquad\qquad\qquad\qquad\qquad BR_{\widetilde{\chi}_2^\pm}$=$0.30(Z)$/$0.08(h)$
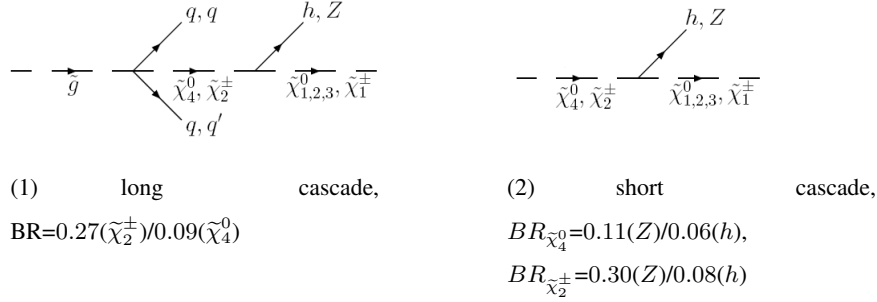
Figure 4.12: *Two of the main cascades of supersymmetric particles that lead to a h/Z production in $SU2$. The branching ratio for the first decay in each graph is presented.*

As in $SU1$ we get a short and a long cascade, where the difference in final state is that the long cascade will have two more jets in addition to the ones produced in the decays in figure 4.10. These jets might have higher p_T than the others, since they are produced earlier in the cascade as demonstrated in figure 4.12 (1). Both chains could also get final states with leptons and/or additional $\not{E}_T$ from neutrinos (BR~ 0.2) in-stead of the two quark jets at the end of the cascade, but this is less probable than getting the non-lepton final state (BR~ 0.8). Since the gauginos can decay into two quarks and the LSP the final states from both the long and the short cascade in $SU2$ will be very rich in quark jets, since the long cascade will give four additional jets, while the short will have two additional, low p_T jets.

4.4.3 Bulk - SU3

The histograms in figure 4.13 show the mother of the produced Z and h bosons in the $SU3$ mSUGRA point.

(1) h (2) Z
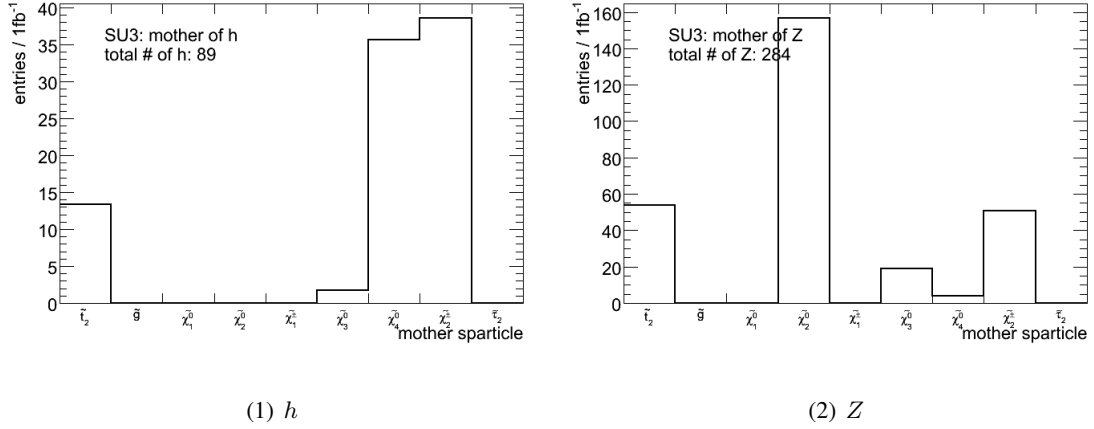
Figure 4.13: *The mother of the produced Z and h bosons in the signal sample $SU3$ for $1fb^{-1}$.*

The number of h bosons in this sample is relatively small (89), while the number of Z bosons (284) are more than three times higher. The h mainly comes from the decay of the $\widetilde{\chi}_4^0$ and $\widetilde{\chi}_2^\pm$, while the Z boson mainly stems from $\widetilde{\chi}_2^0$ decays. Both h and Z have approximately the same fraction of **s**top as the mother **s**particle. Some of the most probable decays into h and Z are sketched in figure 4.14

(1) BR=0.25(Z)/0.20(h)   (2) BR=0.25(Z)/0.20(h)

(3) BR=0.25(Z, from $\widetilde{\chi}_3^0$)/0.18(h)   (4) BR=0.10(Z, from $\widetilde{\chi}_3^0$)/0.07(h)

(5) BR=0.37(Z)/0.09(h)
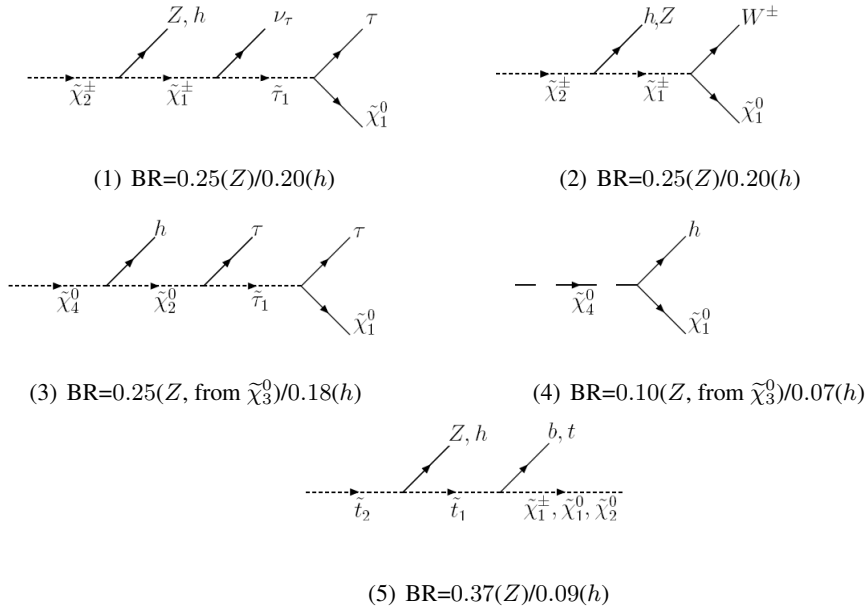
Figure 4.14: *The different diagrams for Z and h production in the signal sample $SU3$. The Z has similar diagrams (3) and (4) as h provided $\widetilde{\chi}_4^0$ is replaced with $\widetilde{\chi}_3^0$. Branching ratios for the first decay in each graph is presented*

The branching ratios for Z production are in all cases much higher than for h production, which reflects the numbers in figure 4.13. In case of a $\widetilde{\chi}_2^\pm$ as the mother sparticle, the decay into h or Z would create a $\widetilde{\chi}_1^\pm$ in addition, as in figure 4.14 (1) and (2). The lightest chargino will further decay to either a stau-neutrino pair (BR = 0.68), as in figure 4.14 (1) or $W^\pm$ (BR=0.30) and the LSP, as in figure 4.14 (2). This will lead to final states with $\not{E}_T$ (from the LSP and ν_τ) and a τ or a lepton/quark pair, somehow dependent on the decay of $\widetilde{\chi}_1^\pm$ and $W^\pm$.

When the h stems from the decay of the heaviest neutralino ($\widetilde{\chi}_4^0$) it could decay either directly to a h and the LSP, as in figure 4.14 (4), or through the more probable and longer cascade with h and $\widetilde{\chi}_2^0$, as in figure 4.14 (3). The latter case will have a final state with two τs (approx 20% of the events will have two electrons or two neutrinos in-stead), $\not{E}_T$ and h, while the first will be without leptons or τs.

The stop quark could also be the mother sparticle of both h and Z. The decay chain will then be as in the graph in figure 4.14 (5). The final state will have an additional 3rd generation quark together with the possible decay products of the chargino or neutralinos as discussed above.

Figure 4.15 show the initially produced sparticle and sparticle pair in each event in the $SU3$ mSUGRA point.
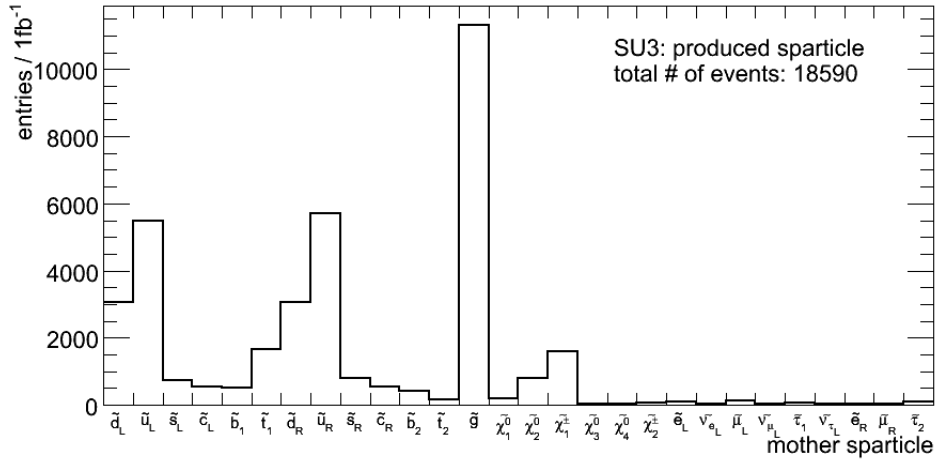
(1) sparticle produced
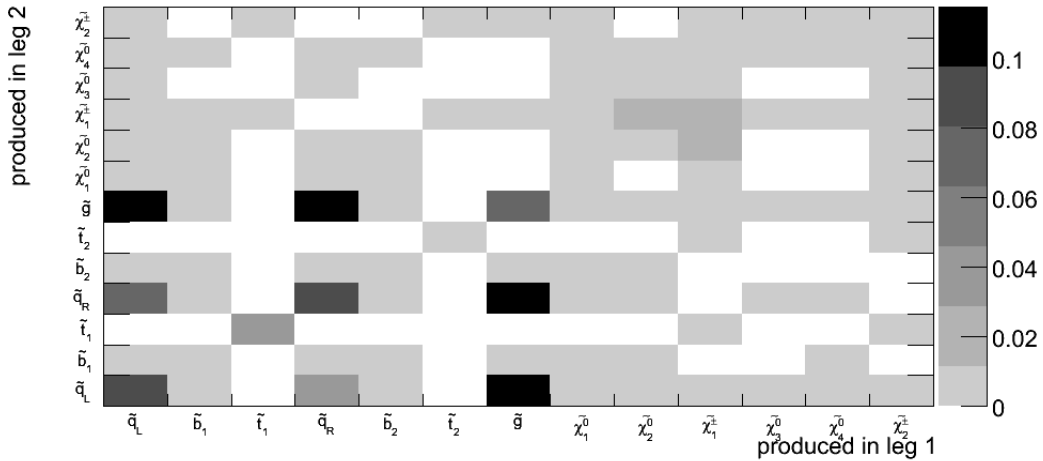
(2) sparticle pair produced

Figure 4.15: (1): The multiplicity of the initially produced sparticles and (2): the various pairs of produced sparticles from each leg per event

From this the most probable is to have production of a gluino or a 1st generation squark. The gluino will most often decay into a right handed squark-quark pair. The right handed squark will nearly always decay into the LSP and a quark, so it is not interesting for Higgs analysis. The gluino has also a decent branching ratio into 3rd generation squark-quark pair or a left handed 1st and 2nd generation squark-quark pair. As discussed above we need production of heavy neutralinos or charginos to produce h in $SU3$.
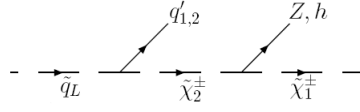
Figure 4.16: *The short cascade (BR=0.02 for the first decay) in $SU3$. The long cascade is similar only with an initially produced gluino decaying into a left-handed squark (BR=0.22).*

The corresponding long cascade will be the same as in figure 4.16 just that a gluino is initially produced, and decays into a left-handed squark. Since the heaviest neutralino ($\widetilde{\chi}_4^0$) and chargino ($\widetilde{\chi}_2^\pm$) are almost as heavy as the 1st and 2nd generation squarks, the branching ratio for a decay into $\widetilde{\chi}_4^0$ or $\widetilde{\chi}_2^\pm$ is very small ($0-0.01$) for these squarks. For Z we have the possibility of production through $\widetilde{\chi}_2^0$, which is lighter and more often produced from squark decays. This is the only production which would give us a decent amount of Z bosons. Somehow for h the branching ratio for $\widetilde{\chi}_2^0 \rightarrow \widetilde{\chi}_1^0 h$ is zero and no Higgs are produced through this decay, which is clear from figure 4.13 (1). The number of h or Z coming from other sources ($\widetilde{\chi}_4^0$ or $\widetilde{\chi}_2^\pm$) is of the same rate and very low. This explains the relatively small number of h bosons (89) in this sample compared with the number of Z bosons (346).

We also have the possibility of having production through **s**top, which is produced from the pp collision, and directly decays into $\widetilde{t}_1$ and Z or h. This is suppressed by the fact that $\widetilde{t}_2$ is relatively seldom produced, as is shown in figure 4.15 (2).

4.4.4 Low mass - SU4

Figure 4.17 details some information about the mothers of the h and Z bosons in the $SU4$ mSUGRA point.

(1) h (2) Z
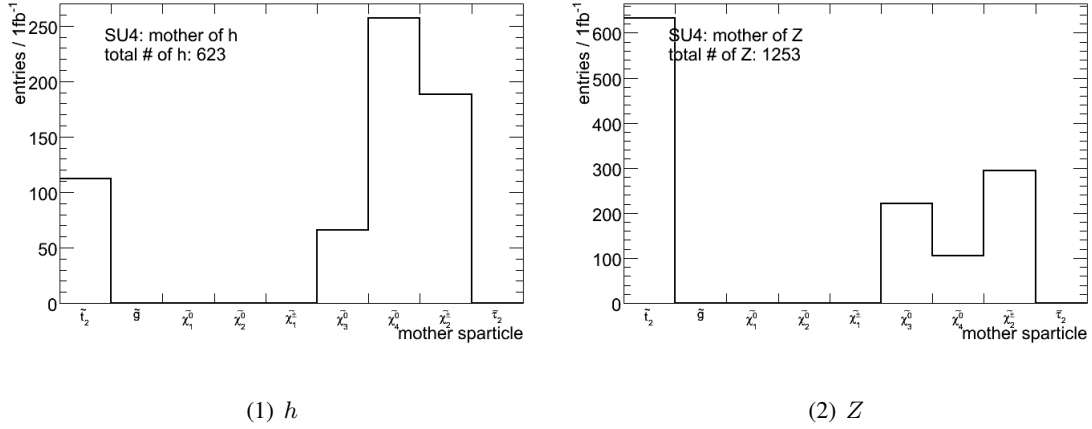
Figure 4.17: *The mother of the produced Z and h bosons in the signal sample $SU4$ for $1fb^{-1}$.*

There are twice more Z bosons (1253) produced in the $SU4$ sample than h bosons (623). Both h and Z are produced through decays of a stop, the heaviest neutralino ($\widetilde{\chi}_4^0$) or chargino ($\widetilde{\chi}_2^{\pm}$) or $\widetilde{\chi}_3^0$. While the Z most often has the stop as the mother the h often stems from the $\widetilde{\chi}_4^0$. The feynman diagrams in 4.18 show the dominant decays into h and Z in $SU4$.

(1) BR=0.16(Z)/0.12(h)   (2) BR=0.43(Z)/0.07(h)

(3) BR=0.20(Z, from $\widetilde{\chi}_3^0$)/0.14(h)   (4) BR=0.11(Z, from $\widetilde{\chi}_3^0$)/0.07(h)
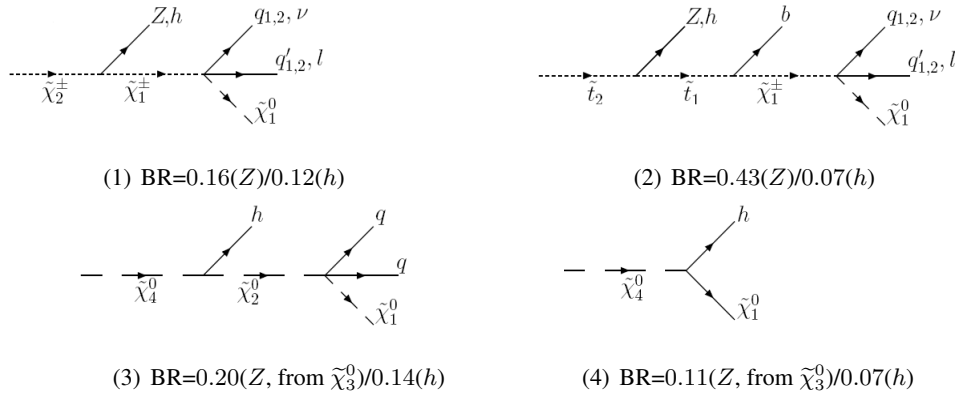
Figure 4.18: *The different diagrams for Z and h production in the signal sample $SU4$. (1) is probable both for h and Z production while (2) is dominant for Z production. The Z has similar diagrams (3) and (4) as h provided $\widetilde{\chi}_4^0$ is replaced with $\widetilde{\chi}_3^0$*

Like in $SU2$ the $\widetilde{\chi}_1^{\pm}$ and $\widetilde{\chi}_2^0$ mostly decay via 3-body decay into LSP and a quark-quark or a lepton-neutrino pair (only for chargino). The $\widetilde{\chi}_2^0$ could possible go into a lepton-lepton pair, but mostly decays into a quark-quark pair (BR=0.75). The same for $\widetilde{\chi}_2^{\pm}$, with a BR=0.65 into a quark-quark pair.

To know what kind of h/Z producing cascades we could expect in $SU4$ we look at the histograms, showing the initially produced sparticles from the pp collision, in figure 4.19.
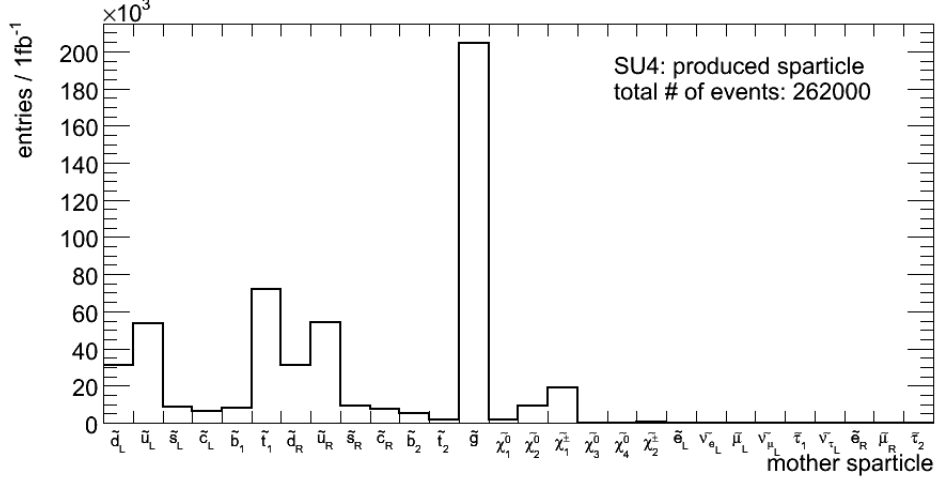
(1) sparticle produced
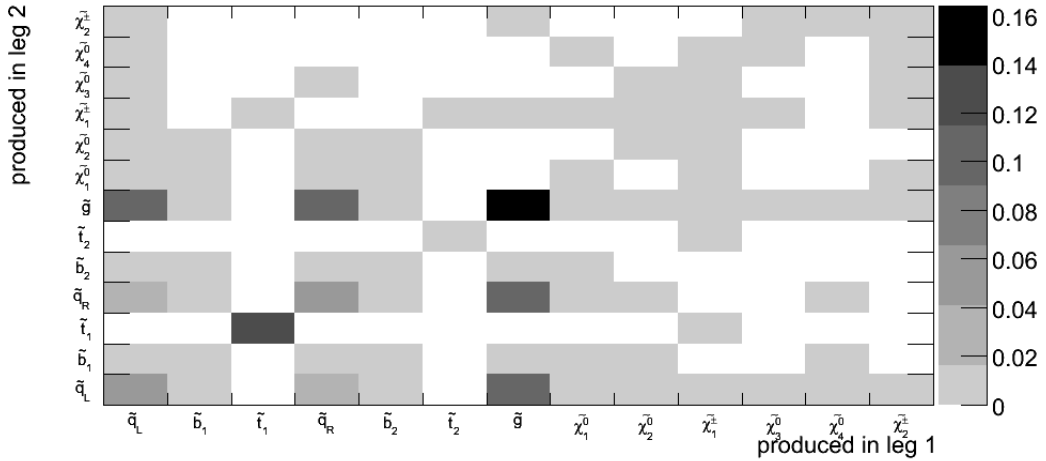
(2) sparticle pair produced

Figure 4.19: *(1): The multiplicity of the initially produced sparticles and (2): the various pairs of produced sparticles from each leg per event*

The $\widetilde{t}_2$ is the heaviest squark in $SU4$ and the only way to produce it is from the initially pp collision, which is not very probable (in $< 2\%$ of the events). To produce either the heaviest neutralino ($\widetilde{\chi}_4^0$) or chargino ($\widetilde{\chi}_2^\pm$) we need to have a gluino or squark produced from the pp collision. A gluino-gluino pair is the dominantly pair produced, but the gluino-squark is also relatively probable. It is

also a lot of $\tilde{t}_1$ pairs produced initially, but they always decay into a $\widetilde{\chi}_1^{\pm}$ and a quark, and are in that case not interesting for h searches. The dominant $\widetilde{\chi}_2^{\pm}$ or $\widetilde{\chi}_4^0$ production is through the decay of a left-handed down squark or a $\tilde{b}_2$. For all the other squarks the branching ratio for this decay is less than one percent. Either we need to have one of these squarks produced initially, which sometimes happens, or an initially produced gluino decays into a $\tilde{b}_2$ (BR ≈ 0.04, the branching ratio for a gluino decaying into a left handed squark however, is zero). This gives us the possible cascades shown in figure 4.20.

<div align="center">
(1) long chain, BR=0.04   (2) short cascade, BR=0.02
</div>
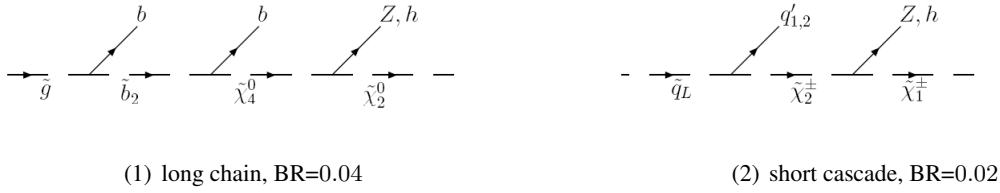
Figure 4.20: *Two of the main cascades of supersymmetric particles that lead to a h/Z production in $SU4$. The branching ratios for the first decay in each graph is presented. For the short cascade the only possibility is a down squark since the up squark has BR ~ 0*

By combining these graphs with the ones in 4.18 we can figure out the expected final states. The diagram in 4.18 (2) is a whole cascade, because the only way to produce $\tilde{t}_2$ is through direct production. The number of jets in the final state will again be different for the long and the short cascade. Both cascades will have two jets (or leptons) produced at the end of the cascade. The long cascade however will have two additional b-jets in the final state while the short cascade will have only a light flavored jet in addition. These jets might have higher p_T than the ones from the end of the cascade.

The conclusion is that the relatively high branching ratio for $\widetilde{t}_2$ to go into Z is the main difference between Z and h production. Both the short and the long cascade will give several jets or leptons, but these cascades are suppressed by the low branching ratio, as shown in figure 4.18.

4.4.5 Funnel - SU6

Figure 4.23 show the mothers of the h and Z bosons in the $SU6$ mSUGRA sample.

(1) h (2) Z
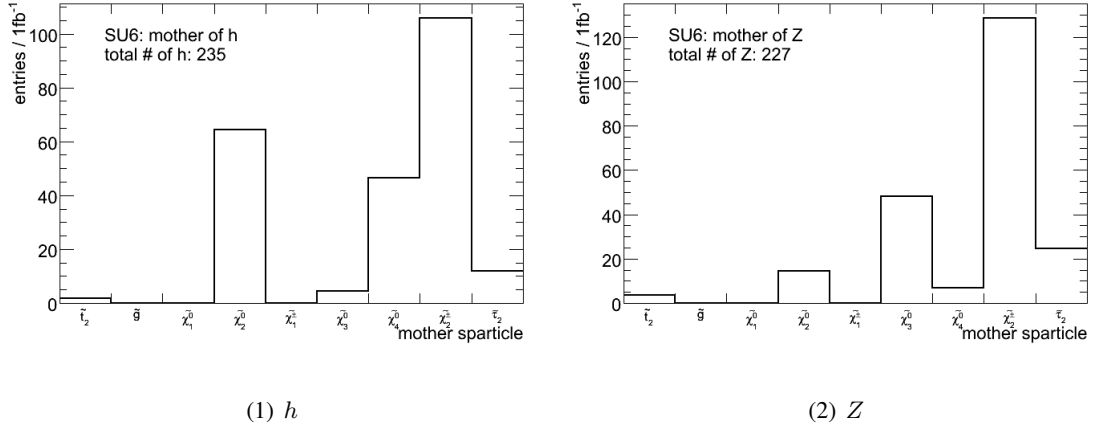
Figure 4.21: *The mother of the produced Z and h bosons in the signal sample $SU6$ for $1fb^{-1}$.*

There is almost the same number of h (235) and Z (227) bosons in the sample, and both are most often produced from the decay of the heaviest chargino ($\widetilde{\chi}_2^\pm$). For h boson production the decay of the heaviest neutralino ($\widetilde{\chi}_4^0$) or $\widetilde{\chi}_2^0$ is also important. For the Z boson the $\widetilde{\chi}_3^0$ decay contribute to the production. The production chains of the two bosons are shown in figure 4.22.

(1) BR=0.20(Z)/0.17(h)   (2) BR=0.15(Z, from $\widetilde{\chi}_3^0$)/0.15(h)

(3) BR=0.08(Z, from $\widetilde{\chi}_3^0$)/0.07(h)   (4) BR=0.01(Z)/0.04(h)
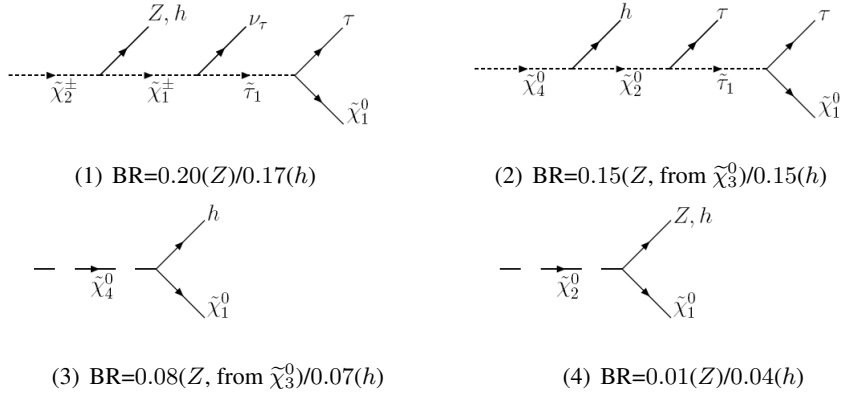
Figure 4.22: *The different diagrams for Z and h production in the signal sample $SU6$. The Z has similar diagrams (2) and (3) as h provided $\widetilde{\chi}_4^0$ is replaced with $\widetilde{\chi}_3^0$. The branching ratio for the first decay in each graph is presented.*

The production of a h or a Z boson often gives final states with two τs or one τ and a corresponding neutrino. In case of a direct decay of the heaviest neutralino or $\widetilde{\chi}_2^0$ into the LSP and h/Z, we do not get any additionally produced sparticles, illustrated in 4.22 (3) and (4).

Figure 4.23 shows the most common sparticles and sparticle pairs that are produced from the pp

collisions in the $SU6$ mSUGRA sample.
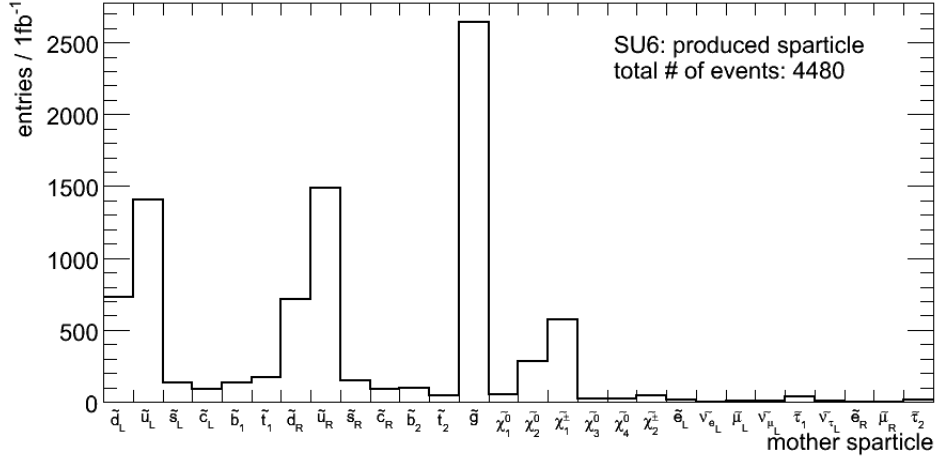
(1) sparticle produced
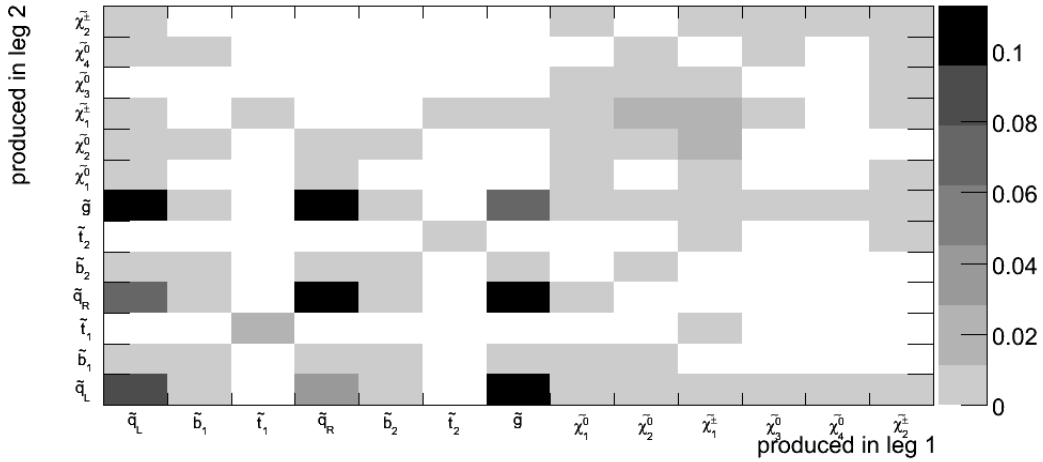
(2) sparticle pair produced

Figure 4.23: *(1): The multiplicity of the initially produced sparticles and (2): the various pairs of produced sparticles from each leg per event*

This shows more or less the same behaviour as in the $SU1$ scenario with gluino-gluino, squark-squark or squark-gluino production as the dominant produced pairs of sparticles.

In case of direct production of a right/left-handed 1st or 2nd generation squark pair we seldom get production of the heaviest neutralino ($\tilde{\chi}_4^0$) or chargino ($\tilde{\chi}_2^\pm$). Only in case of a left handed squark, there is a small branching ratio (between $0.01 - 0.05$) for this. However the decay into $\tilde{\chi}_2^0$ is large

(~ 0.30) and this could lead to the decay in 4.22 (4), although the branching ratio is small (~ 0.04 into h). As in the other scenarios a right handed **s**quark will in nearly 100% of the cases go into the LSP and a quark.

To get heavy gaugino production it is crucial to have at least one gluino produced in the pp collision. The gluino often decays into a 3rd generation **s**quark, which has a decent branching ratio into $\widetilde{\chi}_4^0$ ($0.06 - 0.20$) and $\widetilde{\chi}_2^\pm$ ($0.07 - 0.45$).

From this we can conclude that the dominant cascades producing a h or Z would be the ones in figure 4.24.

(1) long cascade, BR=0.78   (2) short cascade, BR=0.31
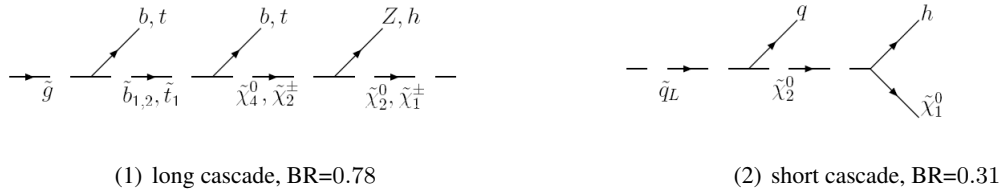
Figure 4.24: *Two of the main cascades of supersymmetric particles that lead to a h production in $SU6$. This is the same cascades as for $SU1$ in figure 4.8. The branching ratio for the first decay in each graph is shown.*

This is similar to what we had in the $SU1$ sample. However the probability of the two chains are different. In $SU6$ the long cascade in 4.24 (1) is more important than in $SU1$. In $SU6$ the long cascade will only produce 3rd generation leptons, in contrast with $SU1$ where we mostly get 1st and 2nd generation leptons. The short cascade is less probable in $SU6$ compared with $SU1$, which is mainly due to the difference in branching ratio for $\widetilde{\chi}_2^0 \to \widetilde{\chi}_1^0 h$ in the two scenarios.

While the long cascade will contain b or t quarks and often τs and neutrinos together with $\not{E}_T$ from the LSP, the short cascade will have only one light flavored jet together with $\not{E}_T$. The $\widetilde{b}_1$ in figure 4.8 (1) could also decay into a $\widetilde{\chi}_2^0$ (BR=0.28), which will give a long cascade, but without additional leptons or neutrinos.

4.4.6 Co-annihilation - SU8.2

Figure 4.25 details some information of the mother of the produced Z and h bosons in the signal sample $SU8.2$.
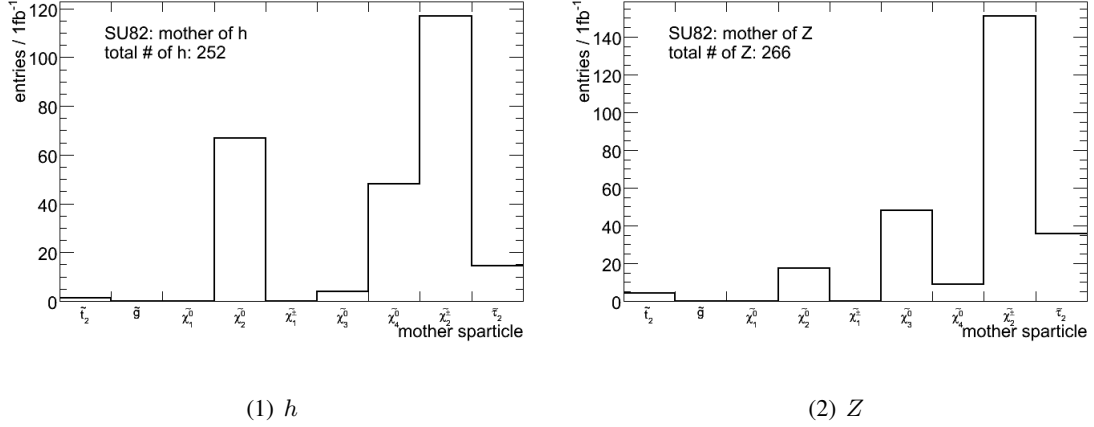
Figure 4.25: *The mother of the produced Z and h bosons in the signal sample $SU8.2$ for $1fb^{-1}$.*

This is very similar to what we had in $SU6$ and $SU1$ with the dominant sources of h from the decays of $\widetilde{\chi}_2^0$, $\widetilde{\chi}_4^0$ and $\widetilde{\chi}_2^\pm$. For Z production the neutralino decays are suppressed, with exception for a small amount from $\widetilde{\chi}_3^0$ the $\widetilde{\chi}_2^\pm$ dominates. The feynman diagrams for the dominant productions of h and Z are shown in figure 4.26.

(1) BR=0.21(Z)/0.17(h)   (2) BR=0.21(Z, from $\widetilde{\chi}_3^0$)/0.15(h)

(3) BR=0.08(Z, from $\widetilde{\chi}_3^0$)/0.06(h)   (4) BR=0.01(Z)/0.03(h)
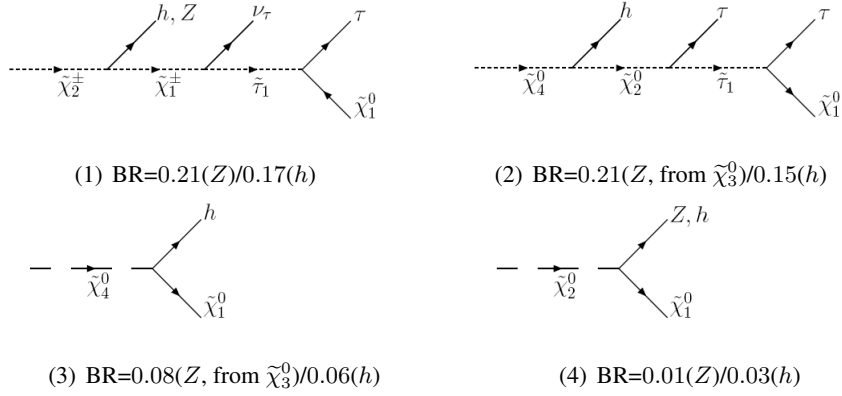
Figure 4.26: *The different diagrams for Z and h production in the signal sample $SU8.2$. The Z has similar diagrams (2) and (3) as h provided $\widetilde{\chi}_4^0$ is replaced with $\widetilde{\chi}_3^0$.*

In figure 4.26 (1) we see that in the case of a chargino as the mother sparticle of the h or Z boson we get signal final states with τs and $\not{E}_T$ (from the LSP and neutrino). The decay of $\widetilde{\chi}_2^\pm$ into $W^\pm$ and LSP is suppressed in this scenario, in contrast with the $SU3$ scenario. In case of a neutralino as the mother sparticle we can get the direct production (figure 4.26 (4)) of h or Z with only $\not{E}_T$ from the LSP in the final state. However we also have the more probable possibility of having a longer

cascades with production of two τs in addition to the h and the LSP, as in figure 4.14 (3).

To find the signature for the different final states with h or Z bosons we have to look at the initially produced sparticles and sparticle pairs from the pp collision. The histograms in figure 4.27 show this.
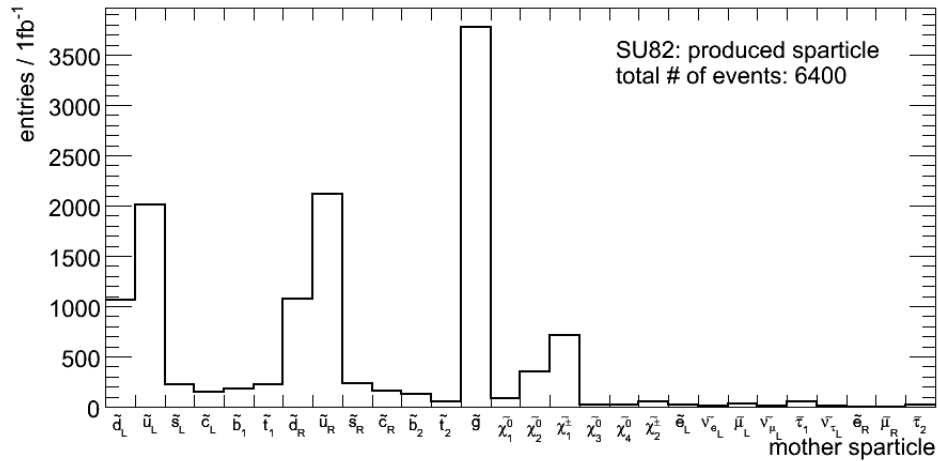
(1) sparticle produced
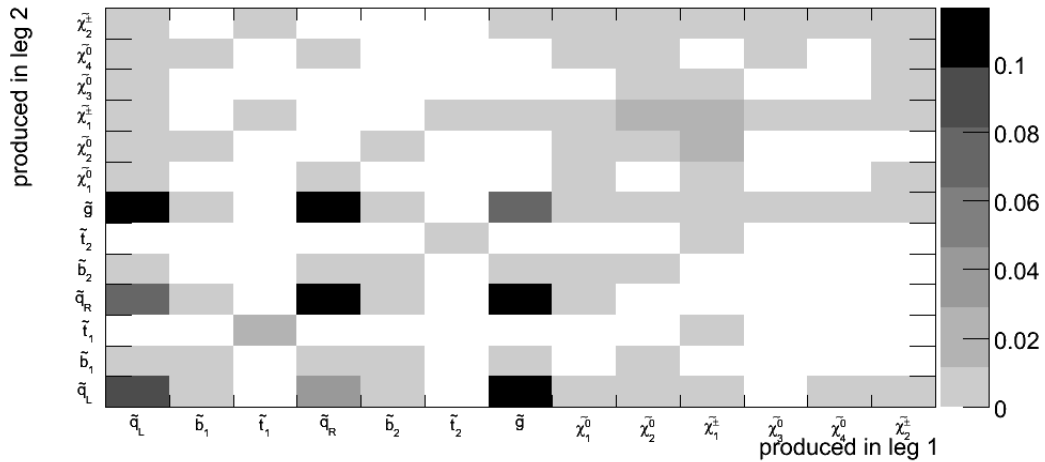
(2) sparticle pair produced

Figure 4.27: *(1): The multiplicity of the initially produced sparticles and (2): the various pairs of produced sparticles from each leg per event*

A gluino is the most probable particle to be produced from the pp collision. From 4.27 (2) it is clear that the most common pair of sparticles produced is a gluino-squark pair. The gluino will most

often decay to a **s**bottom-bottom, **s**top-top or right-handed 1st or 2nd generation **s**quark-quark pair. The latter production, as earlier described, is not interesting for this analysis, because of a branching ratio close to 1 for going directly to a quark and the LSP. However the production of **s**bottom and **s**top is interesting, as they further will decay into $\widetilde{\chi}_2^{\pm}$ or $\widetilde{\chi}_2^0$ and a quark. In case of the **s**bottom quark, decays into the heavier neutralinos ($\widetilde{\chi}_3^0$ and $\widetilde{\chi}_4^0$) are possible.

There is also a decent production of left-handed **s**quarks from the pp collision. These may further decay into a $\widetilde{\chi}_2^0$ and a quark, but only with a branching ratio of about 0.05. They will mostly go into lighter charginos ($\widetilde{\chi}_1^{\pm}$) or neutralinos ($\widetilde{\chi}_1^0$) together with a quark.

From this discussion we can conclude that the main cascades for h or Z production in the $SU8.2$ mSUGRA point will be the cascades in figure 4.28.

        (1) long cascade, BR=0.45   (2) short cascade, BR=0.31
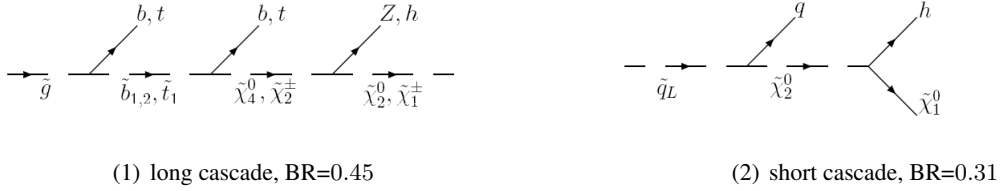
Figure 4.28: *Two of the main cascades of supersymmetric particles that lead to a h production in $SU8.2$. This is similar cascades as for $SU1$ and $SU6$, but with different branching ratios. The branching ratio for the first decay in each cascade is presented.*

This is exactly the same cascades as in the $SU1$ and $SU6$ scenarios. The probability of the long cascade in $SU8.2$ is smaller compared with $SU6$, but is almost the same as in $SU1$. The short cascade has approximately the same probability in both $SU6$ and $SU8.2$.

The long cascade will contain b or t quarks and often τs and neutrinos together with $\not{E}_T$ from the LSP while the short cascade will have only one light flavored jet together with $\not{E}_T$.

4.4.7 Higgs - SU9

Figure 4.29 details some information about the mother of the produced Z and h bosons in the signal sample $SU9$.

(1) h (2) Z
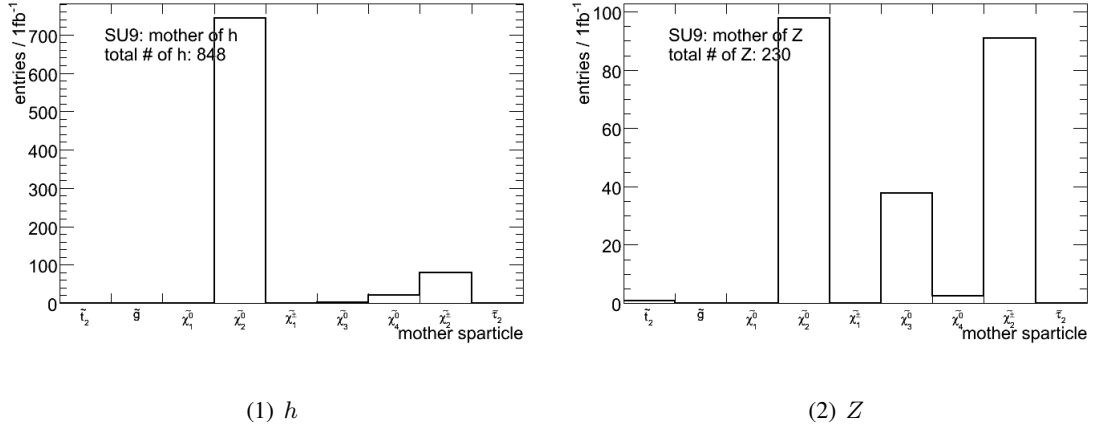
Figure 4.29: *The mother of the produced Z and h bosons in the signal sample $SU9$ for $1fb^{-1}$.*

The $SU9$ mSUGRA point is made especially for Higgs analysis, which means that the branching ratio for $\widetilde{\chi}_2^0 \rightarrow \widetilde{\chi}_2^0\,h$ is relatively large (~ 0.86) compared with the other samples. It is clear from the histogram in figure 4.29 (1) that nearly all the h bosons in the sample come from the decay of $\widetilde{\chi}_2^0$, which give us the same process as in figure 4.26 (4). The number of h bosons (848) in $1fb^{-1}$ in the sample is also much higher compared with the other samples. For Z boson production the decay of $\widetilde{\chi}_2^0$ (the Z-version of the one in figure 4.26 (4)) and the decay of $\widetilde{\chi}_2^\pm$, are the dominant production processes. However the number of Z bosons in the sample is very small (230) compared with the number of hs (848). The decay of $\widetilde{\chi}_2^\pm$ will in this scenario decay into $W^\pm$ and the LSP, like in figure 4.14 (2). The $W^\pm$ could either decay into a lepton-neutrino, lepton-antilepton or a quark-quark pair, giving us the possible final state with $\not{E}_T$ (from the LSP and sometimes from a neutrino) and leptons/quarks. This process is important for Z production only.

The histograms in figure 4.30 show the produced sparticles and sparticle pairs from the pp collision in $SU9$. This is very similar to what we had in the $SU8.2$, $SU6$ and $SU1$ mSUGRA points.
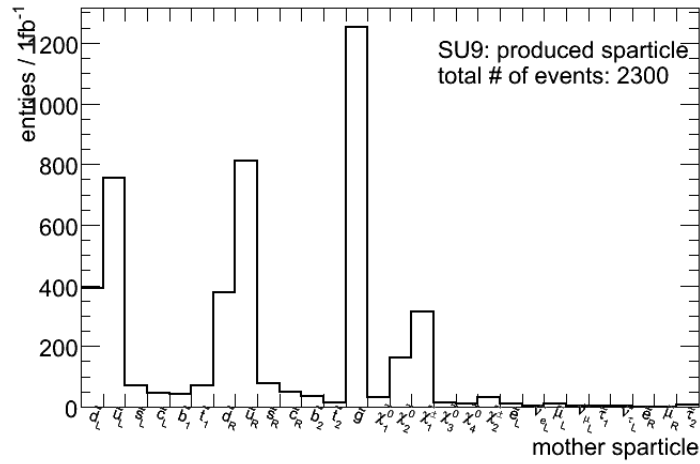
(1) **s**particle produced
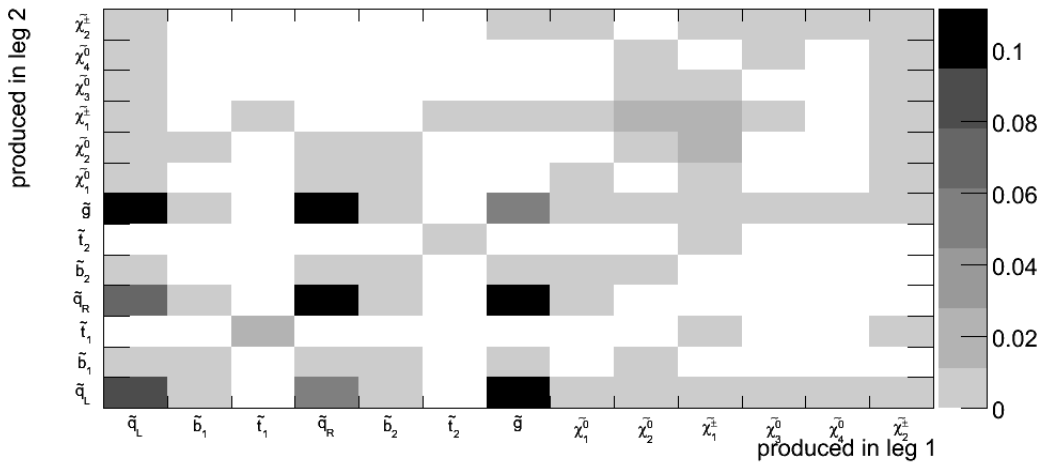
(2) **s**particle pair produced

Figure 4.30: *(1): The multiplicity of the initially produced sparticles and (2): the various pairs of produced sparticles from each leg per event*

The most probable is to have an initial gluon which always decays to a **s**quark-quark pair. In case of a right-handed **s**quark it decays further to a neutralino (mostly $\widetilde{\chi}_2^0$) and a quark. Still the branching ratio for a right handed **s**quark is nearly 1 into a quark and the LSP, so it is not interesting in this analysis. From this we can conclude that the far most dominant cascade leading to a h boson will be the cascade in figure 4.31.
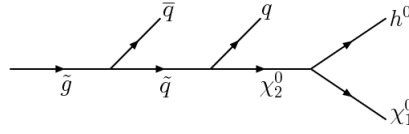
Figure 4.31: *The main cascades of supersymmetric particles that lead to h production in $SU9$. BR= 0.67 for the gluino to decay into a left handed **s**quark or a third generation **s**quark.*

Dependent on whether we get an initially produced gluino (long cascade) or **s**quark (short cascade) these cascades will have final states with one or two jets together with $\not{E}_T$ from the LSP. It will almost never be leptons in the final state with Higgs in this scenario, although it could of course come from the other leg.

4.4.8   Summary

Table 4.5 and 4.6 summarize section 4.4.1-4.4.7. In table 4.5 the probability of production of various pairs with gluinos and $\widetilde{q}_L$ are presented. When a gluino is initially produced it will give a possible long cascade with Higgs production while the production of a $\widetilde{q}_L$ will give a short cascade. In table 4.6 is the typical final states in the various signal samples presented. The fraction of Higgs production from the different cascades are given in parentheses.

Event category	$SU1$	$SU2$	$SU3$	$SU4$	$SU6$	$SU8.2$	$SU9$
$\widetilde{g}\,\widetilde{g}$	0.07	0.10	0.07	0.16	0.07	0.07	0.06
$\widetilde{g}\,\widetilde{q}_L$	0.21	0.00^5	0.22	0.21	0.21	0.21	0.20
$\widetilde{q}_L\,\widetilde{q}_L$	0.08	0.09^5	0.08	0.04	0.08	0.09	0.09
$\widetilde{q}_L\,\widetilde{q}_R$	0.11	0.00	0.11	0.06	0.11	0.12	0.12

Table 4.5: *The fraction of various **s**particle pairs produced in the different signal samples. A gluino will most often create a long cascade while a $\widetilde{q}_L$ will make a short cascade*

---

[5] since the **s**quarks are extremely heavy in $SU2$ the production ratio of $\widetilde{g}\,\widetilde{\chi}_4^0 + \widetilde{g}\,\widetilde{\chi}_2^\pm$ is presented in-stead of the $\widetilde{g}\,\widetilde{q}_L$ production ratio, and the production ratio of $\widetilde{\chi}_2^\pm\,\widetilde{\chi}_4^0$ are shown in-stead of the ratio for $\widetilde{q}_L\,\widetilde{q}_L$ production.

Event category	$SU1$	$SU2$	$SU3$	$SU4$
long	$b,t + l/\nu$ (0.57)	$t,b,q + l/\nu$ (0.20)	$t,b + l/\nu$ (0.84)	b,b,q,q (0.52)
short	q (0.41)	$b,q + l/\nu$ (0.80)	$q + l/\nu$ (0.15)	$b/q + qq/l\nu$ (0.30)

Event category	$SU6$	$SU8.2$	$SU9$
long	$b,t + \tau,\nu$ (0.66)	$b,t + \tau,\nu$ (0.65)	$b, b/q, q$
short	q (0.28)	q (0.26)	q

Table 4.6: *The typical final states in the different scenarios and the ratio of Higgs production through each of the cascades. The separation for $SU9$ is more difficult.*

Chapter 5

Signal and background analysis

In this chapter the goal is to illustrate the techniques and challenges of picking out a $h \rightarrow b\bar{b}$ decay in the different mSUGRA models. All relevant Standard Model backgrounds will be studied in order to see how they differ from the signal. Comparison of signal and background will constrain the value of some measurables in order to reduce the background, hopefully without removing too much signal.

In chapter 4 we saw what would characterize the h final states in each of the signal scenarios. These typical signatures would always contain large missing transverse energy, at least two bs coming from Higgs decay and high p_T jets. However these signal signatures are not unique and there are both Standard Model and SUSY processes that would give very similar final states as the ones discussed.

5.1 Supersymmetric background

From chapter 4 it is clear that SUSY events will contain a lot of b-jets from other sources than h. Gluinos often decay into a $\widetilde{b}_{1,2}b$ pair, which lead to high p_T b-jets. A sbottom quark further decays into a $\widetilde{\chi}^0_{1,2,3,4}$ and a b-quark. It can also decay into a chargino and top or a stop and a $W^{\pm}$, which also will lead to b-jets, since the stop quark may decay into $\widetilde{\chi}^{\pm}_{1,2}, b$ and top mostly decays into $W^{\pm}, b$. The decay of the heavy SUSY Higgs bosons could also decay into b-quark pairs, since the decay into SM gauge bosons are suppressed [11]. These decay channels will be the main sources of high p_T b-jets in SUSY cascades. However b quarks could also stem from Z or $W^{\pm}$ which also are produced in SUSY cascades.

It is clear that all SUSY cascades will lead to the production of a LSP and several hard jets. This is therefore nothing special with the Higgs cascade signature, but common for all SUSY cascades.

5.2 Standard Model background

There are a lot of different Standard Model processes which could be possible background for the interesting SUSY events which were discussed in the last sections. At the production stage[1] the SM backgrounds are divided into different groups, some of which have some *pre selection-cuts* already applied at the generator level (see appendix A for details). The most important backgrounds for this analysis are mentioned below.

5.2.1 $Z + bjets$

Associated production of a Z boson with a b-jet. It is an important background to various processes, including Higgs and SUSY searches, since it contains b-jets such as those stemming from Z decays. In cases where Z decays into a neutrino pair, this will lead to possible final states with both $\not{E}_T$ and b-jets.

5.2.2 WW

This sample has at least two Ws produced where the Ws can decay both leptonically and hadronically. In case of a full hadronic decay both Ws decays to a quark pair. BR($W^\pm \to \bar{q}q'$) $\sim 66\%$ [16]. This will give final states with four jets and no leptons. In case of a full leptonic decay both Ws decay into a lepton-neutrino pair. BR($W \to l\nu$) $\sim 33\%$ [16]. This will give two neutrinos, zero jets and two leptons in the final state. The final possibility is when one of the Ws decays into two quarks and the other into a lepton-neutrino pair. This gives a final state with a neutrino, two jets and a lepton.

5.2.3 ZZ

The Z can decay into two charged leptons, two neutrinos or a $q\bar{q}$ pair with the following branching ratios BR($Z \to q\bar{q}$) $\sim 69\%$, BR($Z \to \nu\nu$) $\sim 21\%$ and BR($Z \to l^+l^-$) $\sim 10\%$. These different decays will have possible neutrinos, leptons or quarks produced. Moreover, Z can decay to $b\bar{b}$.

5.2.4 WZ

Combinations of the decays in 5.2.2 and 5.2.3 above will give final states with possible b-jets, leptons and neutrinos.

---

[1]Monte Carlo simulations

5.2.5 $\mathbf{Z}(\rightarrow \mathbf{l}^+\mathbf{l}^-) + \mathbf{X}$

Production of one Z boson and X, where the Z decays into two charged leptons. X will be a system of particles without any special requirements. This will give final states with at least two leptons.

5.2.6 $\mathbf{Z}(\rightarrow \nu\nu) + \mathbf{X}$

Production of one Z boson and X, where the Z decays into two neutrinos. X will be a system of particles without any special requirements. This will give final states with at least two neutrinos.

5.2.7 $\mathbf{W}(\rightarrow \mathbf{l}^{\pm}\nu) + \mathbf{X}$

Production of one W boson and X, where the W decays leptonically. X will be a system of particles without any special requirements. This will give final state with and at least one lepton and one neutrino.

5.2.8 $\mathbf{t}\bar{\mathbf{t}}$

The BR($t \rightarrow Wb$) $\sim 100\%$ [16]. From section 5.2.2 we saw that the W can decay leptonically or hadronically. This will give a similar possible final state as for the WW background, in addition to two b-jets. The two different $t\bar{t}$ samples are:

$t\bar{t}$: all hadronic (i.e both Ws decay into quarks

$t\bar{t}$: not all hadronic (i.e one of the Ws decays into a lepton-neutrino pair while the other could decay into a lepton-neutrino or a quark pair)

5.2.9 Multi jet events

These samples could be produced in a lot of different ways, and contains many quark jets produced through strong interactions. These processes have very high cross section at LHC. In appendix A the properties of the different background samples within this category used in the analysis are defined.

5.3 Which cuts?

To conclude with a set of cuts to be used in the final analysis, one has to take the effect of the cuts on the rejection of Standard Model background and other SUSY background events into account. This is

done in the following sections by combining reconstructed events and truth information (see section 5.3.2).

5.3.1 Significance

The significance of the signal is an important quantity when studying the effect of cuts. One define the number of signal events S and the number of background events B. The significance of a signal is then calculated by the following formula

$$s = \frac{S}{\sqrt{B}},$$

which is valid as long as $S \ll B$. In the following analysis two significances are calculated. One is the total significance while the other counts only the S and B events in a ± 25 GeV mass window around the Higgs mass position.

In a real situation (i.e in real data) the separation into S and B is only possible once a peak is found and fitted and thereby gives the possibility to compute the significance.

In this study we operate with significances without looking at graphs, simply looking at truth and counting. This is of course fine since this is a simulation. Looking at the significance is the best way to find good cuts. However this method will be more problematic in the real world, since then we only have the significance as guide when some peak structure are present.

Of course, only when we have a peak we can choose the range of the significance calculation in case of real data. In this study we know the theoretically value of the Higgs mass and can use this to set a mass window. Of course, in case we observe a significant $h \rightarrow b\bar{b}$ signal, we will try to fit the mass and the width.

5.3.2 From truth to reconstruction

The truth information used in section 4.4.1-4.4.7 in chapter 4 and in the following is Monte Carlo generated events using the HepMC package [6]. The generated events with the truth information are then matched to the reconstructed events after they have been fully simulated by different methods taking into account the detector performance, material effect etc. The matching is done by looping through all the true b-jets coming from Higgs to find the closest reconstructed jet. If the distance $\Delta R = \sqrt{(\Delta\phi)^2 + (\Delta\eta)^2}$ (see section 3.1.1) between the reconstructed and the true jet is less than 0.4, they are matched.

5.3.3   Event categories

In the analysis on truth the events in the SUSY Higgs samples are divided into 3 main categories.

1. **signal events (SG)**: events with only $b\bar{b}$ pair(s) from Higgs where both of the b-jets are reconstructed. These events will not contain other b-jets, but will have other light jets from decays in the cascade.

2. **uncorrelated bs events (COMB)**: events with $b\bar{b}$ pair(s) from Higgs together with b-jets from other sources. Although these events contain Higgs it will become a noise because the combined b-pairs is not necessarily from Higgs. Contains also events where only one of the b-jets from a Higgs decay is reconstructed.

3. **SUSY BG events (BG)**: b events without any Higgs.

In the following analysis $SU3$ and $SU4$ are not included in the truth analysis, since $SU3$ has very few Higgs bosons and the cascade pattern is very similar to $SU6$ and $SU8.2$. $SU4$ is omitted for the same reason.

5.4   The characteristics of $h \to b\bar{b}$ events

From the previous section it is clear that there are some specific properties characterizing a h final state. First of all the presence of at least two b-jets from the decay of Higgs is crucial. Table 5.1 shows the number of events in each of the three categories, defined in section 5.3.3, for the different signal samples for $10 fb^{-1}$ with a b-tagging efficiency of 60%. It also shows the total number of Higgs (regardless of the decay product) before reconstruction (from section 4.4.1-4.4.7). For comparison the total number of Higgses decaying into $b\bar{b}$ after the reconstruction, where both b-jets are tagged, is also presented. The ratio, between the total number of truth h and the number of reconstructed $h \to b\bar{b}$ is approximately 0.25 for all scenarios. This stems mainly from the b-tagging efficiency ($\varepsilon_{tag} = 0.6$ per b-jet), BR($h \to b\bar{b}$) ≈ 0.80 and the reconstruction efficiency ($\sim 70 - 95\%$ [1]).

	$SU1$	$SU2$	$SU6$	$SU8.2$	$SU9$
# of all h	3040	1110	2350	2520	12167
# of $h->b\bar{b}$	597	166	456	471	2207
Event category					
signal	310	108	161	203	1270
uncorr. bs	1513	473	1213	1296	5343
SUSY BG	72477	48018	43425	62498	26386
total events	74300	48600	44800	64000	33000

Table 5.1: *The upper row shows the total number of Higgs (regardless of the decay product) from truth, while the second row gives the number of reconstructed h which decays into a tagged $b\bar{b}$ pair. The remaining rows show the number of events in each category for the various signal samples before any cuts are done and with a b-tagging efficiency of 60%. All numbers are shown with an integrated luminosity, $\mathscr{L} = 10fb^{-1}$.*

The plots in figure 5.1 and 5.2 show the invariant mass distributions of reconstructed b pairs for the different types of SUSY events, in the two scenarios $SU1$ and $SU9$ respectively.

The invariant mass plots in (1) contain only $b\bar{b}$ pairs from Higgs, so this plot should only contain correct combinations. Sometimes it is produced two Higgs bosons in one event, which will lead to four possible wrong combination in the distribution in (1). However this is very rare ($\sim 0.1\%$ of the events), and are only present in the $SU9$ scenario. The event is in this case counted as a *only Higgs* event, although it may contain some wrong combinations of bs. The distributions in (1) are fitted with a gaussian to show the invariant mass resolution in the two cases. The fitted mass and resolution are found to be around 101 GeV and 16 GeV respectively, in both scenarios. The small tail at high p_T is most probably due to reconstruction inefficiencies, such as the possible big difference between the p_T of the reconstructed and true jet [1]. As already discussed some of the tail in $SU9$ may come from wrong combinations due to two Higgses in one event.

The distributions in (2) show the M_{bb} in events with $b\bar{b}$ pairs from Higgs together with other b-jets. This distribution is much broader than in (1) due to combinations with one b-jet from Higgs and another b from a different source. It would also contain combinations of two b-jets where none of them stem from Higgs. Nevertheless it is possible to see a small signal above the combinatorial

background, reflecting that Higgs often is produced together with other b-jets.

The distributions in (3) contains no Higgs into $b\bar{b}$ and will be purely combinatorial SUSY background. As expected these distributions are very broad since SUSY cascades often will contain a lot of b-jets, as discussed in section 5.1. Especially for $SU1$ this background will be very challenging in the search for the lightest SUSY Higgs.

Table 5.1 and the invariant mass distributions show, as expected from section 4.4.1-4.4.7, that

| (1) signal events | (2) uncorrelated b events | (3) SUSY BG events |
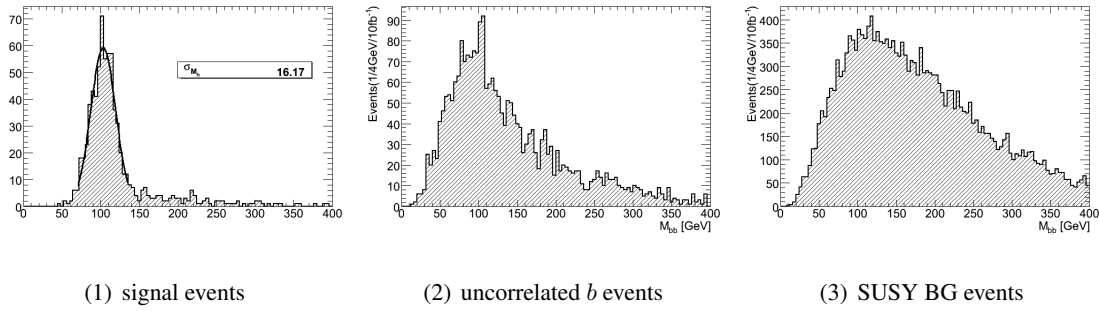
Figure 5.1: *Invariant mass of reconstructed bb pairs in the different categories of SUSY events in the $SU1$ scenario.*

| (1) signal events | (2) uncorrelated b events | (3) SUSY BG events |
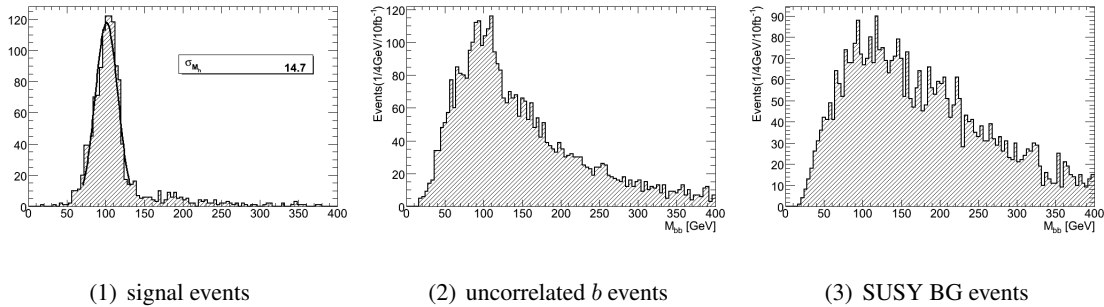
Figure 5.2: *Invariant mass of reconstructed bb pairs in the different categories of SUSY events in the $SU9$ scenario.*

$SU9$ has a lot of *"only Higgs"* events. The most probable cascades in $SU6$ (figure 4.24) and $SU8.2$ (figure 4.28) often have at least one b-jet produced early in the cascade. This is reflected in the ratio between the number of *"uncorrelated bs"* events and the number of *"only Higgs"* events. Since both cascades are relatively probable in $SU1$ (ratio: 4.9), the ratio is more similar to the one for $SU9$ (4.2). For $SU6$ (7.5) and $SU8.2$ (6.4) the long cascade dominates and often produces b-jets, early in the cascade. Therefor the ratios are higher compared to $SU1$ and $SU9$.

CUT #	VALUE
CUT 1	$\not{E}_T > 100\,\text{GeV}$
CUT 2	2 jets $p_T^{1,2} > 100, 50\,\text{GeV}$

Table 5.2: The starting cuts for this analysis, to ensure that all the various background and signal samples start with the same cuts.

In all scenarios we will have both the long and the short cascade, but with different probabilities. Especially $SU6$, $SU4$ and $SU8.2$ would have mostly the long cascade with additional b-jet production. $SU9$ is dominated by the long cascade, since $m_{\tilde{g}} > m_{\tilde{q}}$. $SU1$ will have decent amount of both types of cascades, while $SU2$ will have both long and short cascades, with and without b-jets. $SU3$ also has both long cascades, with additional b-jets, and short cascades. However the multiplicity of Higgs bosons in this sample is very low.

Because of these differences between the samples it could be necessary to have two strategies, one which would favor the long cascades and one which would be good in the case of short cascades. However this could also be difficult since non of the scenarios have only long or only short cascades.

In the following studies the $SU9$, which is dominated by the long cascade, $SU2$ which is dominated by cascades with high jet multiplicity, $SU1$ which has both long and short cascade with and without leptons and $SU6$ and $SU8.2$ which is dominated by long cascades with high p_T b-jets and possible τs and neutrinos, are investigated as examples of the different cascade patterns.

5.5   Background rejection

In appendix A the different backgrounds used in this analysis are defined. For some of the background samples some pre-selection cuts were applied at the generator level. What kind of cuts that is used varies from sample to sample. To be able to compare the different backgrounds and signals we therefor apply some similar *pre-selection-cuts* to be used from the beginning. The *pre-cuts* used here are presented in table 5.2.

To reduce the Standard Model background an important quantity is the missing transverse energy, which mostly will be much higher in SUSY events than in SM events. This is because the Lightest Supersymmetric Particle (LSP) ($m \sim 100\text{GeV}$), in R-parity conserving SUSY scenarios, will be stable and leave the detector without any measurements of its energy or momentum. Since two LSPs

will always be produced in a SUSY event, the $\not{E}_T$ signature is very typical for SUSY events. The only source of missing energy in the SM is the very light neutrinos ($m_\nu < 0.02$GeV). Inefficiencies and other detector effects will also contribute to the missing transverse energy, so a good understanding of the detector is crucial for reliable $\not{E}_T$ measurements [1]. Figure 5.3 shows the $\not{E}_T$ distribution for $SU9$ together with the SM background[2]. All the SM backgrounds are more peaked at low values, but some samples have a tail due to neutrinos and mis measurements of jets.

By combining the fact that SUSY events have large missing transverse energy and high mul-
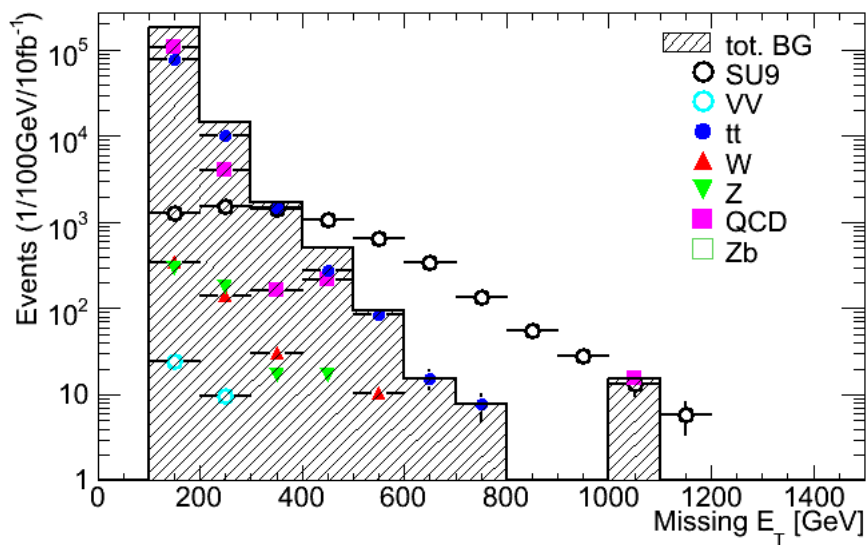
Figure 5.3: *The $\not{E}_T$ distribution for the $SU9$ and the Standard Model background. As expected the $SU9$ peaks at higher values and has longer tails than most of the Standard Model backgrounds. The Standard Model backgrounds with most $\not{E}_T$ are the W, Z and $t\bar{t}$ samples, where the decay of the vector bosons and Ws from top involves neutrinos.*

tiplicity of high p_T jets a variable called effective mass, M_{eff}, is used. This variable sums up all the missing energy, and the momentum of the jets per event. In practice only the four hardest jets per

---

[2]at high $\not{E}_T$, where the statistics is low we get some background events, which look visually a bit strange. This is most dominant for the QCD and top backgrounds. Since the both have large cross sections and because of the limitations on the number of generated events in these samples they need to be scaled with a relatively high scale factor to correspond to $10fb^{-1}$, such that one event eventually become fifteen events. A fluctuation in the limited data sample causes an unnaturally large background in bin (1000,1100) in figure 5.3 This is also the case in some of the distributions shown later.

event are used:

$$M_{eff} = \sum_{i}^{N_{jets}} p_T^i + \sum E\!\!\!/_T,$$ (5.1)

where N_{jets} is the number of jets. This will be much higher in SUSY than in SM events, both because of much $E\!\!\!/_T$ and high multiplicity of high p_T jets in SUSY events. Figure 5.4 shows the distribution of M_{eff} for $SU9$ and the SM background, using formula (5.1) for only the four hardest jets (right) and using all jets in the event (left). It is clear that the difference between these two methods are illustrated in figure 5.4 in the left and right histogram respectively. It is clear that the difference between the two methods is small, so in the following only the four hardest jets will be used in the M_{eff} calculation (eq. (5.1))

Another way to combine different properties is the $E\!\!\!/_T / M_{\text{eff}}$ variable, which is the ratio between
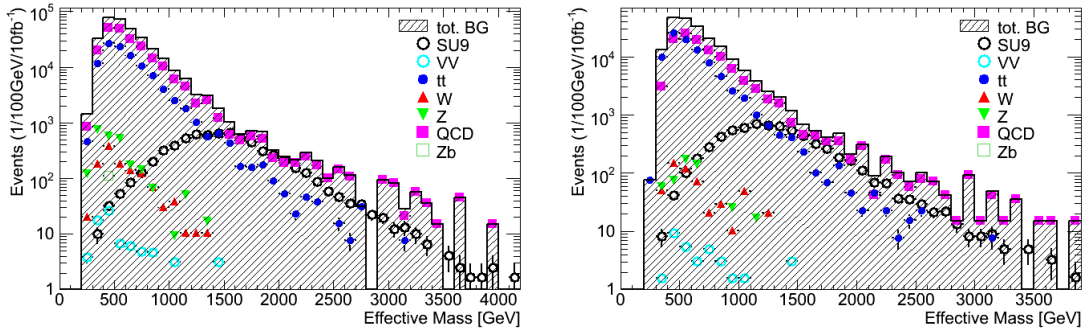
Figure 5.4: *The M_{eff} distribution for $SU9$ and the Standard Model background. Right: just the four hardest jets are used in the calculation. Left: all jets are used. There is a clear difference between the SUSY signal and the Standard Model backgrounds. The peak for the signal is at higher values than for all the SM background. The QCD has very long tails due to the high jet multiplicity. But as illustrated in figure 5.3 much of the QCD background could be removed by using the $E\!\!\!/_T$ signature.*

the missing transverse energy and the effective mass. This variable can be used to specify how much of the total transverse energy that should come from $E\!\!\!/_T$ and how much from M_{eff}. The histogram in figure 5.5 shows the distribution of $E\!\!\!/_T / M_{\text{eff}}$ in the $SU9$ scenario and for the Standard Model background.
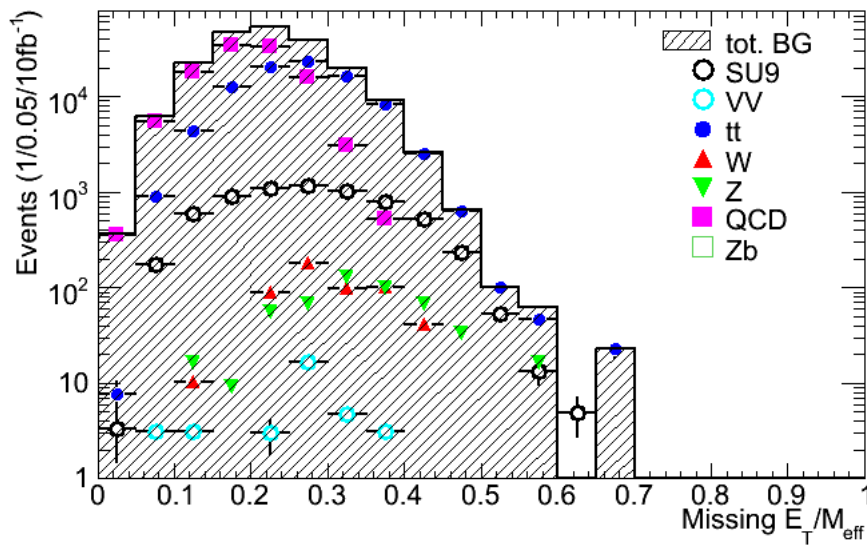
Figure 5.5: *The distribution for $\not{E}_T/M_{\text{eff}}$ for $SU9$ and SM background. Only the four hardest jets are used in the M_{eff} calculation. This variable reflects what is illustrated in figure 5.3 and 5.4. The samples that contain many high p_T jets will peak at low values while the samples which is dominated by $\not{E}_T$ will peak at higher values. (Since SUSY events have much of both jets and $\not{E}_T$ the distribution is more or less flat between $0.15 - 0.4$)*

5.6 Lepton and jet definitions

For a reconstructed lepton[3], an important question is whether it comes from the hard interaction process, or from a heavy flavor jet. From the reconstruction of the events it could also happen that one object in fact is reconstructed as both a jet and an electron. In this case it is important to remove the jet from the event, because this jet would not correspond to a real jet. In all the following studies only jets with $p_T > 20$ GeV and $|\eta| < 2.5$ are used. For the leptons only those with $p_T > 10$ GeV and $|\eta| < 2.5$ are used. In addition there is a requirement on the leptons that the isolation energy in a cone of $\Delta R < 0.2$ around the lepton should be less than 10 GeV [3]. If the leptons and jets fulfill these requirements there is a certain prescription to further define *primary* (leptons from the hard interaction) and *secondary* leptons (leptons from a jet) [3]. A lepton is per definition from a jet (*secondary*) if the distance ΔR between the jet and the lepton is less than 0.4 [3]. Only primary leptons will be used in a possible lepton veto cut in this analysis.

To handle the fact that one object can be reconstructed as both an electron and a jet an *electron jet overlap removal* test is used: If the distance ΔR between the jet and the electron is less than 0.2 the jet is thrown away while the electron is kept. In all the data samples used here a muon and a jet is never reconstructed as the same object (i.e. the *overlap removal* test is not necessary) [3].

5.6.1 Jet flavor definitions

It is important to define how to pick out b-jets from all the jets in the event, since b-jets are important for this study. As was discussed in chapter 4.3 this is a difficult task, and before the LHC starts up and the detector is not well understood it is difficult to say anything exactly about the capability to tag b-jets in ATLAS. In this study a b-tagging efficiency of approximately 60% per b-jet is used ,[4] which is around what is expected in ATLAS and used in most studies [1]. From the plot in figure 5.6 (1), an efficiency of 60% will correspond to $W_{IP3D+SV2} \geq 6$. The mistag and rejection of light jets is then according to the plots in 5.6 (2) and (3) respectively. It shows that the rejection for an efficiency of 60% is approxemantly 40 while the corresponding mistag ratio is 0.025. In ATLAS, with a b-tagging efficiency of 60% it is expected to have a rejection against light jets above 100, while the rejection against c-jets are only around 10 [1]. Since the plots in figure 5.6 show the rejection against all jets (also c-jets) other than b-jets, this value is somehow smaller than this. In the following study these jet

---

[3] a lepton means in the following an electron or a muon or their antiparticles

[4] that means an efficiency of 36% for each b-jet pair
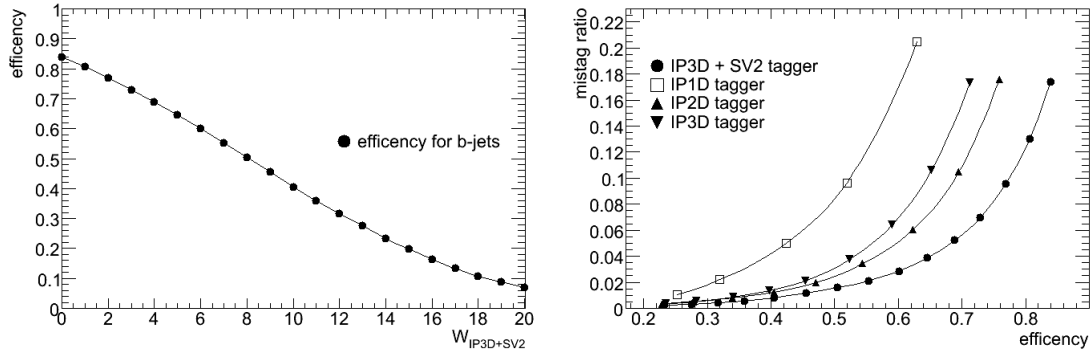
(1) efficiency vs. $W_{IP3D+SV2}$

(2) mistag vs. efficiency
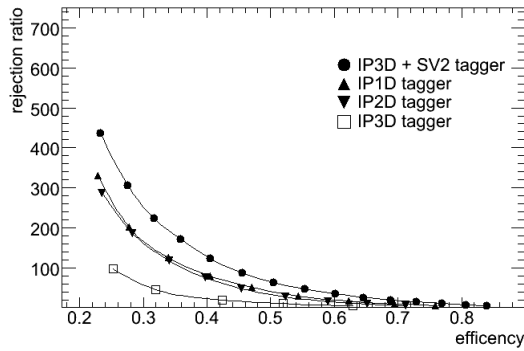
(3) rejection vs. efficiency

Figure 5.6: *(1): The efficiency of b-tagging as a function of the $W_{IP3D+SV2}$. (2) and (3) the mistag/rejection of light jets as a function of efficiency for different types of taggers. As expected the tagger which combine the $IP3D$ and $SV2$ tagger has the best performance. These plots are for the $SU9$ sample, however the same b-tagging performance is achieved with the same value on $W_{IP3D+SV2}$ in the other samples.*

definitions are used

- *light flavored jet (or light jet)*: A jet with $W_{IP3D+SV2} < 6$

- *b-jet*: A jet with $W_{IP3D+SV2} \geq 6$

What is defined as b-jets will of course not be a clean b-jet sample, but also contain mistagged light jets.

The invariant mass of all reconstructed b-jets in each of the signal scenarios are shown in figure 5.7. In the cases where there are more than two b-jets all combinations are used in the calculation. This illustrates that all the SUSY scenarios contain a lot of b-jets, mainly from gluino, **s**bottom and **s**top decays, as discussed in section 5.1. Also ordinary SM processes like the decay of W and Z will contribute to the b-jets produced in supersymmetric cascades. In the $SU9$ scenario we already see a resonance around the Higgs mass, because of the large amount of Higgs bosons in this sample. In $SU1$, with higher integrated luminosity, it may also be possible to extract a resonance. A priori the extraction of a Higgs signal will be difficult in the other scenarios, even with much higher luminosity.

The corresponding distributions in figure 5.8 illustrate that the SM also contains a huge amount of

(1) $SU1$ (2) $SU2$ (3) $SU6$

(4) $SU8.2$ (5) $SU9$
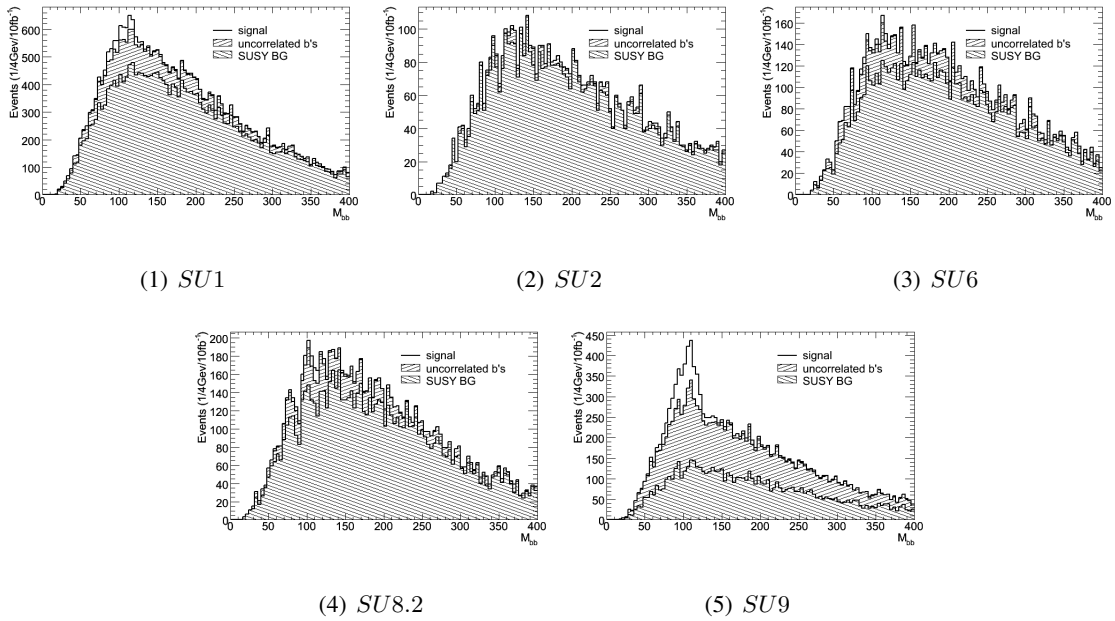
Figure 5.7: *Invariant mass of all tagged jets in the different signal scenarios after the cuts in table 5.2 are applied and a b-tagging efficiency of 60%. In $SU9$ a peak around the Higgs mass is already dominant.*

b-jets, which has to be reduced. As expected, the $t\bar{t}$ background is dominant.
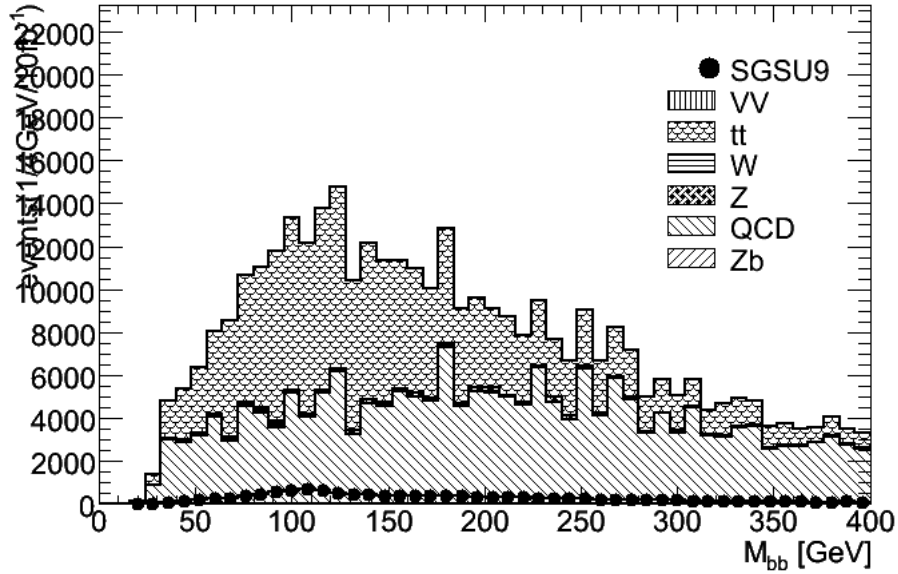
Figure 5.8: *Invariant mass of all tagged b-jets for different standard model processes with the cuts in table 5.2 applied and a b-tagging efficiency of* 60%.

5.7 *b*-**jets**

Since our channel for discovering Higgs is the decay into a *b*-quark pair, the presence of at least two *b*-jets in the event is important. In figure 5.9 and 5.10 (taken from [1]) the energy resolution and the light jet rejection are shown as a function of energy and p_T of the jets, respectively. These plots show that both the energy resolution and the light jet rejection get worse at low E/p_T. The energy resolution steadily improves at high energies, whereas the light jet rejection increases with p_T, reaches a maximum at $p_T \sim 150$ GeV and decreases for higher p_T values. This should be kept in mind when we pick out the *b*-jets.

The histograms in figure 5.11 illustrates that the hardest *b*-jets coming from Higgs most often have $p_T > 50$ GeV, while the second hardest could be softer. This is confirmed by table 5.3, showing the effect of two different p_T requirements on the two *b*-jets. The table 5.3 illustrates what is expected from the histograms in figure 5.11, that we lose much of the *b*-pairs from Higgs when requiring $p_T > 50$ GeV on both of the *b*-jets. A better cut will be to require $p_T > 50$ GeV for the hardest *b*-jet and the second hardest with $p_T > 20$ GeV. The cuts presented in table 5.4 are further used, for which the significance is better for all samples. The invariant mass distributions after the cuts in table 5.4 are
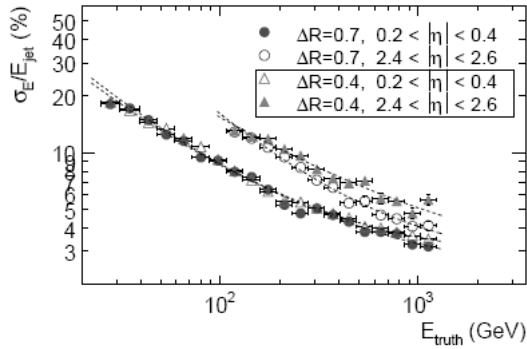
Figure 5.9: *The energy resolution for cone-tower jets with R=0.7 and R=0.4, in two regions of $|\eta|$, as a function of $E_{truth^{jet}}$. The higher the jet energy, the better resolution. Plot taken from [1]*
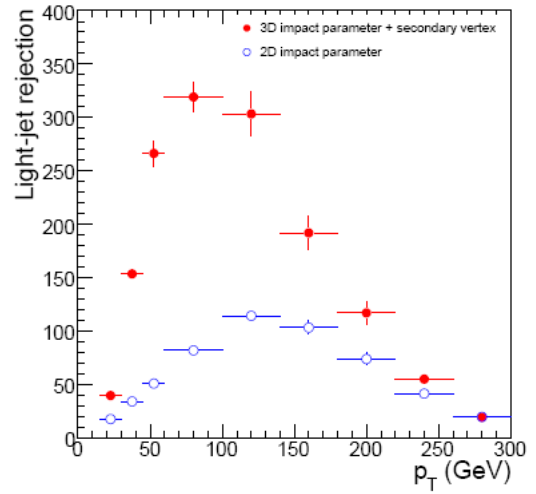
Figure 5.10: *The rejection of light jets (not c-jets) as a function of the transverse momentum for two different b-tagging algorithm. Both are showed with a b-tagging efficiency of 60%. The filled dot is the algorithm which is used in this analysis. Sometimes a requirement of the maximum p_T of the b-jets is also used, since the light jet rejection decreases at high p_T. Plot taken from [1]*
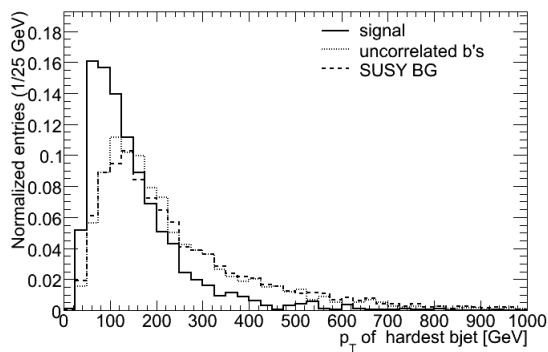
(1) hardest b-jet
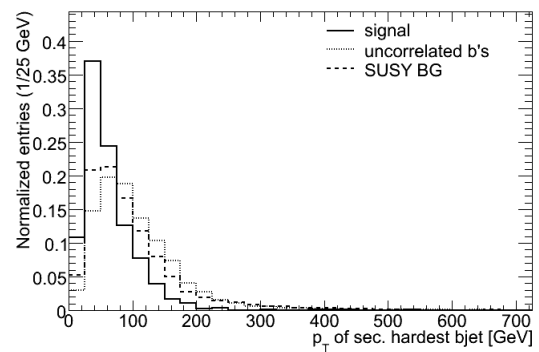
(2) second hardest b-jet

Figure 5.11: *The p_T of the hardest (1) and second hardest (2) b-jet in the different categories of signal after the cuts in table 5.2 are applied.*

$p_T^1 > 50, p_T^2 > 50$						$p_T^1 > 50, p_T^2 > 20$			
	# of events						# of events		
Sample	SG	COMB	BG	$S/\sqrt{B}$		Sample	SG	COMB	BG	$S/\sqrt{B}$
$SU1$	164	408	5400	2.15		$SU1$	258	450	7113	2.97
$SU2$	11	65	2040	0.24		$SU2$	22	72	2412	0.44
$SU6$	88	443	6321	1.07		$SU6$	132	467	7823	1.45
$SU82$	107	425	6162	1.32		$SU82$	171	450	7891	1.87
$SU9$	604	1344	3244	8.92		$SU9$	989	1424	4266	13.1

Table 5.3: *The significance for signal and combinatorial background+SUSY background. This is after requiring at least 2 b-jets with (left): $p_T^1 > 50 GeV$ and $p_T^2 > 50 GeV$ or (right): $p_T^1 > 50$ and $p_T^2 > 20 GeV$. In both tables the cuts in table 5.2 are used together with a b-tagging efficiency of 60%*

CUT #	VALUE
CUT 1	$\not{E}_T > 100$ GeV
CUT 2	2 jets $p_T^{1,2} > 100, 50$ GeV
CUT 3	2 *b*-jets with $p_T^{1,2} > 50, 20$ GeV

Table 5.4: *Cuts used in the analysis.*

applied is shown in figure 5.12 and 5.13 for the signal samples and SM background respectively. The plots in 5.12 do not differ considerably from the plots in 5.7, illustrating that CUT 3 does not remove many of the events with *b*-jets. Although it removes $\sim 80\%$ of the SUSY background events, since they often do not contain *b*-jets at all.

From the discussion in section 4.4.1-4.4.7 in chapter 4 it is clear that *b*-jets are often produced

(1) $SU1$ (2) $SU2$ (3) $SU6$

(4) $SU8.2$ (5) $SU9$
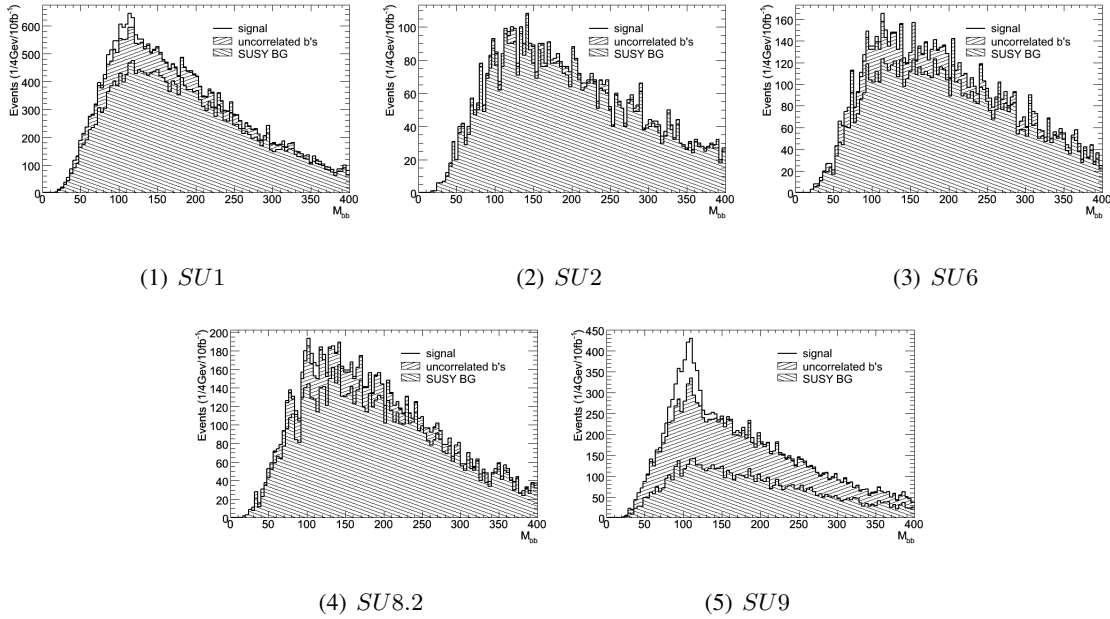
Figure 5.12: *Invariant mass of all tagged jets in the different signal scenarios after the cuts in table 5.4 are applied and a b-tagging efficiency of 60%. These plots are very similar to the ones in 5.7, which illustrate that CUT 3 does not remove much of the signal or the other event categories. Although this cut removes a factor of $\sim 80\%$ of the SUSY background, since this background contain many events without b-jets at all (but this will not be clear from these plots, since they only show events with at least two b-jets).*

from decays of **s**bottom or **s**top in SUSY cascades. These *b*-jets originate from an early stage in the cascade and have therefor usually higher p_T. These *b*-jets do not come from Higgs, and will contribute to wrong combinations in the invariant mass calculation. Figure 5.14 shows for $SU9$ where the different *b*-jets come from according to their p_T. It is clear from this that the hardest (second hardest) *b*-jet is mostly from other sources than h if there are three (more than three) *b*-jets in the event. This is also reflected in table 5.5 which shows an increase in the significance when this constraint is applied. The cuts presented in table 5.6 are further used in the analysis. The invariant mass distribution for the various signals before (figure 5.12) and after (figure 5.15) the cuts in table 5.6 are applied is shown.
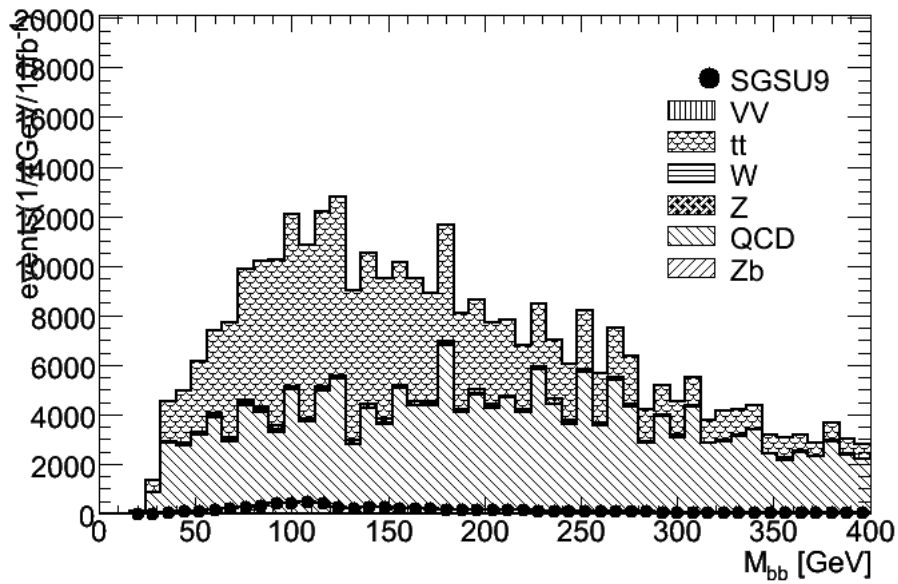
**Figure 5.13:** *Invariant mass of all tagged b-jets for different Standard Model processes with the cuts in table 5.4 applied and a b-tagging efficiency of 60%. For the Standard Model one see a reduction in the number of events compared with 5.8.*

(1) event with 3 *b*-jets

(2) event with 4 *b*-jets
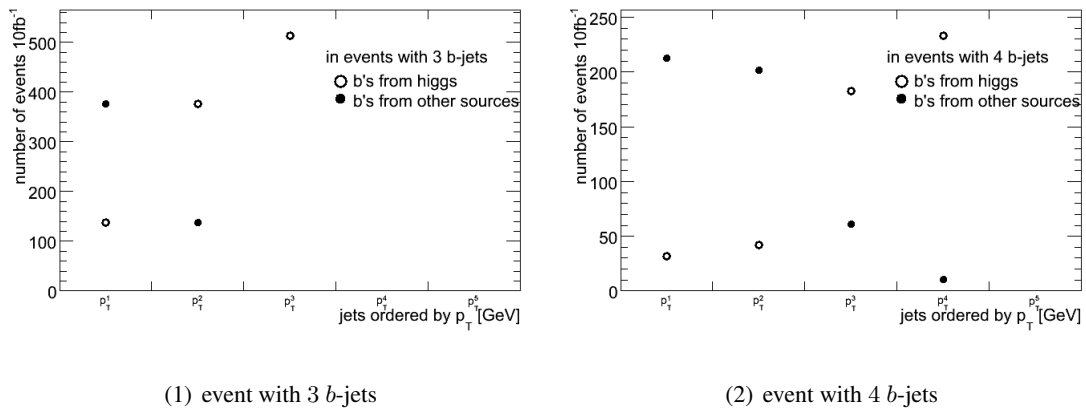
Figure 5.14: *Number of b-jets coming from the decay of h compared to that of other b-jets in events with (1): three or (2): four b-jets for the SU9 signal sample. At the x-axis p_T^1, p_T^2,... correspond to the hardest, second hardest,... b-jet in the event. The y-axis shows how many of the hardest, second hardest... b-jet in each event that comes from Higgs and from other sources.*

CUT	SU1			SU2			SU6		
	S	B	$s_{\pm 25}$	S	B	$s_{\pm 25}$	S	B	$s_{\pm 25}$
use all b-jets	250	5116	3.5	20	1191	0.58	130	5525	1.75
omit b-jet #1 (#2)	250	2792	4.7	20	629	0.79	130	2743	2.48

CUT	SU8.2			SU9		
	S	B	$s_{\pm 25}$	S	B	$s_{\pm 25}$
use all b-jets	167	6245	2.11	980	4197	15.1
omit b-jet #1 (#2)	167	4321	2.54	980	2250	20.7

Table 5.5: *The significance and the number of signal (S) and background (B) events in a $\pm 25 GeV$ mass window around the Higgs mass for the two different methods.* **Upper row**: *Use all b-jets in the event in the M_{bb} calculation.* **Second row**: *the hardest (two hardest) b-jet(s) are omitted from the invariant mass calculation in case of three (four) b-jets in the event. This is after the cuts in table 5.4 are applied and for only SUSY signal and background.* $\mathscr{L} = 10 fb^{-1}$.

CUT #	VALUE
CUT 1	$\not{E}_T > 100$ GeV
CUT 2	2 jets $p_T^{1,2} > 100, 50$ GeV
CUT 3	2 b-jets with $p_T^{1,2} > 50, 20$
CUT 4	omit the hardest (sec. hardest) b-jet in events with 3 (> 3) b-jets in the M_{bb} calculation

Table 5.6: *The cuts used further in the analysis.*

The same is shown for the SM backgrounds in figure 5.13 (before) and 5.16 (after)).

(1) $SU1$ (2) $SU2$ (3) $SU6$

(4) $SU8.2$ (5) $SU9$
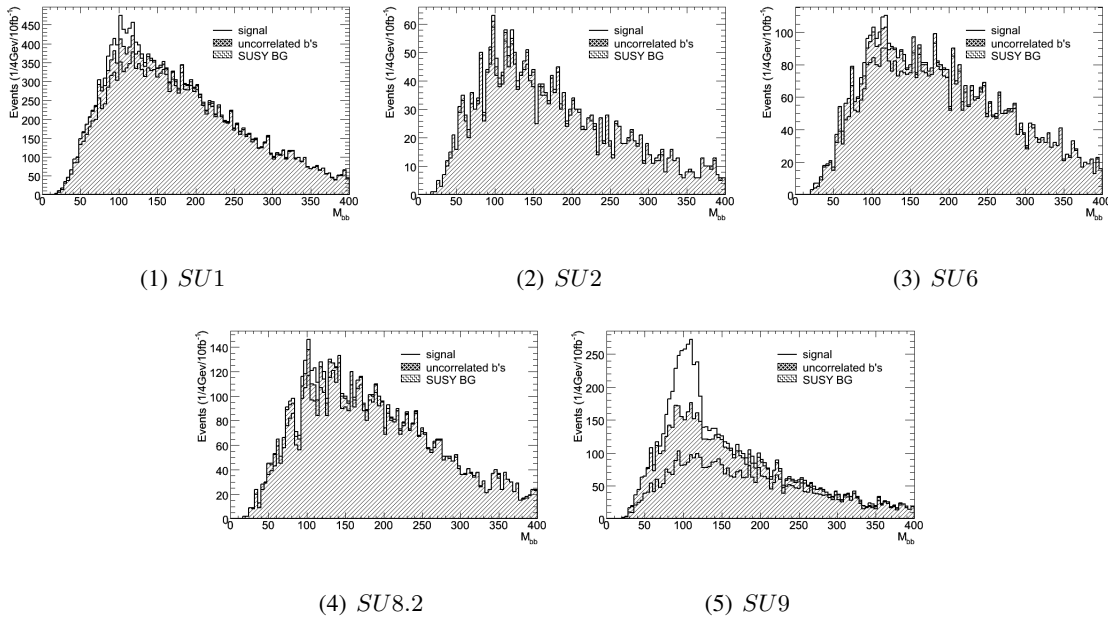
***Figure 5.15:*** *Invariant mass of all tagged jets in the different signal scenarios after the cuts in table 5.6 are also applied together with a b-tagging efficiency of 60%. By adding CUT 4 we remove much of the combinatorial background and the uncorrelated SUSY background while the signal stays the same.*

5.8 Number of jets

Since this analysis concentrates on Higgs production in supersymmetric cascades at least four jets, two b-jets from Higgs decay and two additional jets from elsewhere in the cascade[5] or in the other leg, should exist in the event. This is the minimum of jets that is expected, but as discussed in the previous sections the number of jets could be higher in scenarios which is dominated by long cascades. The plots in figure 5.17 illustrate the jet multiplicity for the different type of jets and the sum of all jets for the signal and Standard Model background. These distributions illustrate the fact that SUSY events have in general more jets than most of the Standard Model background, however the SM $t\bar{t}$ and QCD backgrounds are also very rich in jets. The $SU2$ scenario contains more jets than the other scenarios. This is due to the fact that the gauginos and the gluinos can decay via 3-body decay into two quarks and the LSP. Since the squarks are extremely heavy, gauginos will be produced at high rate in the

---

[5]will only be called *additional jets* in the following discussions
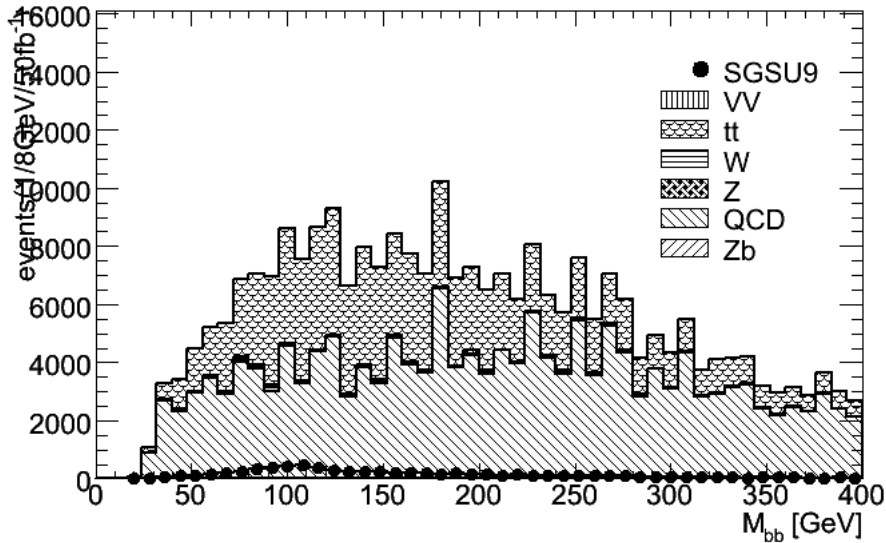
Figure 5.16: *Invariant mass of all tagged b-jets for different standard model processes with the cuts in table 5.6 applied and a b-tagging efficiency of 60%. Cmpared with the corresponding plot in figure 5.13 we see that CUT 4 reduces the SM background. Although CUT 4 is most efficient in removing the combinatorial SUSY background.*

$SU2$, as was shown in section 4.4.2.

The histograms in figure 5.18 show the jet multiplicity in the different types of event categories in some of the signal samples. The solid line shows the distribution for signal events, which always will have at least two jets, since they have two b-jets from the decay of Higgs. These histograms show that all the SUSY scenarios have very similar distributions for the number of jets, except $SU2$ which is a special case discussed earlier. Very seldom a Higgs is produced in events with less than four jets in total, so therefore a requirement of at least two jets in addition to the one from Higgs is a priori a good cut. The cuts in table 5.7 shows the cuts used further

5.9 Summary of cut studies

The goal of this analysis is investigate whether it is possible to isolate a resonance around the expected Higgs mass in the different scenarios by calculating the invariant mass of two b-jets in the event. The SM contains a lot of b-jet candidates that will hide the signal, and the goal is to remove as much of the Standard Model background as possible, while keeping the signal. To achieve this a careful study

SU1

| (1) # of b-jets | (2) # of light fl. jets | (3) # of all jets |

SU2
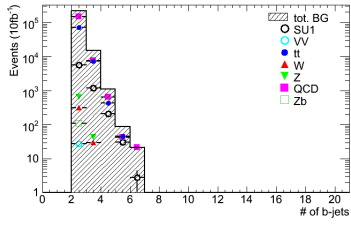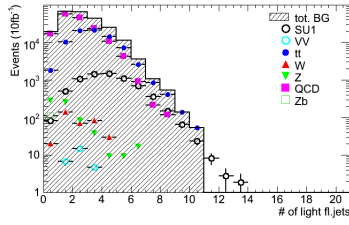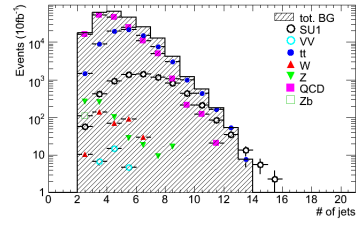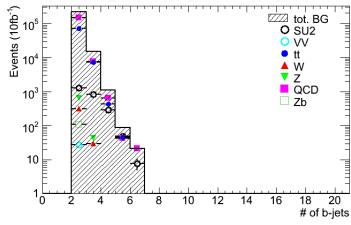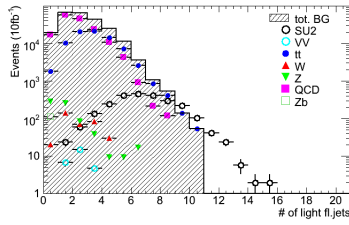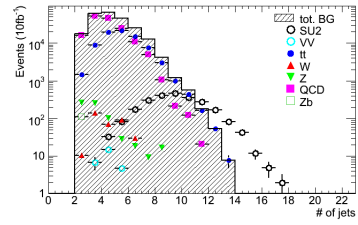
| (4) # of b-jets | (5) # of light fl. jets | (6) # of all jets |

SU3
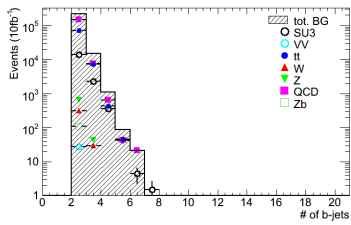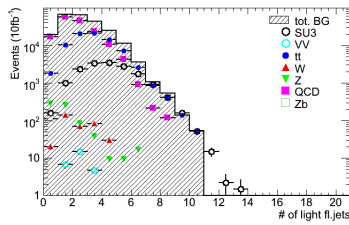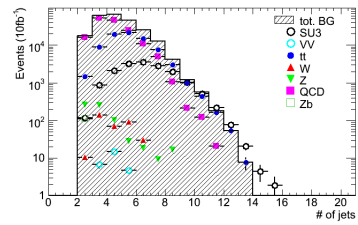
| (7) # of b-jets | (8) # of light fl. jets | (9) # of all jets |

SU4

| (10) # of b-jets | (11) # of light fl. jets | (12) # of all jets |

SU6

(13) # of b-jets

(14) # of light fl. jets

(15) # of all jets

SU8.2

(16) # of b-jets

(17) # of light fl. jets

(18) # of all jets

SU9
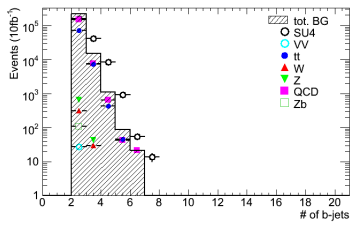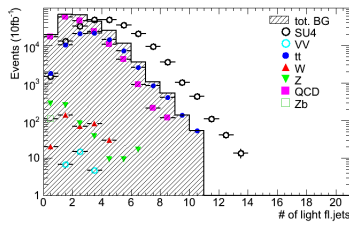
(19) # of b-jets

(20) # of light fl. jets
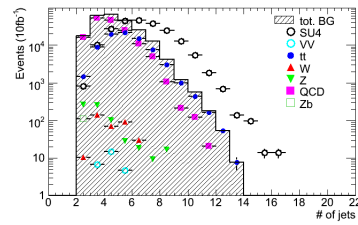
(21) # of all jets
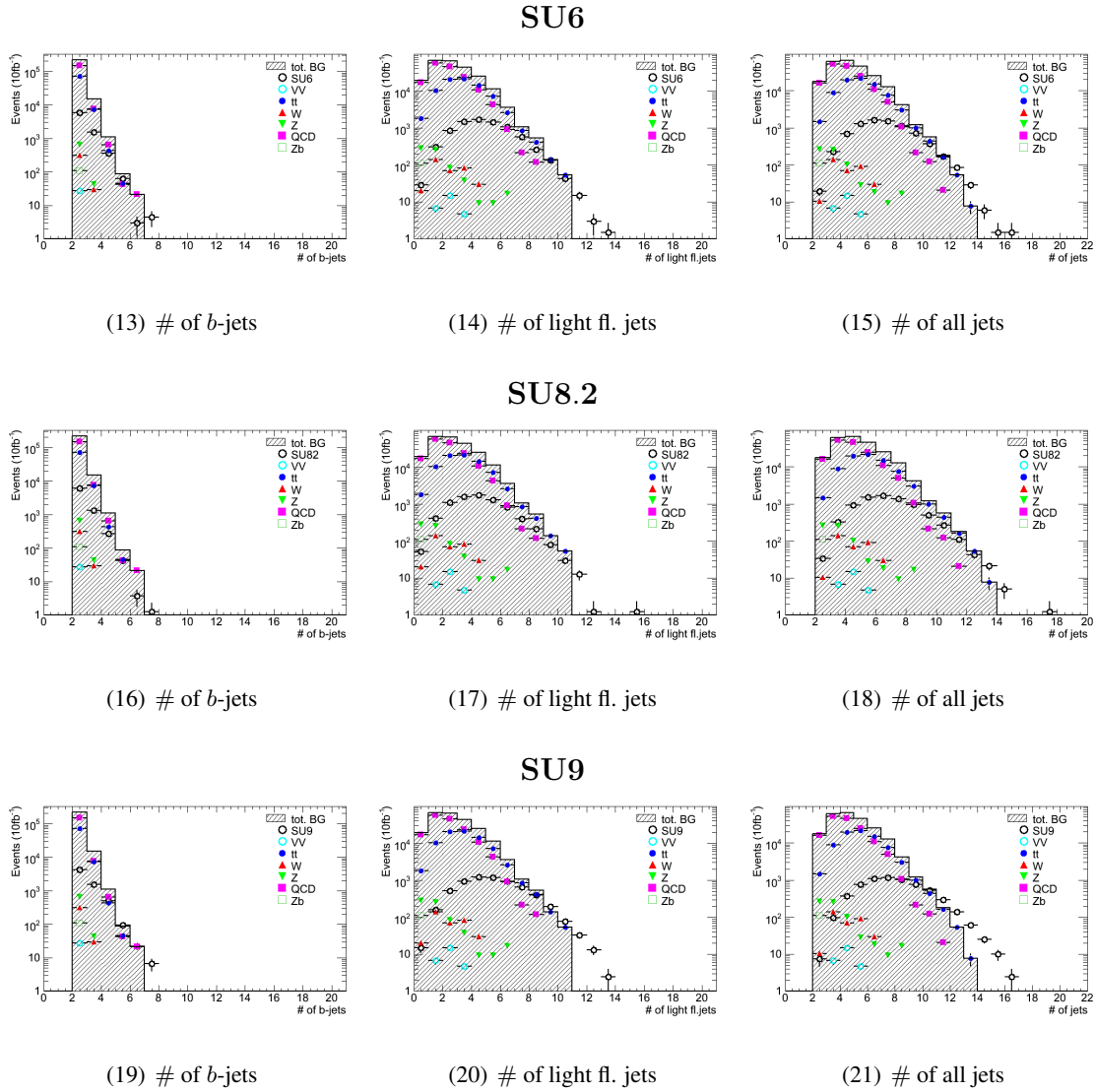
Figure 5.17: *The number of b-jets, light jets and the total number of jets in the various signal samples and for the SM backgrounds. The SUSY signals have high jet multiplicity compared with most of the SM background, except $t\bar{t}$ and QCD which also contains many jets. This is after the cuts in table 5.6 are applied. $\mathscr{L} = 10 fb^{-1}$*

SU1

(1) # of b-jets

(2) # of light fl. jets

(3) # of all jets

SU2
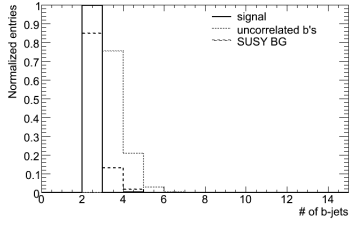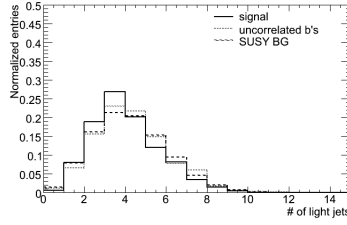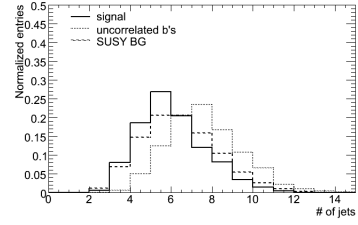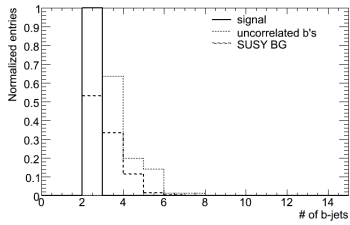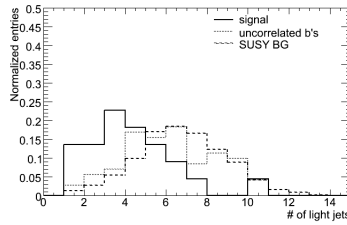
(4) # of b-jets
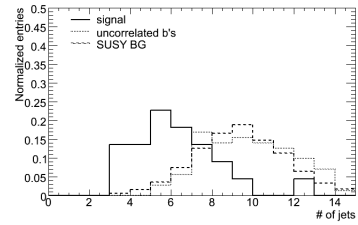
(5) # of light fl. jets

(6) # of all jets

SU6
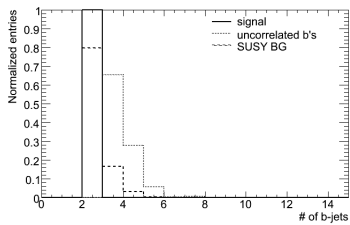
(7) # of b-jets
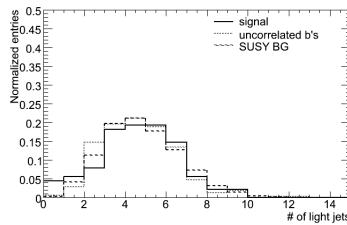
(8) # of light fl. jets
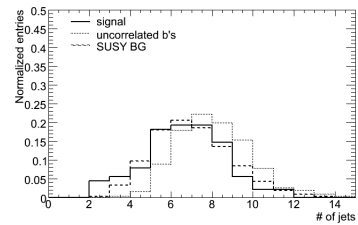
(9) # of all jets

SU8.2
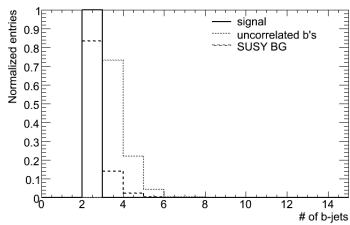
(10) # of b-jets
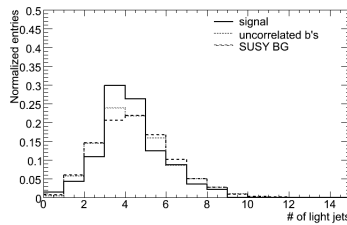
(11) # of light fl. jets
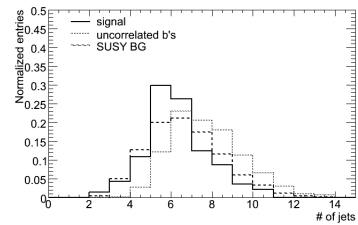
(12) # of all jets

SU9
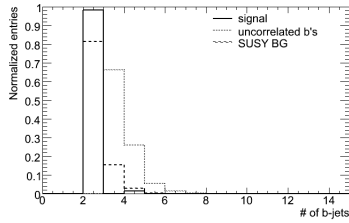
(13) # of b-jets
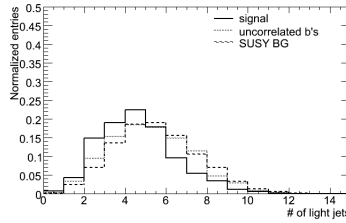
(14) # of light fl. jets
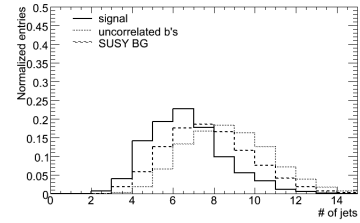
(15) # of all jets

Figure 5.18: *The number of jets in the different categories of event in the signal samples after the cuts in table 5.6 are used. The solid line is only Higgs events, dotted line is combinatorial background while the dashed line is uncorrelated SUSY background. Again $SU2$ is a special case since it contains many jets and both uncorrelated bs and SUSY BG events are peaked at high values.*

CUT #	VALUE
CUT 1	$\not{E}_T > 100$ GeV
CUT 2	2 jets $p_T^{1,2} > 100, 50$ GeV
CUT 3	2 b-jets with $p_T^{1,2} > 50, 20$
CUT 4	omit the hardest (sec. hardest) b-jet in events with more than 3 b-jets from the M_{bb} calculation
CUT 5	≥ 2 additional jets

Table 5.7: *Cuts used further in the analysis.*

of each cut is necessary. The conclusion from section 4.4.1-4.4.7 will be followed in order to avoid cutting away possible signal events.

In the following sections, we perform a detailed study of the effect of different cuts in order to choose the best combination. For each possible cut the significance is calculated, and used as a guidance to achieve the optimal cut. Of course, for the different scenarios, a different set of cuts could in principle be the optimal. The goal is to find as general and effective cuts as possible. It could be that there is need for two different strategies, depending on which of the long or short cascade is dominant.

The distribution in figure 5.19 shows, as an example, that for $SU1$ and $SU9$ all the different categories of events in the sample have very similar distributions for the $\not{E}_T$, M_{eff} and $\not{E}_T/M_{\text{eff}}$. This illustrates the fact that cuts on these variables helps to remove SM background only, but do not improve the significance of the Higgs signal relative to the combinatorial and SUSY backgrounds.

SU1

| (1) $\not{E}_T$ | (2) M_{eff} | (3) $\not{E}_T/M_{\text{eff}}$ |

SU9

| (4) $\not{E}_T$ | (5) M_{eff} | (6) $\not{E}_T/M_{\text{eff}}$ |
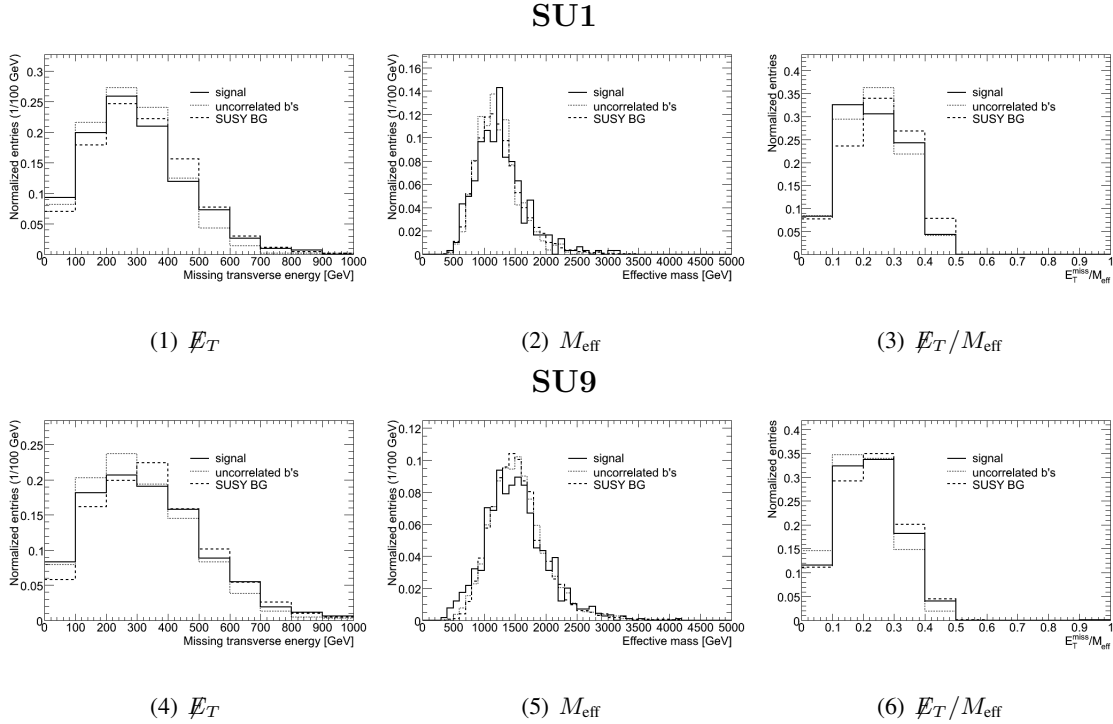
Figure 5.19: *The $\not{E}_T$, M_{eff} and $\not{E}_T/M_{\text{eff}}$ for the $SU1$ (top) and $SU9$ (bottom) scenarios. Signal and SUSY background shapes are similar. This illustrate the fact that the use of these variables do not improve the significance of the Higgs signal relative to the combinatorial and SUSY backgrounds.*

5.9.1 Missing transverse energy, $\not{E}_T$

The standard way to reduce much of the SM background is to use the missing transverse energy signature. Figure 5.20 shows the distribution for the $\not{E}_T$ for the signal samples and standard model background after the cuts in table 5.7 are applied. The $\not{E}_T$ distribution looks very different for SUSY

(1) $SU1$ (2) $SU2$ (3) $SU3$ (4) $SU4$

(5) $SU6$ (6) $SU8.2$ (7) $SU9$
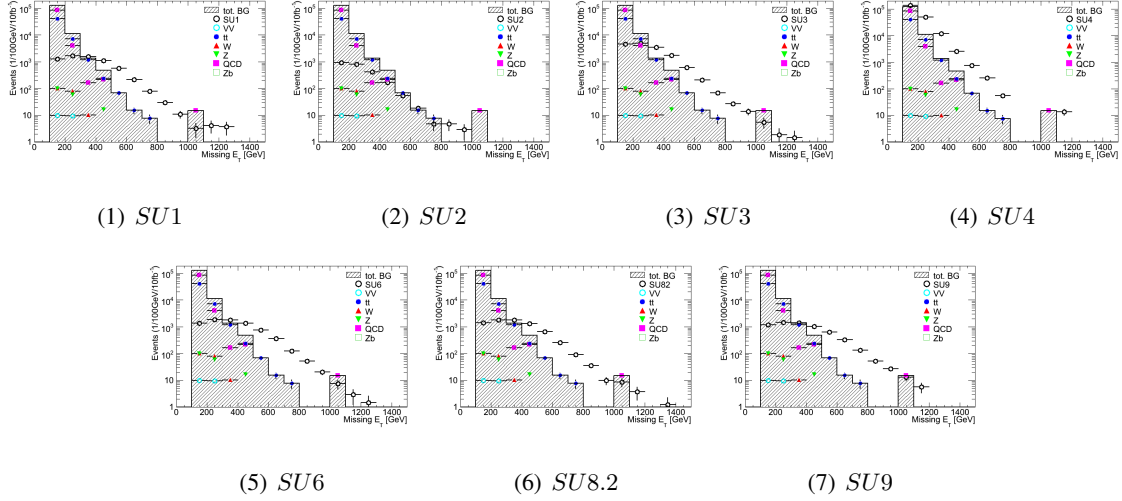
Figure 5.20: *$\not{E}_T$ for the standard model background and signal after the cuts in table 5.7 are applied. The SUSY signals have different distributions compared with the SM backgrounds, which is dominated by $t\bar{t}$ and QCD. $SU2$ is special since the $\not{E}_T$ is relatively low compared with the other SUSY samples. $\mathscr{L} = 10 fb^{-1}$*

signals compared to the SM background, which peaks at relatively low values, while SUSY signals are shifted to the higher values. The tail is also longer for the SUSY samples, but in some of the SM backgrounds there are also long tails, mostly due to decays of W, Z and top involving neutrinos. $SU2$ is again a special case since it contains much less $\not{E}_T$ than the other SUSY samples.

Table 5.8 shows the significance[6] of signal and background for different cuts in $\not{E}_T$. The table illustrates that the highest significance is achieved with a cut in $\not{E}_T > 200 - 300$ GeV for all the signal samples. In the samples where the signal is very small it is difficult to say much about which cuts that may be most efficient. In this case a study of the significances is not the best way to optimize the cuts. Since the signal in $SU2$ is very low, this sample is omitted from the rest of the significance tables.

---

[6]Since the signal is very small in some of the scenarios the integrated luminosity used in this and the rest of the tables in the chapter is $\mathscr{L} = 50 fb^{-1}$.

	SU1				SU2				SU6			
Cut	S	B	all	±25	S	B	all	±25	S	B	all	±25
$\not{E}_T > 100$	719	206161	1.16	1.58	66	200490	0.10	0.15	344	207548	0.54	0.76
$\not{E}_T > 200$	528	22755	4.25	5.21	15	17887	0.27	0.21	262	13161	1.93	2.56
$\not{E}_T > 300$	335	5303	3.54	4.60	10	1915	0.26	0.23	150	5676	1.45	1.99
$\not{E}_T > 400$	172	3430	2.30	2.94	0	1498	0	0	105	3743	1.23	1.71

	SU82				SU9			
Cut	S	B	all	±25	S	B	all	±25
$\not{E}_T > 100$	512	207883	0.78	1.12	3089	201443	4.89	6.88
$\not{E}_T > 200$	394	23386	2.88	3.81	2468	21936	20.4	24.9
$\not{E}_T > 300$	275	5850	2.74	3.60	1747	5390	18.6	23.8
$\not{E}_T > 400$	162	3722	2.10	2.66	1163	3734	14.9	19.0

Table 5.8: *The significances and the number of signal (S) and background events (SUSY + SM) (B) in a ±25 GeV mass-window cuts in $\not{E}_T$ after the cuts in table 5.7 are applied. For $SU2$ the significance is very low so in this case it does not give precise information about which cut that may be the most efficient. We know from the distribution in 5.3 that a high $\not{E}_T$ cut would remove much of the $SU2$ signal. $\mathscr{L} = 50 fb^{-1}$*

5.9.2 Transverse momenta (p_T) of jets

Since the jets in SUSY events very often come from decays of heavy sparticles early in the cascade, these jets will have high p_T. From the discussion in the last chapter these jets could in principle be of any type of flavor. The plots in figures 5.21 shows the p_T distributions for b-jets, light flavored jets and all jets in each event after the cuts in table 5.7 are used. The p_T distributions for all the signal samples are very similar for all types of jets. The $t\bar{t}$ background has very similar distribution as the signals, while the QCD has the same shape but longer tails. For all the signal samples the distributions of the p_T of all jets become very small for values above 1500GeV except for the $SU2$ which is relatively small already at 1000GeV. This is because the $SU2$ sample has extremely heavy squarks so $m_{\widetilde{g}} >> m_{\widetilde{q}}$, and it is mostly produced gauginos or gluinos initially. The gluino decays into a gaugino and two quarks, while the gauginos either decay into W, Z or h and a quark (in case of $\widetilde{\chi}_2^\pm$ and $\widetilde{\chi}_4^0$) or via 3-body decay into two quarks and the LSP (in case of $\widetilde{\chi}_2^0$) (see section 4.4.2). Since the gauginos are not as heavy as the squarks in the other scenarios, this will give relatively lower p_T jets compared with the other scenarios.

The histograms in figure 5.22 shows the p_T of the hardest, second hardest and third hardest jet in each event in the five example scenarios with the cuts in table 5.7. For $SU2$ the distribution is not very precise since much of the clean signal events already are removed by the cuts in table 5.7, as already discussed.

The discussion above demonstrate that there are very often several high p_T jets in cascades of SUSY particles. A requirement on the p_T of the hardest jet could therefor be used to suppress the SM background. However, as is clear from the distributions in 5.22, it is important to not make this cut too hard, since then we would reject much of the signal. This is especially important in the scenarios with small signals. Although, as already discussed this cut should at least require one jet with $p_T > 100$ GeV, since this already is done in some of the background samples (see appendix A). Table 5.9 shows the significance achieved with different cuts on the p_T of the two additional jets.

It is from this difficult to say anything exact because the difference in the significances are

	SU1				SU6				SU82			
Cut	S	B	all	±25	S	B	all	±25	S	B	all	±25
$p_T^{1/2} > 100/50$	719	207095	1.13	1.54	344	207548	0.53	0.72	512	207833	0.77	1.11
$p_T^{1/2} > 100/100$	627	115955	1.26	1.84	307	116632	0.61	0.90	456	116854	0.85	1.33
$p_T^{1/2} > 200/100$	564	72906	1.48	2.09	269	74068	0.69	0.99	406	74117	0.98	1.49
$p_T^{1/2} > 250/150$	412	32000	1.55	2.30	165	32930	0.64	0.91	275	32838	0.96	1.52
$p_T^{1/2} > 300/200$	262	15349	1.49	2.12	104	16042	0.58	0.83	169	15971	0.83	1.34

	SU9			
Cut	S	B	all	±25
$p_T^{1/2} > 100/50$	3089	201443	4.79	6.74
$p_T^{1/2} > 100/100$	2828	112564	5.56	8.43
$p_T^{1/2} > 200/100$	2691	71660	6.87	10.1
$p_T^{1/2} > 250/150$	2269	33663	8.19	12.4
$p_T^{1/2} > 300/200$	1814	17428	9.08	13.7

Table 5.9: *The significance and the number of signal (S) and background events (B) in a ± 25 GeV mass-window for different p_T requirements on the two additional jets. This is after the cuts in table 5.7. The significances are presented with an integrated luminosity of $50 fb^{-1}$*

relatively small. But since we have very small signals in some of the scenarios, the cut should be kept relatively low, as is clear from the distributions in 5.22. In the $SU9$ scenario, where the signal is big and is dominated by the long cascade, harder p_T requirements can be applied with an increase in the

SU1
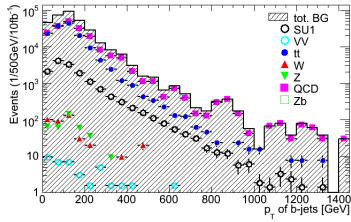
(1) p_T of b-jets
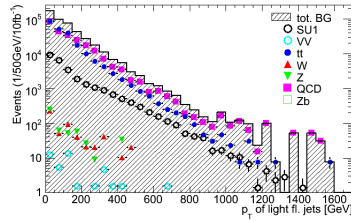
(2) p_T of light fl. jets
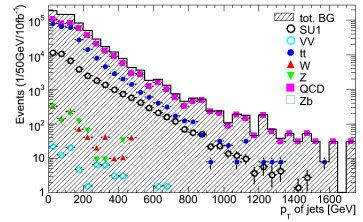
(3) p_T of all jets

SU2
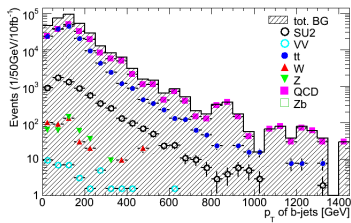
(4) p_T of b-jets
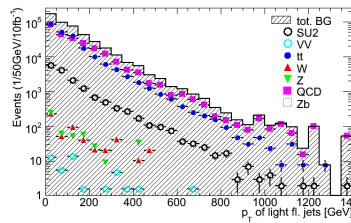
(5) p_T of light fl. jets
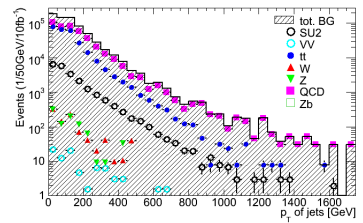
(6) p_T of all jets

SU3
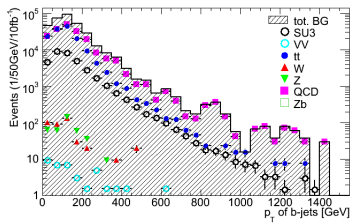
(7) p_T of b-jets
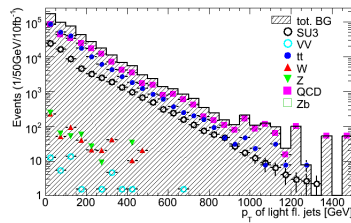
(8) p_T of light fl. jets
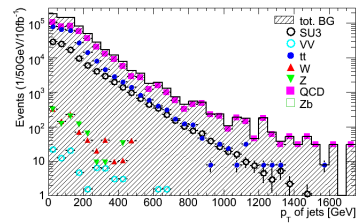
(9) p_T of all jets

SU4
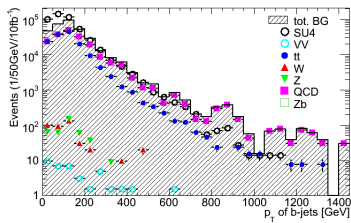
(10) p_T of b-jets
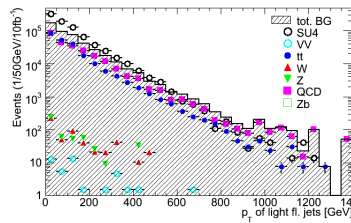
(11) p_T of light fl. jets

(12) p_T of all jets

SU6

(13) p_T of b-jets

(14) p_T of light fl. jets

(15) p_T of all jets

SU8.2

(16) p_T of b-jets

(17) p_T of light fl. jets

(18) p_T of all jets

SU9

(19) p_T of b-jets

(20) p_T of light fl. jets
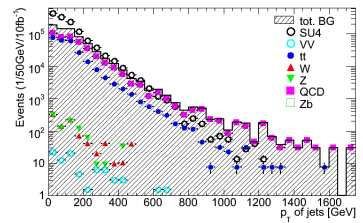
(21) p_T of all jets
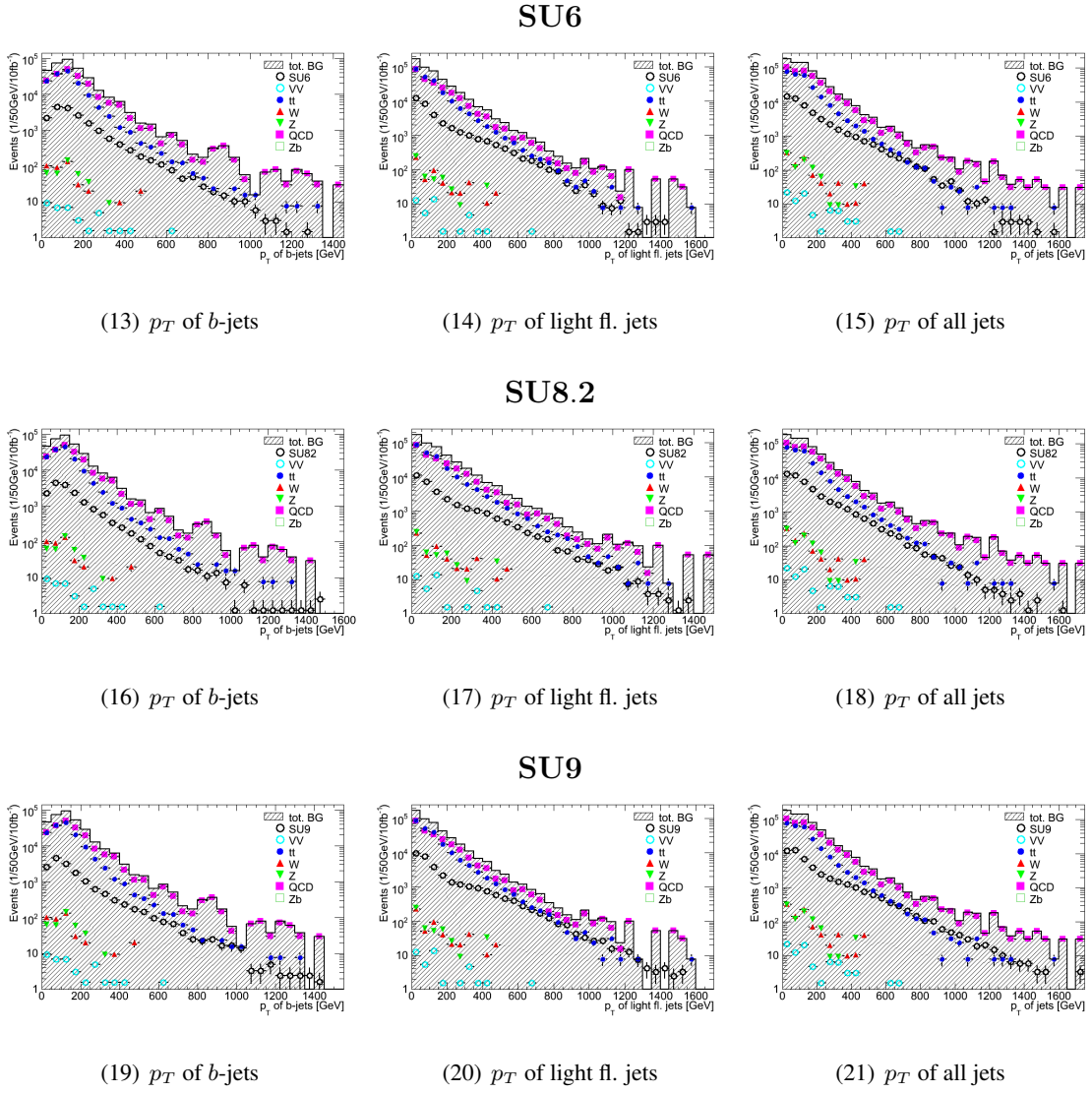
Figure 5.21: *The p_T of the different types of jets in each event for the various signal samples and SM backgrounds. The distributions for both signal and SM background (i.e the dominant ones, $t\bar{t}$ and QCD) is very similar. The other SM backgrounds contains much less high p_T jets.*

SU1
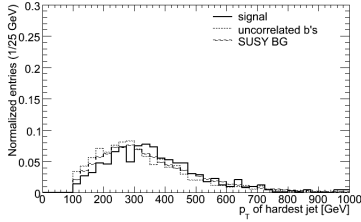
(1) p_T of hardest jet
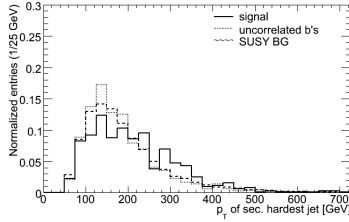
(2) p_T of second hardest jet
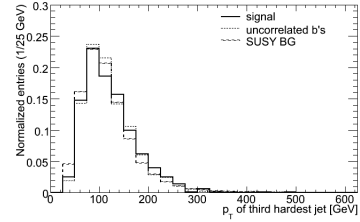
(3) p_T of third hardest jet

SU2
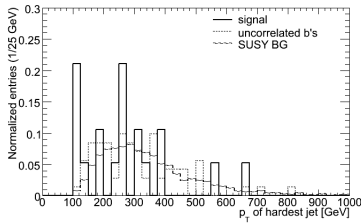
(4) p_T of hardest jet
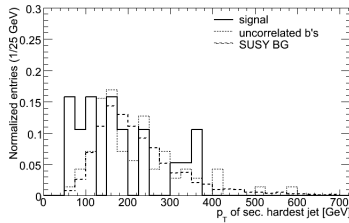
(5) p_T of second hardest jet
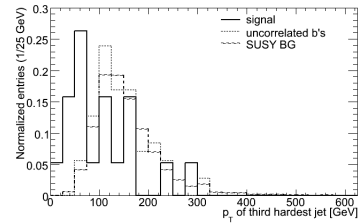
(6) p_T of third hardest jet

SU6
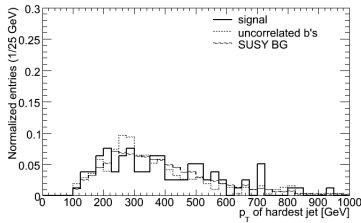
(7) p_T of hardest jet
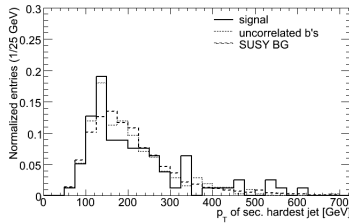
(8) p_T of second hardest jet
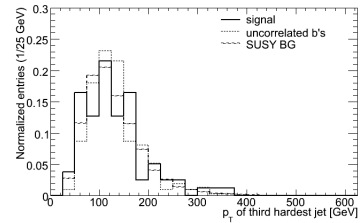
(9) p_T of third hardest jet

SU8.2
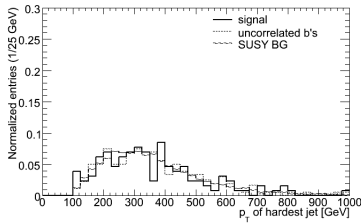
(10) p_T of hardest jet
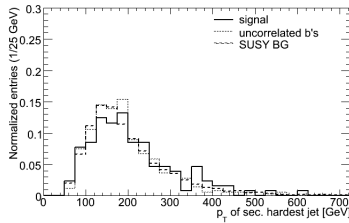
(11) p_T of second hardest jet

(12) p_T of third hardest jet

SU9

(13) p_T of hardest jet   (14) p_T of second hardest jet   (15) p_T of third hardest jet
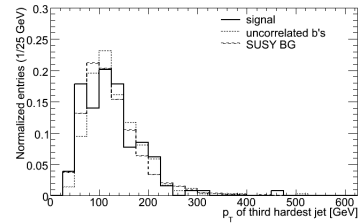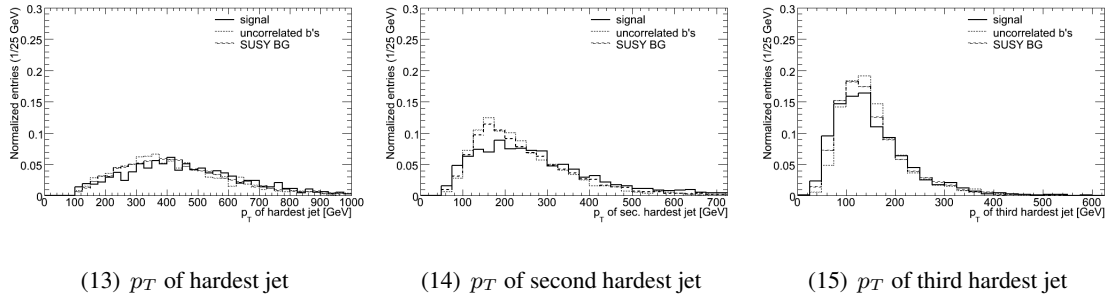
Figure 5.22: *The hardest, second hardest and third hardest jet in each event for the different signal samples after the cuts in table 5.7.*

significance.

As already discussed some of the scenarios have the long cascade as the most important Higgs production. In these scenarios the requirement of one more additional jet (in total 5 jets) could be a way to reject much of the background while keeping the signal. Often the additional jets from these long cascades are b-jets, which also could be used as a requirement. The signal in the samples dominated by the long cascades are very small and it is more convenient to look at the rejection of background events (all events **without** Higgs) compared with the efficiency of the signal events (events **with** Higgs) for the different cuts. Table 5.10 shows the rejection (R) and efficiency (ε) for different cuts requiring two or three jets in addition to two b-jets from Higgs. This shows that in the

		$SU1$	$SU2$	$SU6$	$SU82$	$SU9$
		efficiency				
Cut	R	ε	ε	ε	ε	ε
2 jets (100,100)	0.64	0.88	0.80	0.91	0.89	0.94
2 l-jets (100,100)	0.89	0.53	0.53	0.46	0.53	0.71
1 b-jet + 1 other (100,100)	0.92	0.44	0.49	0.63	0.54	0.43
3 jets (100,100,100)	0.89	0.61	0.72	0.68	0.68	0.78
3 l-jets (100,100,100)	0.98	0.16	0.30	0.15	0.19	0.34
1 b-jet + 2 other (100,100,100)	0.93	0.45	0.51	0.62	0.53	0.46

Table 5.10: *The rejection (R) and efficiency (ε) for different jet cuts in the signal scenarios. The rejection is the same for all samples. The p_T of the required jets are given in parenthesis (GeV). The rejection is for SUSY and SM background. This is after applying the cuts in 5.7.*

CUT #	VALUE
CUT 1	$\not{E}_T > 100 \text{ GeV}$
CUT 2	2 jets $p_T^{1,2} > 100, \mathbf{100}$ GeV
CUT 3	2 b-jets with $p_T^{1,2} > 50, 20$
CUT 4	omit the hardest (and sec. hardest) b-jet in events with more than 3 (4) b-jets in the M_{bb} calculation
CUT 5	≥ 2 additional jets

***Table 5.11:** Cuts used further in the analysis.*

$SU9$ scenario where the long cascade dominates it could be efficient to require three additional jets, since it would reject much background (0.89) while keep most of the signal (0.78). This will however not be a good cut for $SU1$, since it has much of the Higgs production through the short cascade. In $SU8.2$ and $SU6$ we often get additional b-jets produced with Higgs, and to require one of the two additional jets to be a b-jet could be a possibility. Although, since the signal already is low in these scenarios this may cut away to much of the signal.

The most general cut that will be used further is the requirement of two additional jets with $p_T > 100$ GeV. This reflects also the conclusions from the chapter 4, that all the scenarios studied here produce Higgs through both the long and short cascades, except in $SU2$, where the short cascade dominates. However since this scenario has small $\not{E}_T$ it is difficult to remove the SM background without also removing most of the signal. In the further analysis we therefore change CUT 2 in table 5.7 to require at least two jets with $p_T > 100$. The cuts are summarized in table 5.11

5.9.3 Effective mass, M_{eff}

The histograms in figure 5.23 shows the distribution for effective mass after the cuts in table 5.11 are applied. The distributions for M_{eff} looks very different for the signals and the SM background. While the SUSY signals peaks at relatively high values ($1000 - 1500$ GeV) the SM backgrounds are peaked at lower values ($400 - 500$ GeV). It is clear from this that a cut in M_{eff} would be an efficient way to

(1) $SU1$ (2) $SU2$ (3) $SU3$ (4) $SU4$

(5) $SU6$ (6) $SU8.2$ (7) $SU9$
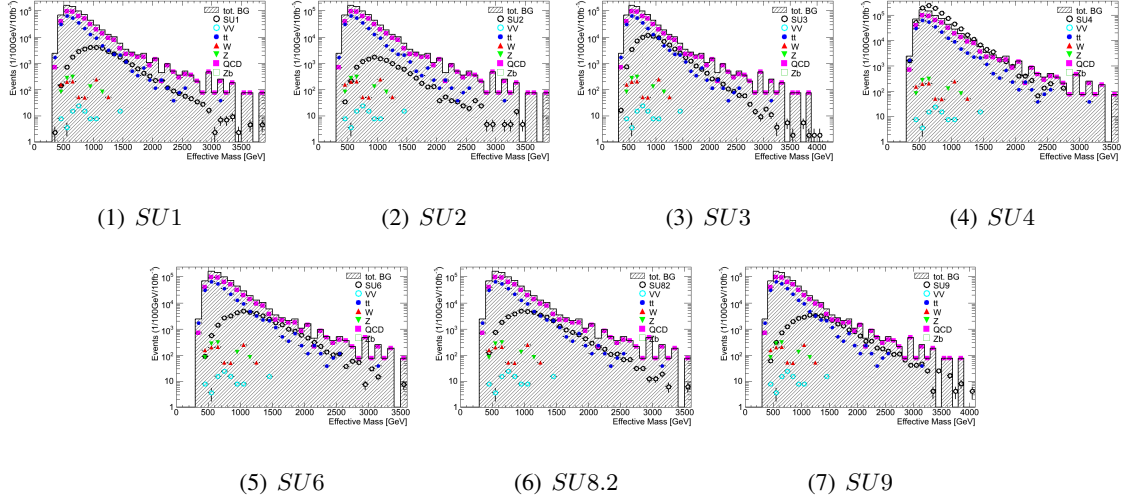
Figure 5.23: M_{eff} *for the standard model background and signal after the cuts in table 5.11 are applied and with an integrated luminosity of* $\mathscr{L} = 10\,fb^{-1}$. *It is clear that the distribution for the SUSY signals peaks at much higher values than the SM background.*

remove much SM background while keeping most of the signal. Again $SU2$ is somehow a special case since it has a shorter tail for high values compared with the other signals. Table 5.12 shows the significance (with $\mathscr{L} = 50\,fb^{-1}$) for different cuts in M_{eff} . The $SU2$ sample is omitted since the significance is very small due to almost no signal events. As was expected from the distributions in 5.23 an increase in the significance in all samples are achieved with a cut in M_{eff} .

5.9.4 Missing transverse energy divided by effective mass, $\not{E}_T / M_{\text{eff}}$

Another possible way to suppress the standard model background is to use the $\not{E}_T / M_{\text{eff}}$ variable. The distributions for this, for the standard model background and signal is showed in figure 5.24. The distributions for the signal samples have a broad peak between $0.2 - 0.4$. The SM background has a clearer peak around 0.2. From the distributions a cut around $0.1 - 0.2$ would probable be the most efficient. The table 5.13 shows the significance with different types of cuts on the $\not{E}_T / M_{\text{eff}}$ variable. It is clear from the table that a cut in the $\not{E}_T / M_{\text{eff}}$ variable also would be an efficient way to reduce the SM background.

	SU1				SU6			
Cut	S	B	all	±25	S	B	all	±25
$M_{\text{eff}} > 600$	609	74232	1.55	2.23	299	75110	0.75	1.09
$M_{\text{eff}} > 1000$	386	16033	2.19	3.05	202	16312	1.08	1.58
$M_{\text{eff}} > 1200$	232	7008	1.89	2.77	120	7564	0.96	1.38

	SU82				SU9			
Cut	S	B	all	±25	S	B	all	±25
$M_{\text{eff}} > 600$	456	75293	1.07	1.66	1774	71102	6.91	10.4
$M_{\text{eff}} > 1000$	262	16241	1.46	2.06	2277	18149	12.0	16.9
$M_{\text{eff}} > 1200$	150	7380	1.20	1.75	1867	9419	13.4	19.2

Table 5.12: *The significance and the number of signal (S) and background events (B) in a ±25 GeV mass-window for various cuts in M_{eff} for an integrated luminosity of $50 fb^{-1}$. This is after the cuts in table 5.11.*

(1) $SU1$ (2) $SU2$ (3) $SU3$ (4) $SU4$

(5) $SU6$ (6) $SU8.2$ (7) $SU9$
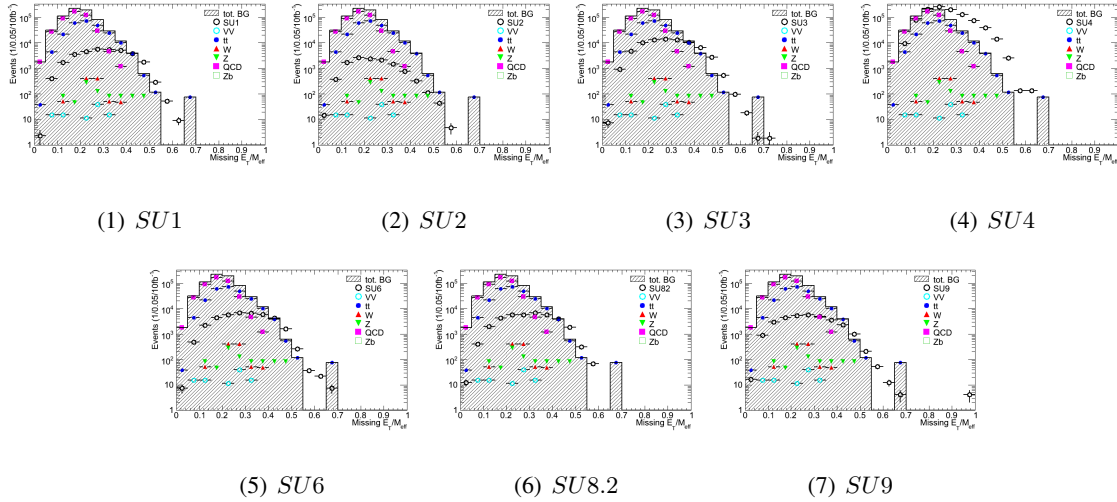
Figure 5.24: *$\not{E}_T/M_{eff}$ for the standard model background and signal after the cuts in table 5.11 with an integrated luminosity of $\mathscr{L} = 10 fb^{-1}$. Again we see a SM background event at high value due to the scaling, as discussed earlier*

	SU1				SU6			
Cut	S	B	all	±25	S	B	all	±25
$\not{E}_T/M_{\mathrm{eff}} > 0.05$	627	115668	1.26	1.84	307	116345	0.61	0.90
$\not{E}_T/M_{\mathrm{eff}} > 0.10$	612	112856	1.25	1.82	307	113543	0.62	0.91
$\not{E}_T/M_{\mathrm{eff}} > 0.20$	487	59506	1.31	2.00	254	59447	0.66	1.04

	SU82				SU9			
Cut	S	B	all	±25	S	B	all	±25
$\not{E}_T/M_{\mathrm{eff}} > 0.05$	456	116568	0.86	1.34	2828	112277	5.55	8.44
$\not{E}_T/M_{\mathrm{eff}} > 0.10$	456	113747	0.87	1.35	2770	108996	5.52	8.39
$\not{E}_T/M_{\mathrm{eff}} > 0.20$	356	59447	0.94	1.46	2054	57487	5.49	8.57

Table 5.13: *The significance and the number of signal (S) and background events (B) in a ± 25 GeV mass-window for different cuts in $\not{E}_T/M_{\mathrm{eff}}$ after the cuts in table 5.11 are applied. $\mathscr{L} = 50 fb^{-1}$.*

5.9.5 Invariant mass with soft cuts

To illustrate the challenges to discover a resonance in the samples other that $SU1$ and $SU9$ the invariant mass plots of selected b-pairs are shown in figure 5.25 after the cuts in table 5.11 and with an integrated luminosity of $\mathscr{L} = 50 fb^{-1}$.[7] It is clear from these distributions that it will be difficult to extract any signal from SUSY scenarios other than $SU1$ and $SU9$, since we have to apply harder cuts than what is used here in order to remove more of the SM background. As we have seen, the cuts for removing SM background will remove the same amount of signal as SUSY background, so these cuts will not increase the ratio of signal and SUSY background.

5.9.6 Lepton veto

The discussion in chapter 4 concluded that the short cascades always are without leptons, while for the longer cascades the production of leptons are possible. Of course a lepton could also be produced

---

[7]These plots and the plots in the following chapter are shown with an integrated luminosity of $50 fb^{-1}$. This because the signal is in many cases very small, and to keep the errors small we have to increase the luminosity. It is clear that many of the histograms have a non-smooth form. This is most probable an artifact of the scaling factors (see appendix A for the various scaling factors in the different samples). This means that even though a Higgs, e.g. in $SU1$, in real life actually would be quite clean for some cut combination since both background and signal would be smooth. Therefore in the $50 fb^{-1}$ histograms an identification of the peak is not really possible. In this case the simulation shows a more pessimistic view than what real life would.
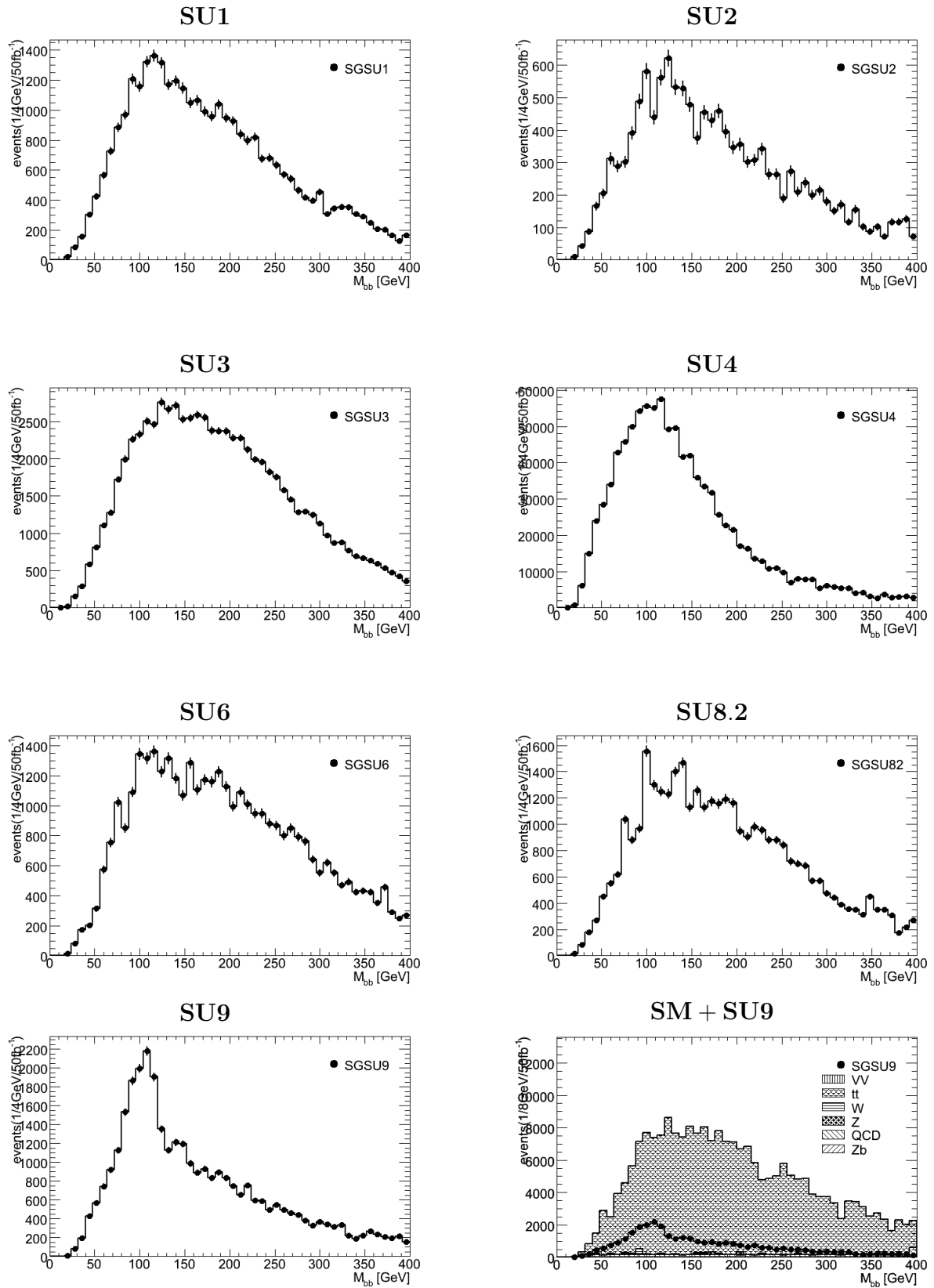
Figure 5.25: *The invariant mass of selected b pairs in all the SUSY scenarios after the cuts in 5.11 is applied and with an integrated luminosity of $50\,fb^{-1}$. At the lower right the $SU9$ signal and SM background is plotted to illustrate that the SM still is dominant.*

in the other leg. Although requiring no leptons in the event could be a way to reduce the $t\bar{t}$, W, Z and di-boson background, and enhance the signal in some scenarios. Table 5.14 shows the fraction of events with and without leptons for various SM background and signals after the cuts in table 5.11 are applied. The $SU9$ sample is dominated by cascades with no lepton production (85% of the events without leptons), like in figure 4.31. The scenario with production of 1st or 2nd generations leptons is especially $SU2$, which will have leptons in both the short and the long cascade. This is reflected in the relatively low values of SG (0.64) and COMB (0.47). The $SU1$ scenario will also have production of leptons, but often together with additional b-quarks, and therefore these events are in the *COMB* category (0.53). The $SU6$ and $SU8.2$ will have mostly τ and ν_τ produced, which is not regarded as leptons in this context.

Whether or not a lepton veto will be efficient for other scenarios than $SU9$ are shown in table

SM BG	QCD	top	VV	W	Z	Zb
with leptons	0.01	0.43	0.83	0.36	0.22	0
without leptons	0.99	0.57	0.17	0.64	0.78	0

Signals	$SU1$			$SU2$			$SU6$		
	SG	COMB	BG	SG	COMB	BG	SG	COMB	BG
with leptons	0.31	0.47	0.44	0.36	0.53	0.50	0.24	0.31	0.36
without leptons	0.69	0.53	0.56	0.64	0.47	0.50	0.76	0.69	0.64

Signals	$SU82$			$SU9$		
	SG	COMB	BG	SG	COMB	BG
with leptons	0.17	0.26	0.30	0.15	0.28	0.33
without leptons	0.83	0.74	0.70	0.85	0.72	0.67

Table 5.14: *The fraction of events with and without leptons for SM background and the signal samples. For the signal samples the events are divided into the three categories. This is after the cuts in table 5.11 are applied. SG means clean signal event, COMB is the uncorrelated bs events and BG is uncorrelated SUSY background.*

5.15, presenting the rejection of background (all events **without** Higgs) and efficiency for signal

(events **with** Higgs) **with** and **without** a lepton veto. At this stage in the analysis, table 5.15 reveal

	SU1		SU2		SU6		SU82		SU9	
	rejection and efficiency									
Cut	R	ε	R	ε	R	ε	R	ε	R	ε
lepton veto	0.19	0.61	0.19	0.55	0.19	0.74	0.19	0.76	0.19	0.80

Table 5.15: *The rejection (R) and efficiency (ε) with a lepton veto applied for the various signal scenarios. The rejection is for SUSY and SM background after the cuts in table 5.11.*

that it is not much to gain in the signal significance by applying a lepton veto. Except for $SU9$ this will remove much of the signal, which will be fatal in the scenarios where the signal already is very small.

Chapter 6

Results and Conclusions

This chapter presents the results obtained after the studies in the last two chapters. As already discussed it could be necessary with different strategies, depending on the most probable cascade patterns in the different models. The invariant mass of selected b-pairs are plotted to show the effect of the different strategies, in each case.

6.1 General cuts

Based on the studies in chapter 5 we use a certain set of cuts to reject the SM background. The general cuts used in this analysis are presented in table 6.1.

6.1.1 Two light jets

We start requiring both of the additional jets to be light. The invariant mass plots in this case are shown in figure 6.1 and should be compared to the plots in figure 5.25 without light jet requirement. The corresponding significances, number of signal and background events and the the total number of Higgs bosons left after this additional requirement are shown in table 6.2. The total $\#h$ is the total number of Higgses left in the sample after the cuts. These are Higgs bosons appearing both in the clean signal events (S), with no additional b-jets, and in the background events (B), together with other b-jets. From the table 6.2 we see that $SU9$ has almost 800 Higgs bosons left after all the cuts in table 6.1. By comparing this number with the number of Higgs after only pre-cuts in table 5.1 (11035) we see we have lost 93%. Although since the $SU9$ sample contains such many Higgses we can still see a signal in the plot in figure 6.1. For the other samples the total numbers of Higgs were much less

CUT #	VALUE
CUT 1	2 b-jets with $p_T^{1,2} > 50, 20$
CUT 2	remove hardest (and sec. hardest) b-jet in events with more than 3 (4) b-jets
CUT 3	$\not{E}_T > 300$ GeV
CUT 4	$M_{\text{eff}} > 800$ GeV
CUT 5	≥ 2 additional jets $p_T^{1,2} >$ 100, 100 GeV

Table 6.1: *The general cuts used in this analysis.*

$SU1$					$SU2$					$SU6$				
$\#h$	S	B	all	±25	$\#h$	S	B	all	±25	$\#h$	S	B	all	±25
476	399	18948	2.90	3.90	15	15	5723	0.20	0.21	284	202	22686	1.34	1.84

$SU82$					$SU9$				
$\#h$	S	B	all	±25	$\#h$	S	B	all	±25
419	325	22032	2.19	3.05	3047	2298	17675	17.3	22.7

Table 6.2: *The significance in a ±25 GeV mass window (±25), the total significance (all), the number of Higgs left after the cuts ($\#h$) and the number of signal (S) and background (B) events are shown after the cuts in table 6.1 requiring the two additional jets to be light flavored. $\mathscr{L} = 50\,fb^{-1}$.*
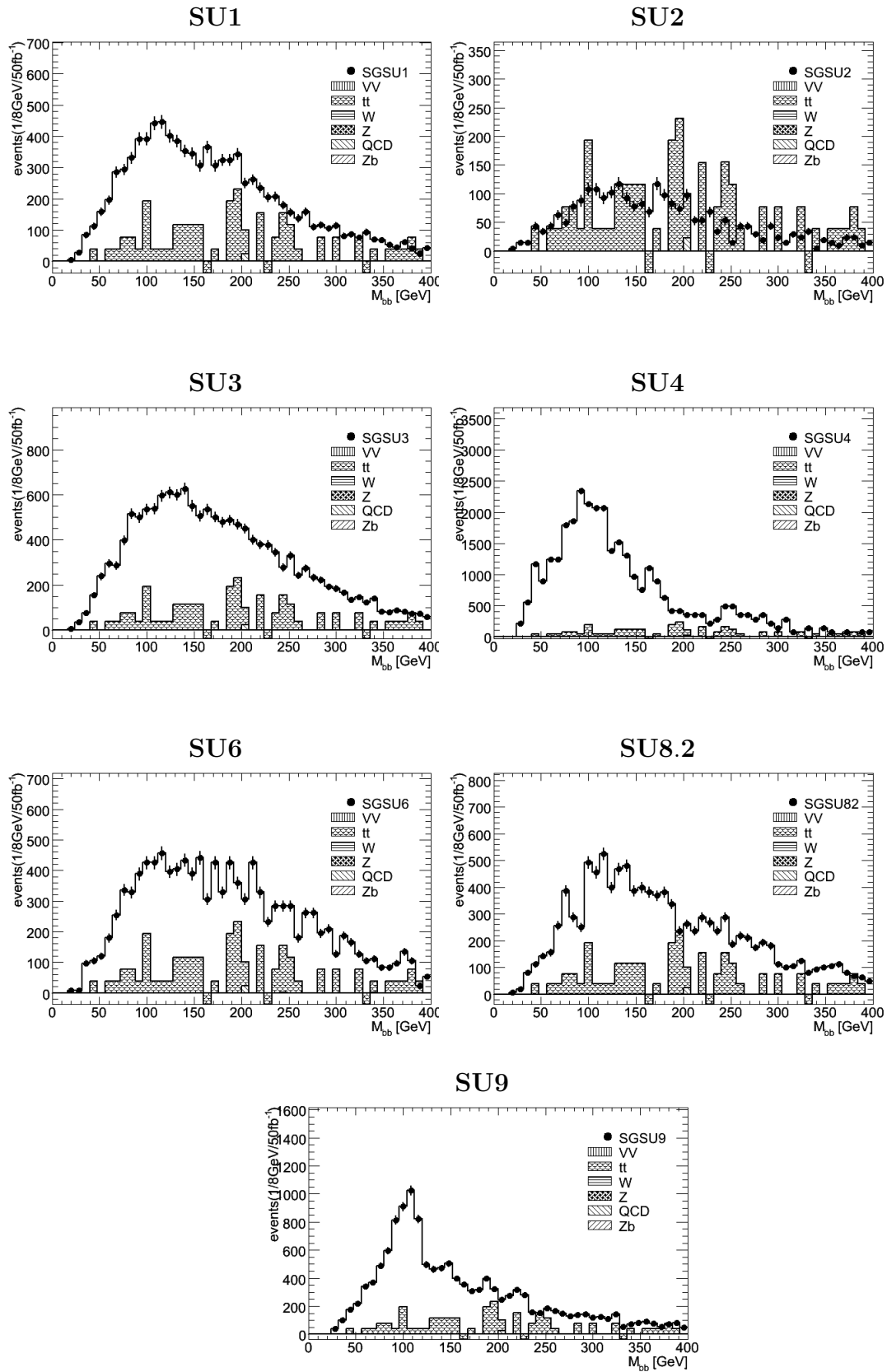
Figure 6.1: *The invariant mass plots for the various signal scenarios and SM background with the cuts in table 6.1 applied and requiring **both** of the additional jets to be **light** jets.*

than in $SU9$. By calculating the rejection of signal events by using the information in table 5.1 it is clear that we also have lost a large fraction of the generated Higgs bosons in the other samples. This is more fatal in these cases since the originally number of Higgs bosons are much smaller compared to $SU9$.

The numbers in table 6.2 illustrate that the majority of the Higgses left after the cuts are produced together with other b-quarks, except in the $SU9$ scenario. This can be seen by comparing the numbers of S events with the number of Higgs bosons left. The S events are clean signal events, meaning no other bs than the two from Higgs. This motivates us to try and require one of the additional jets to be a tagged b-jet.

6.1.2 One tagged b-jet and one other jet

To enhance the signal in the scenarios where additional b-jets are often produced in the Higgs cascade we require one of the additional jets to be a b-jet. The invariant mass distributions after this requirement are shown in figure . The corresponding significances, number of signal and background events and the number of Higgses left are shown in table 6.3.

Since we now require at least three b-jets, all the signal (S) events will be removed. This is

SU1					SU2					SU6				
#h	S	B	all	±25	#h	S	B	all	±25	#h	S	B	all	±25
180	0	6602	0	0	5	0	4574	0	0	239	0	7866	0	0

SU82					SU9				
#h	S	B	all	±25	#h	S	B	all	±25
184	0	7501	0	0	1163	29	9380	0.30	2.54

Table 6.3: *The significance in a ±25 GeV mass window (±25), the total significance (all), the number of Higgs left after the cuts (#h) and the number of signal (S) and background (B) events are shown after the cuts in table 6.1 requiring that one of the additional jets should be tagged as a b-jet. $\mathscr{L} = 50\,fb^{-1}$. Since we require at least three b-jets in this case we remove all the clean signal events, and are only left with events where Higgs is produced together with other b-quarks. Therefore the numbers of signal events are 0. In SU9 we sometimes have the possibility of having two Higgses in one event. This explains the non-zero number of signal events in this scenario.*

because the signal events are samples without any additional b-jets. Therefore we are left with Higgses only in the background events (B) after this cut, except in $SU9$ where we sometimes have two
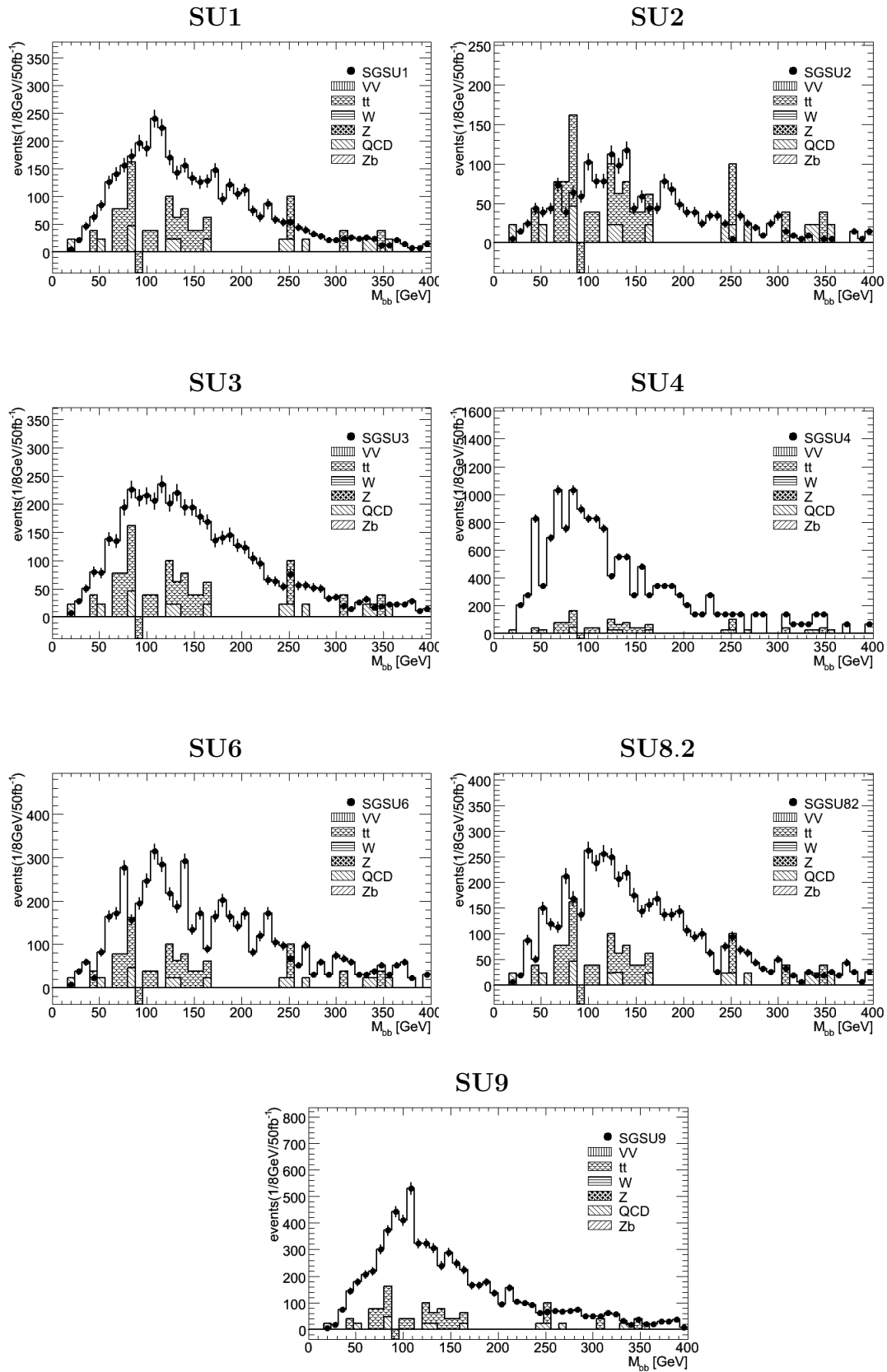
Figure 6.2: *The invariant mass plots for the various signal scenarios and SM background with the cuts i table 6.1 requiring **one** of the additional jets to be a* b*-jet.*

Higgses, and thereby will contain four b-jets and pass the cut. We see from the plots and the table that we reject some of the SM background, but we also loose a lot of Higgs bosons.

The requirement of one additional b-jet is too tough, especially in the $SU9$ scenario. There is however a hint that in $SU1$ in figure 6.2 has a signal.

6.1.3   Lepton Veto

To try to increase the significance more we also can require a lepton veto. From chapter 5 we saw that a lepton veto can be efficient in some of the scenarios, mainly $SU6$, $SU8.2$ and $SU9$. Although this will probably not be a efficient cut for $SU1$.

We use the results from the last section and require the two additional jet to be light. The invariant mass plots after a lepton veto is shown in figure 6.3. The corresponding significances and number of Higgs bosons left after this cut is shown in table 6.4.
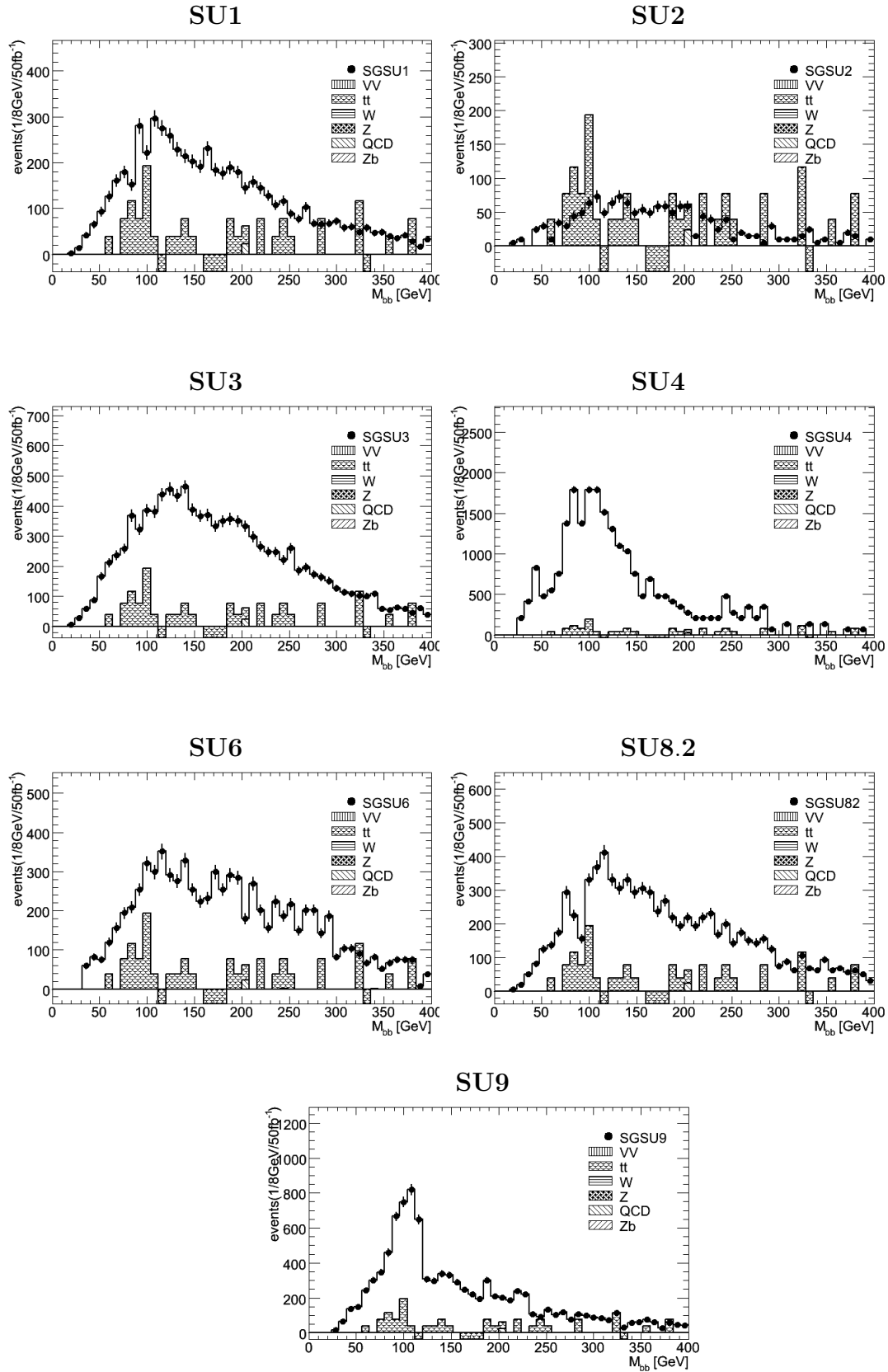
Figure 6.3: *The invariant mass plots for the various signal scenarios and SM background with the cuts i table 6.1 requiring* **both** *of the additional jets to be a* **light** *jet and a lepton veto.*

*SU*1					*SU*2					*SU*6				
#*h*	S	B	all	±25	#*h*	S	B	all	±25	#*h*	S	B	all	±25
66	51	10835	0.49	0.88	15	15	2970	0.28	0.30	194	142	14627	1.17	1.38

*SU*82					*SU*9				
#*h*	S	B	all	±25	#*h*	S	B	all	±25
324	262	15270	2.12	2.94	2613	2000	11708	18.4	23.7

Table 6.4: *The significance in a ±25 GeV mass window (±25), the total significance (all), the number of Higgs left after the cuts (#h) and the number of signal (S) and background (B) events are shown after the cuts in table 6.1 requiring* **both** *of the additional jets to be a* **light** *jet together with a* **lepton veto***.*

As expected for $SU9$ a lepton veto is an efficient cut, since it keeps $\sim 80\%$ of the signal, which was expected from the results in table 5.14 from the last chapter. In the $SU8.2$ scenario (keeps 80% of the signal) we might see a tendency to a small peak around the expected Higgs mass value. By only counting the number of events in the small peak we find approximately 80 events, which is close to the number of signal events in table 6.4. As we expected a lepton veto is not especially efficient for $SU1$, since we loose $\sim 30\%$ of the signal, which could be fatal when the signal already is small. A higher luminosity is required to make further statements concerning other scenarios. This also requires large samples of background events

6.2   *SU*9

We have now tried different strategies, motivated by the discussion in the last chapters, to see if we could extract a resonance around the Higgs mass value in some of the scenarios, other than $SU9$. This seems however to be a difficult task. We therefore end this section by looking at the $SU9$ sample, where we see a clear peak. The plots shown above were based on low generated luminosity (for most of the scenarios) that have been scaled up. We use in this section therefore a luminosity of $mathscrL = 10 fb^{-1}$, since the signal is clear.

Figure 6.4 shows the invariant mass of selected b-jet pairs for $SU9$ after the cuts in table 6.1 with an additional requirement for the two additional jets to be light flavored. The distribution is fitted with a gaussian superimposed to a second degree polynomial. The fit gives a mean value of about 102.1 GeV, which is 12 GeV below the theoretical value. We saw the same effect in the fitted distribution of the clean $h \rightarrow b\bar{b}$ sample in 5.2, so this can not be a possible background sitting close to the peak

(for instance $Z \rightarrow b\bar{b}$). This could instead be either other physics effects such as hadronisation and radiation, or something stemming from detector effects not taken into account properly in the reconstruction or calibration.

The fit used does only fit the signal and the SUSY background since the Standard Model background not is very smooth, as has been discussed earlier.

The number of events under the Gaussian is calculated (681) within one σ around the mean value. The same is done with the SUSY background, described by a second degree polynomial (777). The Standard Model background events (123) are only counted within the same mass window. From this a significance of 22.7 is found.
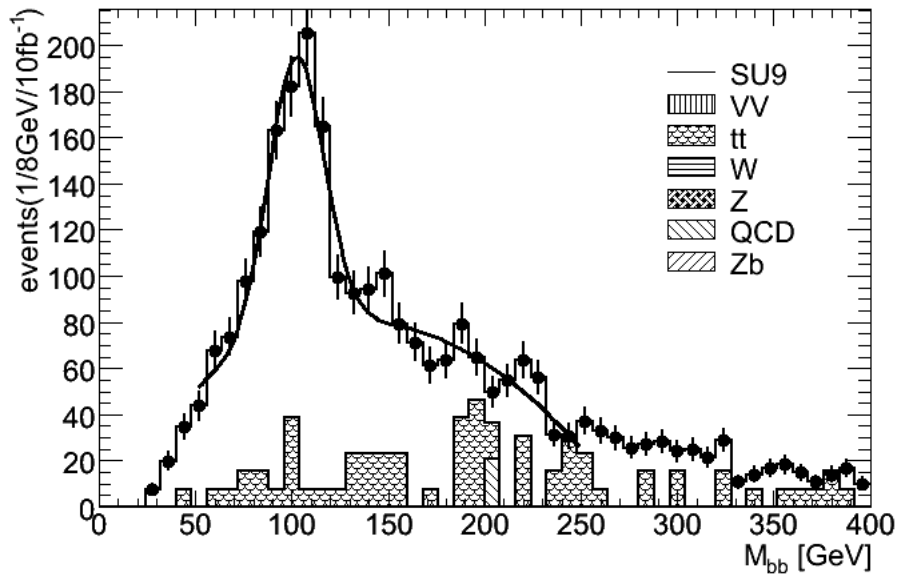
Figure 6.4: *Invariant mass of b-jets in $SU9$ with an integrated luminosity of $10 fb^{-1}$ after the cuts in table 6.1 and the requirement of the two additional jets to be light flavored.*

6.2.1 Systematics

Since LHC will operate at an energy scale which has never been reached by any other experiment before, it is difficult to know exactly how the Standard Model background will look like. One way to account for this is to multiply the SM background by a constant factor, and then calculate the significance. However in the case of a study where the goal is to extract a peak the shape of the peak will still be seen even though the SM background increases. If the background becomes very large

compared to the signal it may be difficult to also see a shape, since the shape eventually could be part of the statistical fluctuations in the background.

If we scale the SM background with three to account for systematics in the case above, the significance stays almost the same. This is because the SM is very small. This could also be misleading as we had to scale and weight the generated backgrounds to account for luminosities of order $10 fb^{-1}$.

6.3 Conclusion

This study deals with the search for the lightest supersymmetric Higgs boson in SUSY events. As we have seen, because of its low mass, the branching ratio for h into $b\bar{b}$ is huge $70 - 80\%$. Due to the large QCD background for this channel it is difficult to use the same production channels as are used in ordinary SM Higgs searches, such as for instance gluon-gluon fusion. However by using the properties of a supersymmetric cascade it has been possible to remove a lot of the SM background without loosing all the signal. By using, especially the missing transverse energy signature, it has been possible to reject most of the SM backgrounds. Also the fact that SUSY cascades contain several high p_T jets has been used to further remove SM background. The conclusion from this is that the SM is not the most challenging background.

As has been discussed the SUSY cascades can produce b-jets through several different channels. This will therefore be one of the main backgrounds that must be tackled, since these events also contain $\not{E}_T$, and can not be removed in the same way as the SM background.

The different mSUGRA scenarios have different probabilities of producing Higgs through various channels. However the main channels overall are through neutralino and chargino decay, but also decays of $\widetilde{t}_2$ and $\widetilde{\tau}_2$ decays are possible.

When the $\widetilde{ll}$ channel is kinematically accessible to the $\widetilde{\chi}_2^0$ this decay dominate its width. This gives signatures suitable for di-lepton searches and end-point measurements [3]. However if the $\widetilde{\chi}_2^0 \rightarrow \widetilde{ll}$ decay is suppressed we have shown that the $\widetilde{\chi}_2^0 \rightarrow \widetilde{\chi}_1^0 h$ dominates. The $\widetilde{\chi}_2^0$ is produced at high rate in SUSY cascades, mainly from squark decays. Therefore scenarios with large branching ratio for the decay $\widetilde{\chi}_2^0 \rightarrow \widetilde{\chi}_1^0 h$ contain many Higgses, like we have in $SU9$. However if this decay is suppressed Higgs needs to be produced through other channels, mostly through heavier gauginos. The heavier gauginos are produced at lower rates than the $\widetilde{\chi}_2^0$ in SUSY cascades, leading to less produced Higgses. In addition the branching ratios for the $\widetilde{\chi}_4^0$, $\widetilde{\chi}_3^0$ and $\widetilde{\chi}_2^\pm$, although kinematic accessible, are

never dominated by the decay into Higgs.

In this study we have tried to systematically go through all the models and find the characteristic of the cascades leading to $h \rightarrow b\bar{b}$. We tried to find different strategies to search for the Higgs coming from other decays than $\widetilde{\chi}_2^0$. This study has revealed that in all the scenarios studied there are very similar final states, except for small variations like the flavor of the additional produced jets, additional lepton production and the number of additional jets. Nevertheless, as this study shows, these small variations between the samples will probably not have any impact on the methods to use. The biggest concern is that the number of produced Higgs bosons in cases where the $\widetilde{\chi}_2^0$ is suppressed, are very small. This makes it difficult to extract the b-pairs from Higgs from all the uncorrelated SUSY background, which we have seen is huge for most scenarios.

To be able to search for Higgs in scenarios other than $SU9$ one would possible need more generated luminosity both for background and signal. Also more sophisticated methods need to be used which possibly would suppress the SUSY background further. However, this is out of the scope for this thesis. In the scenarios with very small signals an increase in the b-tagging efficiency would also be effective, however the b-tagging efficiency used in this analysis is the one foreseen at ATLAS and it is not expected to achieve a better performance than what is used in this study. Results from the CDF experiment at TEVATRON also state that b-tagging is a very difficult task, and it will take a long time before ATLAS reaches the wanted b-tagging performance.

If nature is supersymmetric the prospects for a discovery of the lightest supersymmetric Higgs boson will be very dependent on what type of SUSY is revealed. As we have seen, in the $SU9$ the Higgs may be discovered early and the $\widetilde{\chi}_2^0 \rightarrow \widetilde{\chi}_1^0 h$ channel can also be used for end-point analysis [3]. However if some of the other scenarios are the correct a discovery of the lightest supersymmetric Higgs boson, and using the methods presented in this thesis, may take a long time since one then is very dependent on excellent b-tagging performance as well as high luminosity.

Appendix A

Details of background and signal samples used in the analysis

A.1 Background samples

In the following a more detailed description of each data sample used in the analysis is given.

A.1.1 Boson production and QCD

The samples in table A.1 have production of a boson. This boson then decays into two leptons or neutrinos (to which kind is specified in the name of the dataset). The datasets beginning with J are pure QCD samples, where the number indicates the number of QCD jets. These have, as expected in a hadron collider, very high cross sections. All the samples in table A.1 have the following cuts

- At least two jets with high p_T

- $p_T^{jet\,1} > 80\text{GeV}$

- $p_T^{jet\,2} > 40\text{GeV}$

- $\eta_{max} = 5$

Some of the samples may also have a cut in $\not{E}_T$, this is specified in the table.

dataset	ID	pre-cuts[1]	xsec[pb]	L[fb^{-1}]	EF[%]	num. events	SF ($50fb^{-1}$)
$We\nu$	8270	$\not{E}_T > 80GeV$	343	1.02	14.3	50000	49
$W\mu\nu$	8271	$\not{E}_T > 80GeV$	343	1.05	8.35	30000	48
$W\tau\nu$	8272	$\not{E}_T > 80GeV$	343	0.97	16.3	54250	52
Zee	8194	-	46.2	0.049	100	2250	1020
$Z\mu\mu$	8195	-	46.4	0.52	20.7	5000	96
$Z\tau\tau$	8191	$\not{E}_T > 80GeV$	46.3	1.11	9.72	5000	45
$Z\nu\nu$	8190	$\not{E}_T > 80GeV$	246	0.6	16.8	25250	82
$J4$	8090	$\not{E}_T > 100GeV$	$3.16 \cdot 10^5$	0.72	0.29	66037	69
$J5$	8091	$\not{E}_T > 100GeV$	$1.25 \cdot 10^4$	0.235	2.85	83800	213
$J6$	8092	$\not{E}_T > 100GeV$	344	0.48	19.6	32150	104
$J7$	8093	$\not{E}_T > 100GeV$	5.3	0.66	100	3500	76
$J8$	8094	$\not{E}_T > 100GeV$	$2.21 \cdot 10^{-2}$	192	100	4250	0.3

Table A.1: *Background datasets used in my analysis. The sample ID, cross section and number of events generated are presented. The EF factor should be multiplied by the cross section to get the effective cross section. The luminosity generated for each file is also shown together with SF($50fb^{-1}$) which is the scale factor that is used when scaling the histograms up to an integrated luminosity of $50fb^{-1}$.*

A.1.2 Di-Boson production and Zb

Datasets for all the possible combinations of production of two vector bosons in a pp collision are listed in table A.2. In addition the production of a Z and b-jets are also included, because it has high cross section and is an possibly important background for my analysis. The decay of the vector bosons are not specified, so they can decay both to quarks and leptons. All the datasets in table A.2 have the following cuts.

- *Lepton filter*: an electron or muon to be found in *truth* with $p_T > 10$ GeV

- $|\eta| < 2.8$.

---

[1]in addition to the one already mentioned

dataset	ID	xsec[pb]	L[fb^{-1}]	EF[%]	num. of events	SF ($50fb^{-1}$)
WW	5985	70	2.04	35	50000	25
ZZ	5986	11	14.0	19	29050	4
WZ	5987	27	6.37	29	49900	8
Zb	5178	205	0.12	75	18900	416

Table A.2: Di boson production background used in my analysis. The sample ID, cross section are given. The total number of events in the file and the corresponding integrated luminosity (fb^{-1}) is also shown. SF ($50fb^{-1}$) is the sale factor which is used when scaling the histograms up to an integrated luminosity of $50fb^{-1}$.

A.1.3 Top samples

The production of two top quarks at LHC have large cross section, in addition it is an important background for my final state, since it will contain many b-jets. The top samples used in the analysis are listed in table A.3. There are two datasets, one with purely hadronic decay[2], and one with not purely hadronic decay (i.e. at least one of the W's decays leptonically).

dataset	ID	pre-cuts	effective xsec[pb]	L[fb^{-1}]	comments	num. of events	SF
$T1$	5200	-	461	1.30	not all hadronic	597100	38
$t\bar{t}$	5204	p_T of one of the t's > 200GeV	369	0.27	all hadronic	97950	185

Table A.3: Top backgrounds used in my analysis. The sample ID, effective cross section are shown. The number of generated events in the sample with the corresponding integrated luminosity (fb^{-1}) is also shown. SF ($50fb^{-1}$) is the sale factor which is used when scaling the histograms up to an integrated luminosity of $50fb^{-1}$.

---

[2]since BR($t \to bW$) $\approx 100\%$, hadronic decay means that the W decays into quarks

dataset	ID	xsec[pb]	L[fb^{-1}]	num. events	SF ($50 fb^{-1}$)
SU1	5401	7.43	21	158950	2.3
SU2	5402	4.86	10	49700	5
SU3	5403	18.59	26	496750	1.9
SU4	6400	262	0.73	190250	68
SU6	5404	4.48	6.7	29950	7.5
SU8.2	5407	6.40	8	51200	6.3
Higgs	6404	3.30	12	39850	15

Table A.4: *Signal datasets used in my analysis showing the dataset ID, the calculated cross section, number of generated events and the corresponding luminosity (fb^{-1}). The scale factor (SF) to use when working with a luminosity of $\mathscr{L} = 50$ is also shown.*

A.2 Signal samples

Table A.4 is a list of the signal datasets used in my analysis.

Bibliography

[1] Atlas collaboration, atlas technical paper, atlas technical paper (2008).

[2] Atlas collaboration, b-tagging csc0 note:, b-tagging performance (2008).

[3] Atlas collaboration, susy csc5 note, atlas note csc-susy5 (2008).

[4] W. d. Boer. Search for susy and higgs particles, 1998.

[5] ATLAS Collaboration. Atlas technical design report. Technical report, 1999.

[6] M. Dobbs and J. B. Hansen. The hepmc c++ monte carlo event record for high energy physics. *Computer Physics Communications*, 134(1):41–46, 2001.

[7] Z. Dolezal. The atlas semiconductor tracker - design and status of construction. *Nuclear Physics B - Proceedings Supplements*, 150:128–131, 2006.

[8] G. S. F. Mandl. *Quantum Field Theory*. John Wiley and Sons, revised edition, 1984.

[9] A. Pukhov G. Belanger, S. K. Comparison of susy spectrum calculations and impact on the relic density constraints from wmap. *Phys.Rev:*, D72:015003, 2005.

[10] H. Georgi, H. R. Quinn, and S. Weinberg. Hierarchy of interactions in unified gauge theories. *Phys. Rev. Lett.*, 33(7):451–454, Aug 1974.

[11] X. T. Howard Baer. *Weak Scale Supersymmetry, From Superfields to Scattering Events*. Cambridge University Press, 2006.

[12] P. Luc and T. Daniel. Supersymmetry facing experiment: much ado (already) about nothing (yet). *Reports on Progress in Physics*, (11):2843, 2006.

[13] R. L. Michele Consonni. Higgs searches in cascade decays of susy particles in minimal sugra models. *ATLAS Internal Notes*, 2007.

[14] C. Neu and U. Pennsylvania. *CDF b-tagging: Measuring efficiency and false positive rate*. 2006.

[15] A. Sfyrla, A. Abdesselam, S. G. Basiladze, R. Brenner, M. Chamizo-Llatas, G. Codispoti, P. Ferrari, B. Mikulec, P. Phillips, H. Sandaker, and E. Stanecka. The detector control system for the atlas semiconductor tracker assembly phase, 2006.

[16] W.-M.Yao. Particle data group. *J. Phys. G 33*, 1, (2006) and 2007 partial update for the 2008 edition.